Titre: Title:	Modeling and Experimental Validation of the Performance of Phase Change Material Storage Tanks in Buildings
Auteur: Author:	Katherine D'Avignon
Date:	2015
Type:	Mémoire ou thèse / Dissertation or Thesis
Référence: Citation:	D'Avignon, K. (2015). Modeling and Experimental Validation of the Performance of Phase Change Material Storage Tanks in Buildings [Thèse de doctorat, École Polytechnique de Montréal]. PolyPublie. https://publications.polymtl.ca/1973/

UNIVERSITÉ DE MONTRÉAL

MODELING AND EXPERIMENTAL VALIDATION OF THE PERFORMANCE OF PHASE CHANGE MATERIAL STORAGE TANKS IN BUILDINGS

KATHERINE D'AVIGNON

DÉPARTEMENT DE GÉNIE MÉCANIQUE

ÉCOLE POLYTECHNIQUE DE MONTRÉAL

THÈSE PRÉSENTÉE EN VUE DE L'OBTENTION

DU DIPLÔME DE PHILOSOPHIAE DOCTOR

(GÉNIE MÉCANIQUE)

DÉCEMBRE 2015

UNIVERSITÉ DE MONTRÉAL

ÉCOLE POLYTECHNIQUE DE MONTRÉAL

Cette thèse intitulée :

MODELING AND EXPERIMENTAL VALIDATION OF THE PERFORMANCE OF PHASE CHANGE MATERIAL STORAGE TANKS IN BUILDINGS

présentée par : D'AVIGNON Katherine

en vue de l'obtention du diplôme de : Philosophiae Doctor

a été dûment acceptée par le jury d'examen constitué de :

M. PELLETIER Dominique, Ph. D., président

M. KUMMERT Michaël, Doctorat, membre et directeur de recherche

M. PASQUIER Philippe, Ph. D., membre

M. ATHIENITIS Andreas K., Ph. D., membre externe

DEDICATION

To Sylvain,
because you stayed put whilst I jumped into the void,
you smiled while I panicked,
you fed me when pauses were rare,
you let me grow and learn at my own rhythm,
thank you.

À Sylvain,
parce que tu es resté fixe alors que je sautais dans le vide,
que tu m'as souris alors que je paniquais,
que tu m'as nourri quand les pauses se faisaient rares,
que tu m'as laissé grandir et apprendre à mon rythme,
merci.

"We have to continually be jumping off cliffs
and developing our wings on the way down."
- *Kurt Vonnegut*

ACKNOWLEDGEMENTS

I started this doctoral project quite naively. Reaching this point has been like crossing the desert; an apparently infinite struggle to no end. Somehow, here I am with a complete thesis. This could not have been possible without the help and support of many, to whom I address these few words.

To start, I must give my sincere thanks to my thesis supervisor, Professor *Michaël Kummert*. He trusted me with his laboratory and did not despair when things went awry. He gave me the opportunity to try different things, to delve into side-tracks and let me find my way on my own. He remained patient, calm and supportive while I freaked out, lost time and broke test tube after test tube. It is because of him that I got into this doctorate and thanks to him that I got through it.

I must underline the support and encouragement I received from Professors Michel Bernier and *Philippe Pasquier* throughout the years. Thank you for the advice, the time and the material you lent out so earnestly. I should also note the helpful advice of Professors *Bantwal Rabindranath Baliga* and *Bruno Detuncq*.

I would like to thank the students who participated in various parts of this project: *Antonin Paquette-Rufiange*, *Dustin Goyer*, *Jonathan Lazaro*, *Christophe Chilini*, *Lin Chun Pang*, *Eva Ngansop* and *François Mercier-Boulet*. Though you might have felt like small cogs in a big wheel, your little nudges of progress helped nonetheless.

My thanks go out to the other MECBAT students, past and present, with whom I have shared unforgettable moments: *Aurélie Verstraete*, *Romain Jost*, *Marilyne Rancourt-Ouimet*, *Mathieu Lévesque*, *Antoine Courchesne-Tardif*, *Matthieu Grand*, *Massimo Cimmino*, *Parham Eslami-Nejad*, *Humberto Quintana*, *Kun Zhang*, *Samuel Lettelier-Duchesne*, *Simon Maltais Larouche*, *Bruno Marcotte*; and all the others. Special thanks to *Benoit Delcroix* who, like me, shared in the "joy" of modelling phase change materials.

I would like to mention the technical assistance of *Philippe Massé* in the commissioning of the Semi-Virtual Laboratory and *Thierry Lafrance* from Mëkanic for his contribution to the instrumentation of the PCM capsule.

Finally, I would like to thank Professors *Andreas Athienitis, Dominique Pelletier* and *Philippe Pasquier* for having accepted to be members of the jury.

This project was made possible with funding from the "*Fonds de recherche du Québec – Nature et technologies* (*FRQNT*)", of the *NSERC Smart Net-Zero Energy Buildings Strategic Research Network* (*SNEBRN*) and the *Canadian Foundation for Innovation*.

My warmest thanks to all,

Katherine D'Avignon

Montreal, December 2015

RÉSUMÉ

Le stockage d'énergie thermique dans les bâtiments permet d'atténuer les pointes d'appel de puissance sur le réseau électrique et de synchroniser la demande énergétique à la disponibilité de ressources énergétiques renouvelables, telle l'énergie solaire. Les matériaux à changement de phase (MCP) peuvent être utilisés afin de permettre un tel stockage d'énergie thermique. Ceux-ci offrent une haute densité de stockage énergétique (principalement sous forme d'énergie latente) et un changement de phase à température quasiment constante.

L'intégration de MCP dans un réservoir où circule un fluide caloporteur permet de créer un système de stockage actif. La charge et décharge énergétique du réservoir peuvent alors être contrôlées par le débit du fluide caloporteur envoyé dans le réservoir ou vers un contournement. Afin d'assurer une performance adéquate du réservoir de stockage à MCP dans un bâtiment, le comportement dynamique de celui-ci doit être prévisible. Or, le design du réservoir aura un impact crucial sur son fonctionnement : la température de changement de phase du matériau, la géométrie du réservoir et des capsules de MCP influenceront le comportement dynamique de celui-ci. Afin de permettre un design adéquat du réservoir, des outils permettant la simulation énergétique de tels systèmes sont nécessaires.

Or, la modélisation du changement de phase, souvent basée sur une relation entre l'enthalpie et la température du matériau, présente certaines difficultés. Elle est, entre autre, limitée par les informations rendues disponibles par les manufacturiers, qui sont souvent incomplètes ou erronées. Les MCP ont aussi tendances à se comporter différemment lors de leur fusion et lors de leur solidification (i.e. présence d'hystérèse) et ils exhibent parfois des phénomènes de surfusion dont l'occurrence est plus stochastique que déterministe. De plus, peu de données expérimentales existent sur le comportement dynamique de tels réservoirs. Ainsi, les modèles numériques actuels sont limités à quelques géométries et rarement validés expérimentalement. Toutes ces problématiques sont soulevées dans cette thèse et des solutions sont abordées.

La première partie (chapitre 4) offre une contribution à une méthode de caractérisation normalisée des matériaux à changement de phase, à travers une évaluation critique du traitement des données de la méthode « T-History ». Une proposition est faite quant à la variante qui devrait être adoptée pour déterminer la courbe enthalpie-température de MCP présentant une surfusion

importante afin de fournir toutes les informations nécessaires pour la simulation numérique de leur comportement.

La deuxième partie (chapitre 5) se concentre sur les essais expérimentaux détaillés d'un réservoir horizontal contenant des capsules rectangulaires de matériaux à changement de phase à échelle réelle. Les essais expérimentaux effectués sont minutieux: 14 conditions d'opérations distinctes sont testées, faisant varier le débit d'entrée, l'intervalle de température ainsi que le profil de la charge dans le réservoir. Trois répétitions de chaque test permettent d'étudier la variabilité des résultats.

Finalement, la dernière partie (chapitre 6) se concentre sur le développement ainsi que la validation numérique et expérimentale d'un nouveau modèle permettant la simulation de réservoirs de MCP. Le modèle est basé sur une discrétisation semi-explicite et représente le changement de phase du matériau par la méthode enthalpique, permettant aussi la simulation d'un MCP avec de l'hystérèse entre ses processus de fusion et de solidification. Le modèle est d'abord validé numériquement par comparaison de ses résultats avec ceux de modèles détaillées à éléments-finis. Les données expérimentales du chapitre précédent sont ensuite utilisées pour effectuer une validation expérimentale exhaustive. La comparaison des résultats numériques aux données expérimentales selon les principes de la ligne directrice 14 de l'American Society of Heating, Refrigerating and Air-conditioning Engineers confirme la validité des résultats du modèle pour cette géométrie.

ABSTRACT

Thermal energy storage in buildings can attenuate peak power demand to the electric grid and synchronize the heating or cooling load to the availability of renewable energy, such as solar energy. Phase change materials (PCM) can be used to allow such storage of thermal energy. They offer high energy storage density (mainly through latent energy) and a quasi-constant phase change temperature.

The integration of PCMs in a tank where a heat transfer fluid can circulate allows the creation of an active thermal storage system. Charging and discharging energy from the reservoir can be controlled by directing the heat transfer fluid into the tank or towards a by-pass. To ensure an adequate performance of the PCM storage tank in a building, its dynamic behaviour must be predictable. The PCM tank's design will have a crucial impact on its operation: the material's phase change temperature, the geometry of the tank and PCM capsules will influence the transient behaviour of the tank. To allow an adequate design of the tank, tools allowing the energy simulation of such systems are required.

However, the modelling of phase change itself, often based upon a relation between the enthalpy and temperature of the material, presents some difficulties. It is, amongst other things, limited by the information made available by manufacturers, which are often incomplete or erroneous. PCMs have also the tendency to behave differently during their fusion and solidification processes (i.e. presence of hysteresis) and they exhibit at times a phenomenon of supercooling whose occurrence tends to be more stochastic than deterministic. Moreover, little experimental data exists on the transient behavior of such PCM storage tanks. The existing numerical models are limited to a few geometries and have rarely been validated experimentally. All these problems are explored in this thesis and solutions are addressed.

The first section of this thesis (Chapter 4) offers a contribution towards a standardised characterisation method for phase change materials through a critical evaluation of the data processing in the T-History Method. A proposal is made concerning the data processing variant which should be adopted to determine the enthalpy-temperature curve of PCMs presenting an important degree of supercooling so that all the required information necessary for its numerical simulation is available. The second section (Chapter 5) concentrates on the detailed experimental testing of a real-scale horizontal storage tank containing rectangular PCM capsules. The

experimental tests are thorough: 14 different operating conditions are tested with combinations of different inlet flowrates, temperature intervals and load profiles to the tank. Three repetitions of each test allow the assessment of the variability of results.

Finally, the last section (Chapter 6) focusses on the development as well as the numerical and experimental validation of a new model for the simulation of PCM storage tanks. The model is based on a semi-explicit discretization and represents phase change in the material by the enthalpy method, allowing the simulation of a PCM with hysteresis between its fusion and solidification processes. The model is first validated numerically by comparing its results to those of detailed finite-element models. The experimental data from the previous chapter are then used to perform an exhaustive experimental validation. The comparison of numerical results to the experimental measurements following the principles of Guideline 14 from the American Society of Heating, Refrigerating and Air-conditioning Engineers confirms the validity of the model results for the studied geometry.

TABLE OF CONTENTS

DEDICATION III

ACKNOWLEDGEMENTS IV

RÉSUMÉ VI

ABSTRACT VIII

TABLE OF CONTENTS X

LIST OF TABLES XIV

LIST OF FIGURES XV

LIST OF SYMBOLS AND ABBREVIATIONS XIX

LIST OF APPENDICES XXI

CHAPTER 1 INTRODUCTION 1

CHAPTER 2 LITERATURE REVIEW 5

2.1 Modeling the phase change process 5

2.1.1 Enthalpy method 6

2.1.2 Effective heat capacity method 8

2.1.3 Issues with modelling the phase change process 10

2.2 Modeling PCM encapsulated in flat, rectangular capsules 13

2.2.1 Gaseous heat transfer fluid 13

2.2.2 Liquid heat transfer fluid 14

2.3 Experimental data on phase change material thermal storage tanks 16

2.4 Applications of PCMs in building systems 17

2.4.1 PCM in construction material 18

2.4.2 Applications in solar energy systems 19

2.4.3 Applications of PCM in hot water storage tanks 20

2.4.4 Free cooling applications 21
2.4.5 Follow-up of real applications in buildings 22
2.5 Conclusion 24
CHAPTER 3 OBJECTIVES AND THESIS ORGANISATION 25
3.1 Thesis objectives 25
3.2 Thesis organisation 26
CHAPTER 4 ARTICLE 1: ASSESSMENT OF T-HISTORY METHOD VARIANTS TO OBTAIN ENTHALPY-TEMPERATURE CURVES FOR PHASE CHANGE MATERIALS WITH SIGNIFICANT SUBCOOLING 28
4.1 Abstract 28
4.2 Introduction 29
4.3 Literature review: PCM characterization methods 31
4.4 Experimental test 32
4.4.1 Setup 32
4.4.2 Procedure 33
4.4.3 Experiment 34
4.5 Results 36
4.5.1 T-history method – Z 36
4.5.2 Time-delay method – M 38
4.5.3 Sandness & Rekstad’s Method – SR 41
4.5.4 Thermal-delay method – K 44
4.6 Discussion and recommendations 47
4.7 Conclusion 49
4.8 Acknowledgements 50
4.9 Nomenclature 50

4.9.1 Subscript....50
4.10 References....51
CHAPTER 5 ARTICLE 2: EXPERIMENTAL ASSESSMENT OF A PHASE CHANGE MATERIAL STORAGE TANK....55
5.1 Abstract....55
5.2 Keywords....55
5.3 Introduction....56
5.4 Experimental set-up....57
5.5 Test methodology....61
5.6 Results and discussion....62
5.6.1 Step tests....62
5.6.2 Interrupted tests....75
5.6.3 Fixed temperature change rate tests....78
5.6.4 Constant power tests....80
5.7 Comparison of useful energy from the tank for all tests....82
5.8 Conclusion....85
5.9 Acknowledgments....86
5.10 References....87
CHAPTER 6 ARTICLE 3: MODELING HORIZONTAL STORAGE TANKS WITH ENCAPSULATED PHASE CHANGE MATERIALS FOR BUILDING PERFORMANCE SIMULATION 91
6.1 Abstract....91
6.2 Introduction....91
6.3 Mathematical model....93
6.3.1 Significant flow conditions | Pe > 2....97

6.3.2 Negligible flow conditions | Pe < 2 100
6.3.3 Enthalpy-temperature curve and hysteresis 101
6.4 Preliminary study through detailed model analysis 103
6.4.1 Fluid flow 103
6.4.2 Heat transfer surface 109
6.4.3 Lateral conduction between PCM nodes 110
6.4.4 Grid and time step analysis 110
6.5 Model adjustments 113
6.6 Experimental validation 115
6.6.1 Experimental set-up 115
6.6.2 Comparison to experimental results 118
6.7 Discussion 124
6.8 Conclusion 125
6.9 Acknowledgements 126
6.10 References 126
CHAPTER 7 GENERAL DISCUSSION 130
CHAPTER 8 CONCLUSION AND RECOMMENDATIONS 133
BIBLIOGRAPHY 135
APPENDICES 151

LIST OF TABLES

Table 4.1: PCM properties specified by manufacturer 34

Table 5.1: PCM properties of S27 as specified by the manufacturer.....58

Table 5.2: Duration of the useful power output 71

Table 5.3: Total energy variation in the test for each process and operating condition.....84

Table 6.1: Material characteristics 105

Table 6.2: Data for simulation test cases.....105

Table 6.3: Characteristics of phase change material S27.....117

Table 6.4: Validation metrics for all PCM tank tests.....120

Table A.1: S27 properties supplied by the manufacturer.....152

Table B.1: List of temperature sensors.....160

Table B.2: Measurement accuracy for NI 9217 specified by the manufacturer 163

Table B.3: Detailed calculation of random uncertainty for thermocouple TC - 12 165

Table B.4: Maximum combined uncertainty for every sensor.....167

Table B.5: List of uncertainty sources, associated uncertainty reduction methods and conclusion 169

LIST OF FIGURES

Figure 1-1: Schematic of different PCM storage tank geometries a) flat plate, b) shell-and-tube with crossflow, c) cylindrical capsules, d) coil submerged in PCM, e) packed bed of spherical capsules and f) heat pipe 3

Figure 2-1: Evolution of a material's specific enthalpy as a function of material temperature for a) a pure substance and b) a binary mixture 7

Figure 2-2: Evolution of a material's apparent specific heat capacity as a function of material temperature 9

Figure 2-3: Evolution of a material's specific enthalpy as a function of material temperature in the presence of a) supercooling or b) hysteresis 11

Figure 4-1: Temperature evolution during a full cycle of the T-history experimental procedure .34

Figure 4-2: T-history data from six of the PCM samples tested for the third cooling and heating cycle 35

Figure 4-3: Division of the T-history curves following the method Z for a) the reference sample and b) the PCM sample 37

Figure 4-4: T-history curve of PCM sample indicating two alternate ways of treating subcooling in method M 39

Figure 4-5: Enthalpy-temperature curves resulting from the method presented by method M according to the way subcooling is treated 40

Figure 4-6: Comparison of enthalpy-temperature curves for every PCM sample, for both heating and cooling for method M 41

Figure 4-7: Comparison of enthalpy-temperature curves for every PCM sample by method SR .42

Figure 4-8: Method K for a) the reference sample and b) the PCM sample 44

Figure 4-9: Effective specific heat curves as a function of temperature for sample K19, calculated with method K using a 10 s time interval for a) heating and b) cooling process data 46

Figure 4-10: Enthalpy as a function of temperature for all samples, as per method K, for both heating and cooling processes 47

Figure 4-11: Enthalpy-temperature curves produced by method M (with absolute temperature interval), method K and method SR for all PCM samples, from both cooling and heating test data 48

Figure 5-1: Instrumented PCM capsule 58

Figure 5-2: PCM tank viewed from the inlet, including 1) perforated plate, 2) capsule support and 3) PCM capsules 59

Figure 5-3: Position of the instrumented PCM capsule in the tank as viewed from the outlet 59

Figure 5-4: Schematic representation of the PCM tank testing zone of the Semi-Virtual Lab 60

Figure 5-5: Temperature profiles for a heating test at $v = 0.3$ L/s and $\Delta T = 10$ °C 63

Figure 5-6: Temperature profiles for a cooling test at $v = 0.3$ L/s and $\Delta T = 10$ °C 63

Figure 5-7: PCM temperature measured by "long" sensor as a function of time for all cooling and heating test repetitions 65

Figure 5-8: PCM temperature measured by the "short" sensor as a function of time for all heating and cooling test repetitions 66

Figure 5-9: Outlet fluid temperature from PCM tank as a function of time for all heating and cooling test repetitions 68

Figure 5-10: Evolution of instantaneous tank power output through logarithmic time 69

Figure 5-11: Melt (in grey) and freeze time (in black) associated with every flowrate and temperature differential combination calculated through the short, $T_{pcm,s}$, and long PCM sensors, $T_{pcm,l}$, as well as the tank outlet temperature, T_{out}. 72

Figure 5-12: Degree of supercooling for all v and ΔT combinations 74

Figure 5-13: Enthalpy-temperature curve followed by PCM according to different authors 76

Figure 5-14: Interrupted heating and cooling tests, $v = 0.3$ L/s, $\Delta T = 10$ °C, with the fourth repetition indicated by dash-dotted lines 77

Figure 5-15: Test results for inlet temperature change rate of 1.25 °C/hr, $v = 0.3$ L/s 79

Figure 5-16: Temperature profiles for a heating test at $v = 0.3$ L/s and constant power input 81

Figure 5-17: Temperature profiles for a cooling test at $v = 0.3$ L/s and constant power input.....81

Figure 6-1: Flat slab-like PCM capsule.....94

Figure 6-2: Modelled section of the PCM storage tank 95

Figure 6-3: Modelled section of the PCM tank (between the two dotted lines) is discretized into several control volumes (illustrated here for 2 PCM control volumes in the y direction).....96

Figure 6-4: Model discretization.....98

Figure 6-5: Schematic of an enthalpy-temperature curve with hysteresis 101

Figure 6-6: Enthalpy-temperature curve followed by PCM according to different authors 102

Figure 6-7: Fluid flow profiles studied 104

Figure 6-8: Velocity profile [m/s] at the half-height of the fluid passage for Model 3 107

Figure 6-9: Outlet fluid temperature for Case 1.....108

Figure 6-10: Temperature distribution at sectional cuts of the PCM capsule, 1500 s into Case 1 109

Figure 6-11: Temperature distribution at sectional cuts of the PCM capsule, 1500 s into Case 1 112

Figure 6-12: Repartition of PCM inside the capsule.....114

Figure 6-13: Schematic of by-pass section and entry/exit volumes.....114

Figure 6-14: Experimental set-up schematic.....116

Figure 6-15: Enthalpy-temperature curve of PCM S27 117

Figure 6-16: PCM capsule tested 118

Figure 6-17: Insulated PCM storage tank 118

Figure 6-18: Tank outlet fluid temperature as a function of time for all step tests.....119

Figure 6-19: Tank outlet fluid temperature as a function of time for interrupted test 122

Figure 6-20: Tank outlet fluid temperature as a function of time for fixed temperature change rate tests.....123

Figure 6-21: Tank outlet fluid temperature for constant power heating test.....124

Figure 6-22: Tank outlet fluid temperature for constant power cooling test 124

Figure A-1: Image of S27 sample equipped with a thermocouple sensor 151

Figure B-1: Raw experimental and correlation predicted temperature difference plotted against the average reference temperature for sensor « 1/10 - 4 » 162

LIST OF SYMBOLS AND ABBREVIATIONS

The following symbols and abbreviations apply to Chapters 1, 2, 3, 7 and 8 of this thesis. The different journal papers presented in Chapters 4 to 6 however have their own nomenclature. The symbols and abbreviations for each journal paper are specific to that Chapter and the reader is asked to refer to each paper's nomenclature for information on the symbols and abbreviations used.

ASHRAE	American Society of Heating, Refrigerating and Air-conditioning Engineers
c_p	Specific heat capacity [kJ/(kg-K)]
$c_{p,App}$	Apparent specific heat capacity [kJ/(kg-K)]
DSC	Differential scanning calorimetry
H	Enthalpy [kJ]
HTF	Heat transfer fluid
HVAC	Heating, Ventilating and Air-Conditioning
k	Thermal conductivity [W/(m-K)]
k_l	Liquid state thermal conductivity [W/(m-K)]
k_s	Solid state thermal conductivity [W/(m-K)]
L	Latent heat of fusion [kJ/kg]
l_f	Liquid fraction [-]
PCM	Phase change material
T	Temperature [K] or [°C]
t	Time [s], [mins] or [hrs]
T_f	Solidification temperature [K] or [°C]
T_m	Fusion temperature [K] or [°C]
TRNSYS	Commercial brand name of a transient system simulation program
x	Length [m]

Greek symbols

∂	Differential [-]
ρ	Density [kg/m^3]
Δ	Variation [-]

LIST OF APPENDICES

Appendix A – Additional S27 properties 151

Appendix B – Temperature sensor calibration and uncertainty 159

CHAPTER 1 INTRODUCTION

An important part of building energy use serves to meet the thermal needs of the buildings such as space heating and cooling as well as hot water heating. In 2010, it is 60% of the energy consumed in Canadian commercial and institutional buildings which could be attributed to thermal needs; in the case of the residential sector, these end-uses accounted for over 80% of building energy usage (Natural Resources Canada, 2013). The sector's energetic future therefore depends in large part on the evolution of building thermal systems energy efficiency.

Building energy demand undergoes a succession of peaks and valleys over the course of a day due to the schedule of occupant behaviour and daily weather cycles. Over a year, seasonal weather variations increase these peaks; northern climates experience peak heating demands in winter time and southern climates see increased needs in the hottest summer days. As they overlap, energy demand peaks from neighbouring buildings become critical for utility companies. Additional production and transport capacity must be planned to meet these peak load, which occur for only a few hours each year. For example, Quebec's peak energy demand reached 38 950 MW at 7h21 on January 8th (Hydro-Quebec, 2014). Though the installed capacity of 36 643 MW is sufficient for usual operation (Hydro-Quebec, 2014), such instances prompt the need to purchase expensive and more environmentally damaging energy for neighbouring utilities. It is no surprise utilities across the globe seek to reduce building peak energy demand.

The inclusion of renewable energy resources tends to accentuate this issue. In fact, the great variability in the availability of renewable energy resources such as wind and solar, often leads to increased de-synchronization of energy supply and demand. The exploitation of these resources therefore does not permit the complete replacement of the more polluting thermal power stations which provide a stable and reliable energy supply. Knowing the limits of planetary energy resources, it is more than a reduction of energy consumption which is required; a better synchronisation of energy demand and supply is also essential.

The introduction of a technology allowing energy to be stored as heat or "cold" in off-peak demand periods and restored when needs are maximum is of prime interest. The storage of latent energy is of particular interest in comparison to that of sensible energy as it allows a larger storage density and releases heat over a narrow temperature range (Agyenim, Hewitt, Eames & Smyth, 2010). Latent energy can be stored in any material which changes phase over the

operating temperature interval. The solid/liquid phase change is of particular interest as the inherent change in material volume is more manageable than for liquid/gas transitions. The large variety of commercially available Phase Change Materials (PCMs) also allows the selection of the correct transition temperature, leading to the adequate outlet heat transfer fluid temperature from the storage unit. Water is a natural PCM, but its uses are limited by the low phase change temperature (0 °C). In the case of building heat load levelling, the desirable interval for heat transfer fluid temperature is between 15 and 90 °C (Farid, Khudhair, Razack & Al-Hallaj, 2004), which requires a range of adapted PCMs.

Different phase change material storage systems exist for use in buildings. PCM enhanced building materials such as wallboards, floor tiles, concrete, bricks and windows can passively augment a building's thermal mass (Khudhair & Farid, 2004). Controlling the timing of heat storage and release is required for peak demand shifting, so in that regards only active storage is of interest. Active PCM storage systems include radiant floors containing PCM material (Kalnæs & Jelle, 2015; Pomianowski, Heiselberg & Zhang, 2013) but most often refer to heat exchangers built to charge/discharge energy from PCM to a heat transfer fluid. Storage units of the shell-and-tube type can be found, as well as heat-pipes. Companies across the world produce encapsulated PCM most often of rectangular, cylindrical or spherical shape which can be installed in storage tanks so as to create a "latent heat thermal energy storage system". These can take the form of vertical or horizontal water tanks including PCM capsules (Belén Zalba, Marin, Cabeza & Mehling, 2003) or air ducts holding PCM capsule banks across which the air flow can circulate (Regin, Solanki & Saini, 2008; Zhu, Ma & Wang, 2009). A schematic of different PCM storage tank geometries is presented in Figure 1-1.

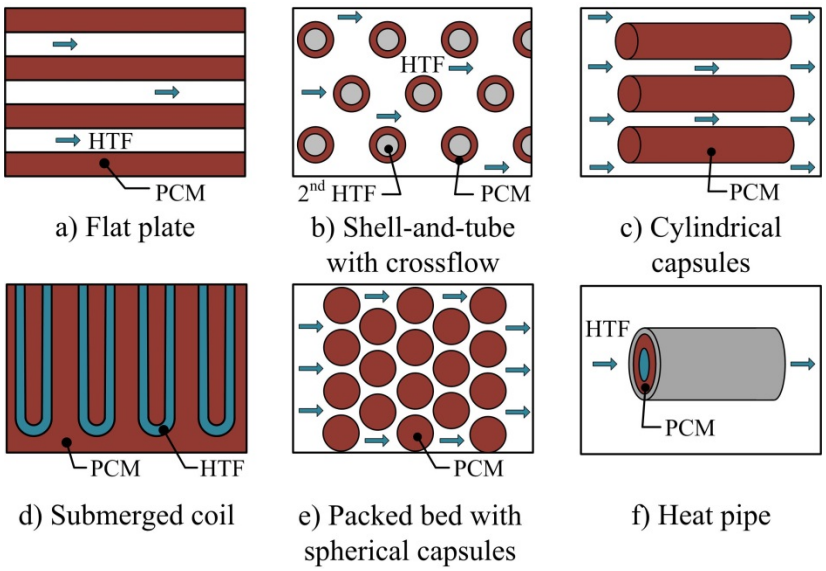

Figure 1-1: Schematic of different PCM storage tank geometries a) flat plate, b) shell-and-tube with crossflow, c) cylindrical capsules, d) coil submerged in PCM, e) packed bed of spherical capsules and f) heat pipe

The deployment of phase change material storage tanks in the building industry remains to this day quite limited. Canada and the province of Quebec are no exception. In fact, installations in the province, despite being functional, have not seen their performance been adequately documented. Recent court cases also seem to indicate that some installed systems did not meet expectations (Larocque, 2014; Siemens Canada ltée c. Groupe Enerstat inc., 2014; Systemex Energies inc. c. Groupe Enerstat inc., 2015); the most frequent complaint appears to be the system's incapacity to supply and maintain the planned power output.

However, the information given by manufacturers is often limited to the thermophysical properties of the pure substances included in the chosen PCM, and the selection of the storage unit is often based on nominal capacity values. These calculations do not reflect the transient behaviour of the storage tank once they have been included in complex heating and cooling systems. The incapacity of Heating, Ventilating and Air-Conditioning (HVAC) system designers to understand and predict the transient behaviour of PCM storage tanks increases the risk that the system will not deliver the expected performance, and they are thus reluctant to include this technology in their design.

To increase the use of PCM storage tanks in the building sector, models must be created to simulate the transient behaviour of such tanks in interaction with electromechanical systems so as to understand how they would impact them. These models must be accessible to HVAC system designers and compatible with energy simulation programs used in the industry.

The first objective of this study is the development of a model for the simulation of the behaviour of horizontal storage tanks with commercially-available PCM capsules of rectangular geometry. The model, based on the enthalpy method, is intended for use in whole building simulations so computational efficiency will be an important factor, as well as accuracy on the time scale of typical building system response.

The second objective of the study is to thoroughly validate the model. As pointed out by past researchers, assumptions which are reasonable for one type of PCM storage tank can often not be applied safely to other geometries (Dutil, Rousse, Ben Salah, Lassue & Zalewski, 2011). These modelling assumptions need to be investigated and verified for the specific geometry under study. Too many past studies have also relied on numerical results from the literature to validate new PCM storage models. Original experimental data is rare and often incomplete, so thorough experimental testing is required for an adequate experimental validation of the model.

CHAPTER 2 LITERATURE REVIEW

This literature review contains elements relating to each of the project objectives described previously. First, the development of an adequate model for the simulation of a phase change material storage tank can be separated into two steps: modelling the phase change process itself and simulating heat transfer mechanisms inside the tank. Section 2.1 of this literature review discusses the existing methods to model the phase change process while Section 2.2 presents existing models of PCM storage tanks of the studied geometry: horizontal tanks with PCM encapsulated in flat, rectangular capsules. Secondly, experimental validation of the model requires thorough testing of the tank on a test bench which can measure the correct experimental data and impose realistic operating conditions. In Section 2.3, a review is made of the existing experimental data on the use of PCM storage systems in order to identify data of importance as well as the areas where information is lacking. Finally, Section 2.4 presents specific applications of PCM storage units in buildings to identify the likely operating conditions and metrics of importance.

2.1 Modeling the phase change process

A material's change of phase from liquid to solid state can be described as the time-wise evolution of the liquid/solid interface through the volume studied. Determining the position of this interface at a specific time is therefore the goal of phase change problems. This position depends directly on the speed at which heat is absorbed by the material, hence on the material's thermal properties. However, those properties (thermal conductivity, specific heat capacity, density etc.) often change significantly between liquid and solid states. Modelling the change of phase therefore implies knowing the position in time and space of the liquid/solid interface so the appropriate properties can be applied on both sides. The complexity of the phase change problem is caused by the fact that this interface position is both the solution to the problem and a required input; such types of problems are named moving boundary problems and have been studied as early as 1831 by Clapeyron and Lamé in their investigation of the formation of the Earth's crust. It was Jožef Stefan's 1889 work on ice formation, however, which truly introduced a general class for these problems, hereafter known as Stefan problems.

According to Shyy et al. (1996), resolution methods for moving boundary problems are divided in two main categories :

1. Lagrangian methods and
2. Eulerian methods.

Lagrangian methods are also known as front-tracking methods. They imply following the phase change front throughout the studied domain by reconfiguring the spatial or temporal grid so the interface is always on a grid limit. This implies the interface between the solid and liquid phases is seen as a discontinuity in the material and its position is an intrinsic part of the problem solution.

Eulerian methods instead establish a fixed grid for the studied volume and reconstruct a phase change front from the properties determined at each point of the domain. These methods are less precise in their definition of the phase change front but when such a precision is not required they offer the advantage of greater computational efficiency and a simpler implementation for the modeller.

2.1.1 Enthalpy method

One of the more popular Eulerian methods is named the “enthalpy method” and was described by numerous authors (Crank, 1984; Lacroix, 1989; Shyy et al., 1996; V. R. Voller, Cross & Markatos, 1987; V.R. Voller & Prakash, 1987). It uses the same equation for both the liquid and solid phases of the material, deducting the phase change front position a posteriori through the temperature determined for each control volume in the grid. To do this, it requires a function linking the material specific enthalpy to its temperature for the whole temperature interval of interest.

For example, in the case of a conduction problem, the governing equation for the phenomena can be written as:

$$\rho \frac{\partial(\mathrm{H})}{\partial \mathrm{t}} = \nabla(\mathrm{k}\nabla \mathrm{T}) \tag{2-1}$$

The equation can be discretized according to the control volume method where the total enthalpy, H, and temperature, T, can be interpreted as average values over the control volume studied. The total enthalpy includes both sensible and latent components as indicated in Equation (2-2):

$$H = c_p \cdot T + l_f \cdot L \tag{2-2}$$

where c_p is the material specific heat capacity, l_f is the control volume liquid fraction and L the material's enthalpy of fusion. The governing equation can be modified to include this definition of enthalpy where the enthalpy of fusion is treated as a source term:

$$\rho c_p \frac{\partial(T)}{\partial t} = \nabla(k\nabla T) - L\frac{\rho\,\partial(l_f)}{\partial t} \tag{2-3}$$

To complete the model, a relation between the material's temperature and liquid fraction must be established. For a pure substance, specific enthalpy is a sharp but continuous function of material temperature (Tittelein et al., 2015) as illustrated on Figure 2-1a. Most real PCMs behave as binary mixtures (Tittelein et al., 2015), with phase change spread out over a temperature interval as illustrated in grey on Figure 2-1b.

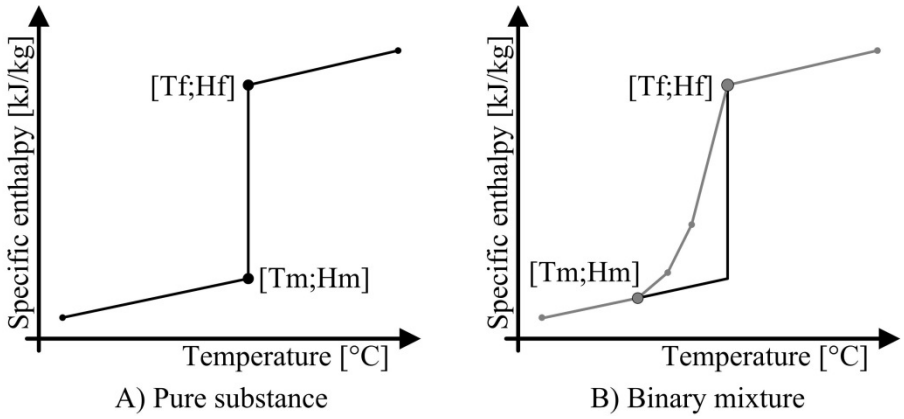

Figure 2-1: Evolution of a material's specific enthalpy as a function of material temperature for a) a pure substance and b) a binary mixture

In that case, temperature T_m indicates the moment the material begins to melt and temperature T_f indicates the end of the melting process. Between these two temperatures is a "mushy zone" where both phases coexist. The liquid fraction, l_f, can then be calculated for each control volume as a function of the temperature field following Equation (2-4):

$$l_f = \frac{T - T_m}{T_f - T_m} \tag{2-4}$$

An alternative exists where the liquid fraction and other properties are updated through the enthalpy value:

$$l_f = \frac{H - H_m}{H_f - H_m} \tag{2-5}$$

This alternative has the advantage of being less sensitive to minor errors on the control volume temperature than that using Equation (2-4). So it is then possible to model the change of phase of a pure substance (isothermal phase change) without losing accuracy.

2.1.2 Effective heat capacity method

Another popular Eulerian method involves reflecting the position of the phase change front in the specific heat capacity value of the material. In this method, when the phase change temperature is reached in a control volume, any energy supplied to the control volume serves to change the specific heat capacity until the additional energy required for phase change has been accounted for. Therefore, in the case of a unidimensional conduction problem, the governing equation can be written as:

$$\rho c_{p,App} \frac{\partial(T)}{\partial t} = k \frac{\partial^2 T}{\partial x^2} \tag{2-6}$$

where $c_{p,App}$ is the apparent specific heat capacity, k is the material thermal conductivity, ρ is the material density and T the material temperature.

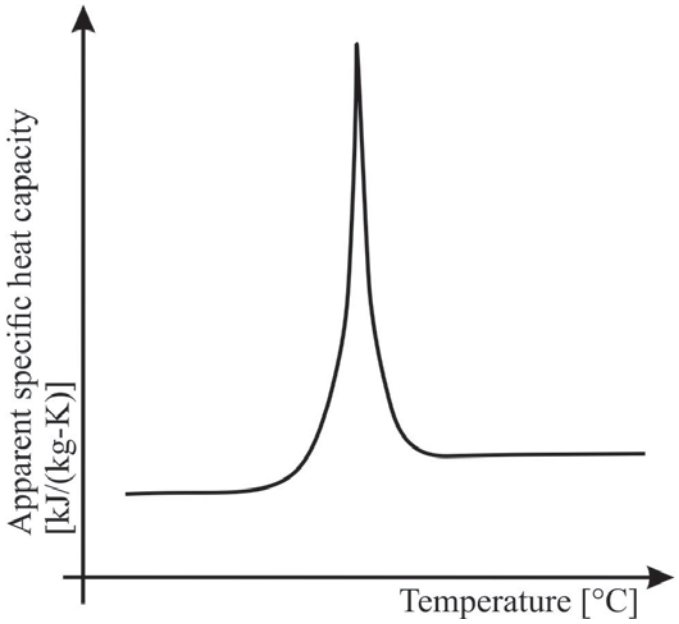

Figure 2-2: Evolution of a material's apparent specific heat capacity as a function of material temperature

The equation then uses variable properties according to the control volume temperature, an example is given in Equation (2-7) for the thermal conductivity:

$$k = \begin{cases} k_s & \text{if } T < T_m \\ k_s(1 - l_f) + k_l l_f & \text{if } T_f \leq T \leq T_m \\ k_l & \text{if } T_f < T \end{cases} \tag{2-7}$$

As is clear from Figure 2-2, the apparent heat capacity is a discontinuous function of the material temperature. Though the method was used by many authors, it often results in non-convergence due to the abrupt changes in the apparent specific heat capacity at the solid/liquid interface. This has been shown to be especially true when implicit time discretization is used (Al-Saadi & Zhai, 2015; Gong & Mujumdar, 1997). Numerous variants have been proposed to resolve these non-convergence issues, rendering the method more complex to implement (Bonacina, Comini, Fasano & Primicerio, 1973; Gong & Mujumdar, 1997; Yang & He, 2010). This method's computational speed is still inferior to most enthalpy methods (Al-Saadi & Zhai, 2015).

2.1.3 Issues with modelling the phase change process

Additional issues commonly arise in the modelling of the phase change process caused by the enthalpy-temperature curve (or apparent heat capacity curve) themselves, specifically the presence of hysteresis between the heating and cooling curves and the presence of supercooling[1]. These effects modify the expected behaviour of the phase change material, making its prediction and modelling more complex or at times even impossible without resorting to statistical probabilities.

Hysteresis is a phenomenon where the melting temperature of a material is different from its solidification temperature, not because the material changes phase over a temperature interval as presented in Figure 2-1b but because an offset exists between the enthalpy-temperature curves representing the cooling and heating processes for the same material. This phenomenon is illustrated on Figure 2-3b. At times, hysteresis is a property of the material or material sample under study but at times its presence is due to the measurement conditions, in which case it is often labelled “apparent hysteresis” (Mehling & Cabeza, 2008).

[1] The terminology employed in Chapter 4, is “subcooling” instead of “supercooling” but it refers to the same phenomenon. Subcooling is generally used by authors in building sciences who model PCM behaviour, and Chapter 4 used that terminology. Chemical engineers and material science authors use supercooling, which is a more rigorous term, and was used in our subsequent work in Chapters 5 and 6.

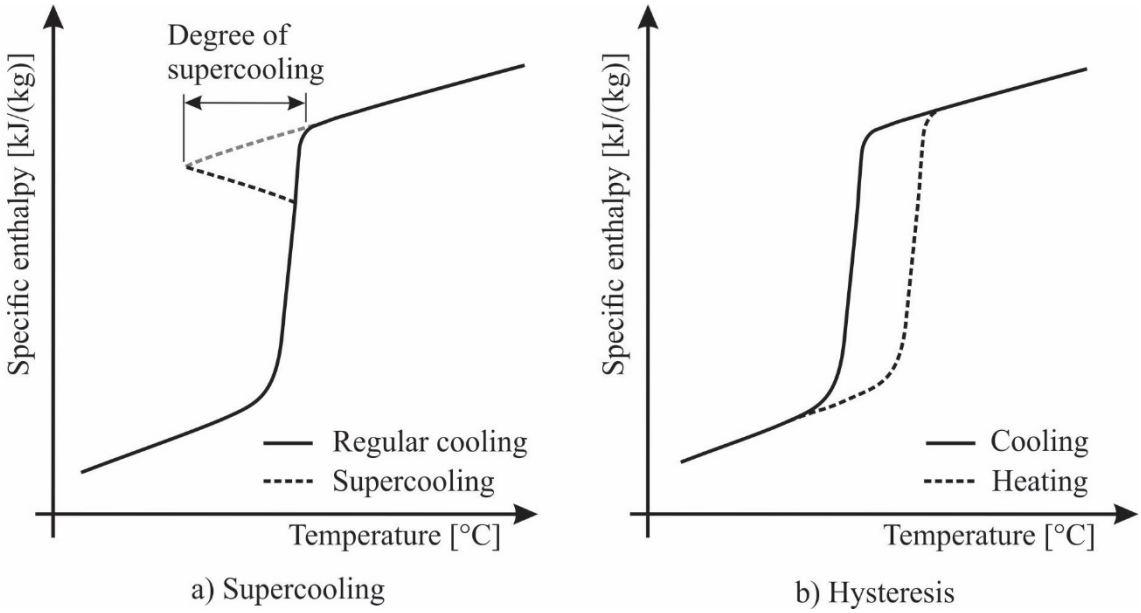

Figure 2-3: Evolution of a material's specific enthalpy as a function of material temperature in the presence of a) supercooling or b) hysteresis

Supercooling, sometimes referred to as "subcooling" in the literature, is a phenomenon where the material being cooled does not start to crystalize immediately upon reaching its solidification temperature. Instead, as illustrated on Figure 2-3a, the material will become a supercooled liquid (indicated in grey on Figure 2-3a) and reach a temperature well below the solidification temperature before the actual solidification process takes place. The difference between the solidification temperature and the real nucleation temperature is known as the degree of supercooling of the material. Supercooling happens in pure materials; water, for example, when pure can at times not solidify before temperatures below -15 °C are reached. This delays the release of the latent heat of fusion and can be a serious problem in thermal storage applications. It is especially frequent in salt hydrates, so manufacturers will often add nucleating agents to reduce its prevalence and importance (Mehling & Cabeza, 2008), though their presence is not always sufficient to prevent its occurrence.

Previous work by Günther, Mehling & Hiebler (2007) attempted to model supercooling numerically to ensure a more accurate prediction of the behaviour of salt hydrates. The paper stated that, as most PCMs do not have a fixed melting temperature but rather a melting range, a fixed degree of supercooling cannot be associated with most PCMs. Instead, a range of

temperatures at which nucleation of the supercooled liquid is likely to start exists and the likelihood of one temperature starting nucleation can be estimated through a statistical distribution within the nucleation range. Another important notion of their modelling technique is the speed of crystallization and its relation to the speed with which heat is transported in the same material. The authors explain that every molecule undergoing the change a phase from liquid to solid will release a fixed amount of latent energy which raises the temperature of the material in proximity. Depending on the relative speed of crystallization to that of heat transport in the material, solidification of one PCM molecule can either inhibit or stimulate the propagation of the phase change front, thereby causing or limiting the formation of a temperature plateau in the material. The numerical model of the supercooling effect performed quite well when compared to experimental data. The main issue with this model is the absence of required information for most PCMs. The additional information required by this modelling method (the crystallization speed and nucleation probability as a function of temperature) is unknown for most materials and requires thorough experimental testing for which no standardized method exist as of yet.

Solomon, Karthikeyan & Velraj (2013) performed a detailed study of the supercooling of a PCM installed in a vertical double pipe annular heat exchanger (i.e. heat pipe) with air serving the role of heat transfer fluid in the set-up's inner tube. The researchers studied the impact of varying the fluid flowrate on the presence and degree of supercooling measured. Results indicated increasing the fluid flowrate, and thus increasing the heat flux to the PCM, augmented the degree of supercooling measured. Similarly, supercooling was more prominent in the PCM which was positioned closest to the fluid entry than that further downstream as it experienced higher cooling rates. However, beyond a certain fluid velocity, any further increases had negligible effects on supercooling. They also found that the degree of supercooling measured at the different cooling rates in their experimental data correlated well with the apparent specific heat curve as a function of temperature obtained through digital scanning calorimetry (DSC) with similar cooling rates. This would indicate that characterisation of a material should be performed at the same heating/cooling rates as those expected in the targeted application for the resulting curves (enthalpy-temperature curve or apparent specific heat-temperature curve) to adequately represent the PCM's expected behaviour.

2.2 Modeling PCM encapsulated in flat, rectangular capsules

2.2.1 Gaseous heat transfer fluid

Phase change material encapsulated in flat rectangular containers has been modelled by different researchers when using air as heat transfer fluid. Dolado et al. (2006) developed various numerical models simulating the behaviour of flat slab-like PCM capsules exposed to air flow, each considering different modelling assumptions. Two of the models are finite-difference based and considered only conduction inside the PCM, neglecting any effect natural convection might have while the PCM is in liquid phase. One model considered one-dimensional conduction in the PCM in the direction normal to Heat Transfer Fluid (HTF) flow while the other considered conduction in the PCM both parallel and normal to the HTF flow. Comparing numerical results to the previous experimental data of Belén Zalba (2002) confirmed that the unidimensional model could reproduce experimental data with the required accuracy. Hence, modelling conduction inside the PCM in the direction of HTF flow did not bring any significant accuracy improvement to the numerical results.

Vakilaltojjar and Saman (2001) developed three numerical models to evaluate the impact of different modelling assumptions in simulating a thermal storage unit with PCMs, installed in an air-conditioning unit. As air was to be the considered heat transfer fluid, all models neglected the fluid heat capacity as well as that of the capsule wall. One model ignored the sensible heat at the initial stages of melting and freezing of the PCM (i.e. the initial temperature of the PCM was set equal to the melting temperature). Another model also assumed the wall temperature inside the PCM capsule was either equal to the melting point of the PCM or equal to the air temperature. Numerical results indicated that assuming a constant air speed profile at the tank inlet did not significantly impact outlet air temperature from the unit in comparison to a fully developed inlet air flow profile. The analysis showed that the air-side heat transfer resistance dominates the overall heat transfer resistance so both the capsule wall and PCM thermal resistances could safely be ignored in this case. This model however has some inherent limitations; among others, its limited capability to predict heat transfer rates.

Halawa et al (2005) developed a model for a roof integrated solar heating system using thermal storage inside PCM slabs. The model accounts for bi-dimensional conduction inside the PCM as

well as the variation of air temperature along the length of the PCM capsules. Arguing neither "constant heat flux" nor "constant temperature" were realistic boundary conditions at the capsule wall, they implemented different Nusselt number values for each control volume over the length of the PCM capsule. Each was calculated for constant temperature boundary conditions but was solely valid over the length of that control volume. Further work (Saman, Bruno & Halawa, 2005) compared this model's numerical results to two tests from Vakilaltojjar's experimental data (2000), one for flat PCM capsules and the other for conical capsules. In both cases, the model demonstrated an interesting fit but had difficulty replicating the tank outlet fluid temperature following rapid changes to the inlet fluid temperature. These differences lead to errors in the simulated heat transfer rate of over 0.5 kW or ~ 28% of the measured value for conical capsules.

Halawa, Saman & Bruno (2010) developed a one-dimensional finite-difference model where, again, the fluid's thermal capacity was neglected. The PCM's thermal resistance was also considered negligible with regards to the capsule wall's thermal resistance. As the thickness of the capsule is small, only one node inside the PCM was modelled. Comparing the outlet fluid temperature from numerical and experimental results demonstrated a satisfactory agreement. However, the model predicted slightly higher values than shown in the experimental results during the 15 minutes following a sudden change in inlet fluid temperature. The difference between these results reached a high of ~ 1.2 °C. The authors noted that the presence of supercooling, neglected in the model, could explain the sudden variations in the experimental data which are not reflected in the numerical data during the cooling process.

2.2.2 Liquid heat transfer fluid

Studies of encapsulated PCM of rectangular geometry are scarce for liquid Heat Transfer Fluid (HTF). Elsayed (2007) studied ice in horizontal capsules exposed to cyclic HTF temperatures using a tri-dimensional implicit model based on the enthalpy method. For simplicity, the author assumed the solid PCM would remain fixed at the centre of the capsule so the capsule symmetry could be exploited. Model results were summarily compared to numerical and experimental data from past research, which showed a good agreement. Though the model was implicit, a maximum time step of 3 secs could be used for results to be independent of mesh size (fluid velocity was not specified). A numerical study let the author conclude that the rate of heat

transfer was more influenced by the HTF temperature than by the heat transfer coefficient. Consequently, the paper postulated that the average fluid temperature could be used to determine the thermal response of a PCM storage unit with reasonable precision.

Liu, Bruno & Saman (2011) developed a unidimensional model to simulate the behaviour of horizontal PCM tanks for use in refrigerated trucks, based on Halawa's "phase change processor" (2010) previously described in Section 2.2.1. The model included the HTF specific heat capacity but did not consider any thermal resistance for the PCM material nor any heat transfer between adjacent PCM nodes in the direction of HTF flow. Results from two experimental tests of a complete melt/freeze cycle showed a close agreement between the outlet fluid temperature measured experimentally and its simulated counterpart. However, the model had some difficulties adequately representing experimental results at the beginning of the melting process following an initial change in inlet HTF temperature. A parametric study (M. Liu, Bruno & Saman, 2011) performed with the numerical model indicated that the inlet fluid temperature to the tank as well as fluid flowrate had a significant impact on the PCM melting time as well as rates of heat transfer.

Langlois (2011) developed a unidimensional model of a horizontal PCM storage tank based on isothermal phase change and implemented it in the TRNSYS building energy simulation program (Klein et al., 2011) as a TRNSYS type. The model considered that only one fluid control volume was associated with each PCM capsule and the capsule itself was only discretized into numerous control volumes over its thickness, not its length. The model is based on a variant of the method proposed by Zivkovic & Fujii (2001) where the same equation is used for both the liquid and solid phases of the PCM and only the equation coefficients are changed from one state to the other. This implies a constant verification of the phase change front is required to choose the correct boundary conditions and thermal properties for each control volume. No experimental validation of the model exists.

Bony & Citherlet (2007b) modified a pre-existing stratified hot water storage tank model from TRNSYS, named Type 60, to include the effects of PCM capsules of various geometries. The model presents various advantages compared to previous propositions: it uses a variable number of nodes over the PCM thickness, considers two-dimensional conduction in the PCM and accounts for both supercooling and hysteresis in the PCM as well as natural convection in the

PCM's liquid phase. Simulation results demonstrated a good fit between experimental and numerical results. Experimental tests only concerned with cylindrical capsules installed vertically in a vertical water storage tank. The model accuracy for horizontal storage with rectangular capsules was not demonstrated, and some model assumptions are not adapted to this configuration. For example, the heat transfer coefficient considered is that of a vertical plate submitted to convective heat transfer in both vertical and horizontal tank orientations. Inherent limitations of Type 60, such as the fact that natural convection is deemed the main heat transfer mechanism in the fluid, could also inhibit the adequate modelling of a horizontal tank. Finally, hysteresis and supercooling being negligible in the paraffin used in the experimental tests, the results did not allow the assessment of the model's treatment of these two phenomena.

Puschnig, Heinz & Steicher (2005) have also developed TRNSYS models capable of representing a water tank filled with PCM capsules of various geometries as well as micro-encapsulated PCM slurries. This model is based upon another existing TRNSYS model, named Type 240, and considers exclusively vertical tank where thermal stratification and natural convection are important components of the heat exchanges between the heat transfer fluid and PCM. Conduction inside the PCM capsules is considered bi-dimensional and convective heat exchange between the fluid and PCM includes both natural and forced convection.

Most other studies where a liquid is used as HTF have considered particular configurations where capsules are heated in an asymmetrical fashion, imposing constant flux or constant temperature boundary conditions over the length of the capsule, (Costa, Buddhi & Oliva, 1998; Hamdan & Elwerr, 1996; Lacroix, 2001; Silva, Gonçalves & Pires, 2002) instead of convective heat transfer from a fluid.

2.3 Experimental data on phase change material thermal storage tanks

Moreno et al. (2014) experimentally tested the use of a horizontal PCM storage tank to shift the daytime cooling load of a small space. The PCM tank was coupled to a water-to-water heat pump and air handling unit, linked to a shed-size building, which was used to represent the indoor space whose temperature must be maintained. The performance of a horizontal water storage tank of identical dimensions was compared to that of the tank stacked with PCM capsules, which are commercially-available, rectangular in shape and made of high density polyethylene. Test parameters were representative of a real-life application, with the heat pump's compressor

switching on and off, fluid flow being interrupted when minimum inlet HTF temperature was reached, etc. Charging time was deemed an important metric and was determined in function of either the outlet fluid temperature or PCM temperature. One of the PCM capsules having been outfitted with a temperature sensor, supercooling was found to be present even though it was not documented in the manufacturer data. Results indicate that for the same footprint, the PCM tank could on average supply 14.5% more cooling energy than the water tank, at the expense of a charging time which was 4.6 times longer.

Dolado et al. (2011) performed thorough experimental testing of a PCM-air heat exchanger which included metal-encapsulated PCM slabs positioned vertically. Detailed figures provide the evolution of the temperature through time, measured at the surface of the PCM capsules inside the unit as well as the fluid inlet and outlet temperatures for the different tests. The impact of varying the fluid flowrate and inlet fluid temperature on the thermal power produced by the unit was evaluated. The time required to fully charge/discharge the tank was also studied and at least one test underwent three repetitions to evaluate the repeatability of the process. One capsule was especially outfitted with three additional sensors placed inside the capsule to measure the PCM temperature itself. These sensors allowed an analysis of the PCM's behaviour inside the specific capsule geometry, indicating for example, longer phase change plateaus at sensors placed further downstream from the tank inlet.

Such detailed experimental tests exist for other PCM capsule geometries such as plastic pouches (Saied Mohammad Vakilaltojjar, 2000; Zukowski, 2007), plastic vertical slabs (Lázaro, Dolado, Marín & Zalba, 2009; B. Zalba, Marin, Cabeza & Mehling, 2004), as well as spherical (Bedecarrats, Castaing-Lasvignottes, Strub & Dumas, 2009; I. W. Eames & Adref, 2002; Nallusamy, Sampath & Velraj, 2007) and cylindrical capsules (J. Wei, Kawaguchi, Hirano & Takeuchi, 2005). However, thorough analysis of the behaviour of the commercially available capsules studied in this project has not been found in the literature.

2.4 Applications of PCMs in building systems

Possible applications of PCM in buildings are numerous and diversified. For example, Buick, O'Callaghan & Probert (1987) numerically studied the contribution of PCM thermal storage on the heat pumps of a central heating system. Authors demonstrated that installing PCM between the heat pumps and distribution system, heat pumps of a reduced capacity could be installed thus

reducing system installation costs. Riffat, Omer & Ma (2001) built a prototype to study the potential of PCM and tube heat exchangers for thermoelectric cooling. Their study demonstrated the use of PCM instead of the cold source (heat sink) improved the system's performance by maintaining a low temperature differential between the cold and hot junctions of the module.

There are however 4 subjects which return more frequently in the literature: the addition of thermal inertia in building materials, thermal storage associated with solar systems, hot water storage tanks in general and free cooling. These subjects stand out, among other things, by their relation to the thermal conductivity of PCMs. In the case of adding thermal inertia to the building envelope, the low thermal conductivity of the PCM is not problematic as charging and discharging occurs over a long period. Active applications such as free cooling, hot water storage tanks generally and specifically associated with solar energy however require quicker charge/discharge time and methods must be put in place to compensate the PCM's low thermal conductivity.

2.4.1 PCM in construction material

Many researchers have studied the inclusion of PCM in construction material such as gypsum, concrete and wallboards in order to increase the building's thermal mass (Athienitis, Liu, Hawes, Banu & Feldman, 1997; Behzadi & Farid, 2011; B. Delcroix, 2015; Farid et al., 2004; Khudhair & Farid, 2004; Nikoofard, Ugursal & Beausoleil-Morrison, 2015; Sharma, Tyagi, Chen & Buddhi, 2009; Tyagi & Buddhi, 2007; X. Wang et al., 2009; D. Wei, Liang, Xing & Yun, 2009; Belén Zalba et al., 2003; Zhou, Zhang, Wang, Lin & Xiao, 2007). These materials aim to reduce the daily variations of temperature inside the building consequently reducing peaks in heating and cooling. In northern climates, the additional thermal mass allows to store solar energy during the day and to discharge it at night to heat the room's ambient air. Similarly, in hotter climates, building thermal mass stores nocturnal coolness allowing the reduction of mechanical cooling during the day. Such an addition of thermal mass to a building is however a passive thermal storage method, since charging and discharging cannot be controlled.

Other storage methods termed « active» permit the control of the charge applied to the PCM as well as the moment the charging/discharging takes place, thus allowing a control over the moment the system's energy is released. One such option is the inclusion of PCM in ventilated façades (Alvaro de Gracia, Navarro, Castell & Cabeza, 2015; Fiorito, 2012; S. Liu & Li, 2015;

Rodriguez-Ubinas, Ruiz-Valero, Vega & Neila, 2012) where air flow is controlled by louvers. This is also the case of a storage tank connected to a building's heating or cooling loop where flow can either enter the tank or by-pass it, such as the configuration studied in this thesis.

2.4.2 Applications in solar energy systems

Studies on the use of PCM in solar thermal systems are frequent and aim mainly to compensate the temporal de-synchronization between the availability of solar energy and the occurrence of heating requirements (Al-Kayiem & Alhamdo, 2012; Bansal & Buddhi, 1992; Bony & Citherlet, 2007a; Esen, 2000). Certain researchers have studied solar panels with a thin layer of PCM added into them (Chen, Gu, Peng, Peng & Wu, 2010; P. C. Eames & Griffiths, 2006; Rabin, Bar-Niv, Korin & Mikic, 1995). Malvi, Dixon-Hardy & Crook (2011) have added PCM to combined photovoltaic and thermal solar panels. Their study showed that by cooling the photovoltaic panel, the PCM increase by 9% the daily energy produced by the system in comparison to ordinary photovoltaic panels.

Cabeza et al. (2006) have experimentally compared the behaviour of a stratified hot water storage tank including encapsulated PCMs to that of a simple storage tank when coupled to solar thermal panels. Their experimental results indicated the use of PCM produces hot water over a longer period without any supplemental heating and reduces the thermal storage tank size. Results from Ibáñez et al. (2006) demonstrate an increase in the solar fraction from 4% to 8% when PCM are added to a hot water storage tank connected to thermal solar panels. Following a similar experiment, Canbazoğlu et al. (2005) compared different encapsulated PCMs inserted in the hot water tank of a thermal solar system. Their results demonstrated a PCM storage tank could store up to 3 times more energy than an ordinary tank depending on the material used.

However, other researchers have found that the use of PCM to store energy produced by a solar thermal system was disadvantageous when compared to a typical sensible storage tank. For example, Bony & Citherlet (2007a) have noted an increase in supplemental heating when PCM is included in a solar system's hot water tank. Talmatsky & Kribus (2008) have numerically simulated a solar thermal system combined with a PCM tank and compared results for different combinations of PCMs and capsule positions inside the tank. They concluded that adding PCM inside hot water storage tanks did not increase the system efficiency. Rather, the annual energy transmitted to the final user is often inferior for PCM systems.

According to Kousksou et al. (2011), the mixed results of these authors demonstrate that PCM thermal storage can have both a positive and negative impact on solar thermal systems depending on the phase change temperature chosen and the comparison criteria used. The variability of these results also indicates the importance of an adequate simulation of the storage system's behaviour at the design stage.

2.4.3 Applications of PCM in hot water storage tanks

As seen in the previous section, the use of PCMs in the storage of solar energy often involves the use of PCM-enhanced hot water storage tanks. The study of such PCM-enhanced tanks is also important for their use in the supply of domestic hot water, whether or not they are connected to thermal solar systems. Domestic hot water is usually provided using electric or gas heaters which have a low efficiency in terms of primary energy due to the fact that they often imply the conversion of fossil fuels to electricity and electricity to thermal energy (Nkwetta & Haghighat, 2014). Domestic hot water storage tanks are also a great opportunity for peak shifting building electric demand to off-peak periods provided that modifications are made to ensure power draw does not occur concurrently with water withdrawal (Lacroix, 1999). Moreover, as the water temperature inside these tanks must be maintained at or above 60 °C to prevent the proliferation of dangerous bacteria such as Legionella (ASHRAE, 2000), the possibility to supply water at a constant temperature with latent systems is of particular interest.

Al-Hinti et al. (2010) discussed the effect of water withdrawal patterns on the performance of both a PCM-enhanced and ordinary domestic hot water storage tanks. Following a withdrawal pattern typical of residential day-time consumption of domestic hot water for a small family, average water temperature in the ordinary tank dropped by 20 °C (71 °C to 51 °C) while the average temperature dropped by only 12 °C (72 °C to 60 °C) in the PCM-enhanced tank. They concluded that in cases of extreme consumption, such as during evening hours, the presence of PCMs resulted in extended operational time of the system without the need for supplementary heating of the water.

Several other studies have also demonstrated that the inclusion of PCMs in hot water storage tanks can increase their storage density and delay the activation of supplementary heating following water withdrawal for a significant amount of time, at times displacing it completely to

off-peak power demand periods (A. de Gracia, Oró, Farid & Cabeza, 2011; Mehling, Cabeza, Hippeli & Hiebler, 2003). This potential can further be enhanced through the use of optimised control strategies (Nkwetta et al., 2014) and the adequate choice of phase change temperature and capsule geometry (Barba & Spiga, 2003). The implicit requirement behind both the evaluation of control strategies and design choices is the availability of adequate modelling tools.

2.4.4 Free cooling applications

Free cooling is another classic application of active PCM storage. Zalba et al. (2004) have experimentally tested the use of a PCM storage tank to store cold from the night-time air and restore it as cooling capacity during the day. The unit was experimentally submitted to step changes in its inlet fluid temperature, using combinations of different inlet temperatures and air flowrates. The study indicated that the use of such a tank in an industrial building is economical in comparison to a conventional air-cooling system as it uses approximately 9 times less electricity.

Arkar & Medved (2007) have numerically compared different modes of free cooling for a residence with low energy consumption including a system with PCM integrated in the ventilation system. Besides cooling the residence at night, cool outside air is also stored in the PCM and released in the residence by day. Though the air flowrate into the PCM unit remained constant during the simulation, the inlet temperature changed following the daily variations in outdoor air temperature surrounding the residence, located in Ljubljana, Slovenia. The study concludes this method is more efficient in the reduction of indoor air temperature than continuous free cooling as well as night-time free cooling where only one opening exists per room (single-sided natural ventilation). Even though the method leads to slightly higher indoor temperatures when compared to cross night-time ventilation (where openings on opposite walls allow the incoming air to sweep across the entire room), it increases air quality in the residence by continuing ventilation of outdoor air during the hot hours of the day. Moreover, air flow required for cross night-time ventilation to be efficient depends on wind and is not guaranteed every night of the hot season.

Turnpenny el al. (2000, 2001) conceived and constructed a cooling system containing heat pipes inserted into PCM and used it conjointly with a ceiling-suspended air heater. Their experimental trials were performed with different air flowrates and step changes in inlet temperature to the

unit. Results indicate this system compares advantageously to chilled ceilings through its inferior mass and the fact no cold water has to be produced. When compared to conventional air-conditioning systems, the study's results indicate the PCM system is more economical and more energy efficient.

Raj & Velraj (2010) performed a detailed review of publications of PCMs used in free cooling. They concluded that in spite of the potential of PCM in free cooling demonstrated by some authors, the low thermal conductivity of both air and most PCMs as well as long PCM charging time remain significant obstacles. As free cooling potential varies greatly as a function of site location and climate, a detailed analysis is required before selecting the correct phase change temperature and heat transfer rate for each application. Knowing PCM thermal properties vary as a function of temperature, the design of any PCM storage system should be based on the analysis of the PCM's transient behaviour.

2.4.5 Follow-up of real applications in buildings

Authors cited previously discuss numerical or experimental results obtained from the study of PCMs. To select the appropriate operating conditions under which to experimentally test a PCM storage tank however, it is the real operating conditions found in actual building HVAC systems which are of interest, not simulation results or experimental tests. To draw a complete portrait of the state of the art on the domain of PCMs in buildings, concrete cases of real PCM storage tanks monitored during their installation in buildings must also be discussed.

2.4.5.1 Ice as phase change material

Most sites where thermal storage with phase change materials has been implemented and its performance monitored used water as PCM. As for other such materials, different configurations exist among which ice-on-coil systems, encapsulated ice and ice slurry based systems are the most common.

Sohn & Nixon (2001) have studied the operation of fire station 506 of the United States Army on the Yuma Proving Ground, in Arizona, where an ice tank has been in service since 1988. This tank consists of a coil submerged in water and is used to produce ice at night to even out peak air-conditioning loads occurring during the day. The general operating conditions required the tank to be fully charged daily, over a 20 hour period by a 281 kW (80-ton) chiller producing ice in the

tank. The tank then supplied cooling to the building while one 774 kW (220-ton) chiller was turned off for four hours each day, from noon to 4 pm, in order to reduce peak electric demand. The tank was thus used to offset a nearly constant power load over this specific period of time. The system reduces the electricity bill by 22 450$ per year resulting in the initial capital investment being paid back in 6.5 years. It must be noted that the system only required minimal maintenance over the 12 years of service investigated in the study.

Wang & Kusumoto (2001) have studied the use of an ice slurry system at the Ritz Carlton Plaza in Osaka, Japan. The building contained 16 ice slurry tanks, spread out amongst the different floors, to reduce peak cooling loads in summer and winter. The design used heat pumps to provide space heating, while their evaporators generated ice in a storage tank, which was in turn used for space cooling. The ice storage discharged during the daytime, cooling recirculated air from the conditioned space. Therefore, operating conditions included constant inlet air temperature and flowrate variations depended on whether the unit functioned at a constant (on/off conditions) or variable flowrate. Their study showed approximately 80% of the electricity required to cool the building was used at night. As lower electrical tariffs applied at night, this method allowed important cost reductions.

Past performance make strong arguments for the use of ice as latent energy storage systems. It must however be noted its use is limited to building cooling (the direct heating of water or air being impossible considering the ice's phase change temperature) and requires the use of refrigerating equipment which can cool a fluid below 0 °C, imposing additional constraints on traditional systems. Therefore, commercial PCMs are required to widen the spectrum of fusion temperatures available and the number of possible applications.

2.4.5.2 Commercially available phase change material

For commercial PCMs, little data is available in the literature on real building-tested applications. Liu et al. (1994) compared the real performance of PCM storage systems (ice and eutectic salts) to the simulated performance of conventional systems. Their results indicated PCM storage systems performed better than expected and induced lower energy costs than traditional chillers used in the same applications.

Paré & Bilodeau (2007) presented a project to replace the chillers at IBM's plant in Bromont, Canada, during which a PCM storage system was also installed. One PCM tank was designed to regulate water temperature to the emergency showers where the flow rate can suddenly vary from 0.1 to 2.5 L/s. Another PCM is installed upstream of the chiller and used continuously to regulate the load to the unit, therefore undergoing several charging/discharging cycles each day. The last PCM tank is installed downstream from the chiller with the purpose to reduce peak power by complementing the chillers' capacity during period of peak cooling demand. A by-pass to the PCM tank is installed so it can either be in a charging, discharging or waiting mode (i.e. when it is completely by-passed). The article presented brief monitoring data which indicated increased efficiency of the cooling system and a reduction of the daily energy consumption.

Other data available on PCM storage tanks installed in buildings originate directly from PCM manufacturers and have not been confirmed independently (Cristopia Energy Systems, 2011; PCM Products Ltd, 2009). These documents contain little information and do not allow an objective analysis of the reported data. Recent court cases in Québec seem to indicate that some installed systems did not meet expectations (Larocque, 2014; Siemens Canada ltée c. Groupe Enerstat inc., 2014; Systemex Energies inc. c. Groupe Enerstat inc., 2015), although – perhaps unsurprisingly – no performance data have been published. The results from current installations require a thorough investigation to ensure we can learn from past mistakes and adequately assess the technology's potential for future applications.

2.5 Conclusion

The literature review presented illustrates the issues and obstacles to the deployment of PCM technology in buildings. The existing models often neglect important phenomena such as hysteresis and supercooling. Models rarely represent the waiting period between successive charging/discharging periods and neglect the thermal equilibrium occurring in the PCM in those instances. The rarity of experimentally validated models is also notable as well as the scarce performance data on real installation of PCM tanks in buildings. When experimental data is available, the repeatability of test results is rarely discussed even though phenomena such as supercooling have been shown to lead to poor repeatability. The development and validation of a model compatible with a complete building energy simulation would be a significant contribution to the deployment of the technology.

CHAPTER 3 OBJECTIVES AND THESIS ORGANISATION

The research project's main subject is the modelling of phase change material storage tanks for use in building heating, ventilating and air-conditioning (HVAC) systems. A model, based upon the enthalpy method, is proposed to simulate the behaviour of horizontal tanks filled with horizontal, rectangular capsules. The heat transfer fluid is a liquid flowing between the capsules.

3.1 Thesis objectives

This thesis has two main objectives, which can each be separated in secondary objectives:

- Develop a numerical model for the simulation of the behaviour of horizontal storage tanks with commercially-available phase change material capsules of rectangular geometry.
    - Develop a preliminary model, based on the enthalpy method, for use in whole building simulations;
    - Evaluate the impact of conduction in the phase change material in the direction of fluid flow;
    - Evaluate the impact of the fluid flow profile;
    - Evaluate the impact of the capsule geometry; and
    - Verify the developed model against numerical data.
- To validate experimentally the performance of the proposed model:
    - Design and construct a test bench for the study of hydronic equipment;
    - Characterize the enthalpy-temperature relation for the phase change material tested;
    - Determine experimentally the behaviour and performance of a horizontal storage tanks with commercially-available phase change material capsules of rectangular geometry; and
    - Compare the behaviour measured experimentally to the simulated response of the tank using the model developed.

3.2 Thesis organisation

The present thesis includes eight chapters and follows the format of an article-based thesis. Chapter 1 presents an introduction to the subject of phase change materials and the reasons for their applications in building systems. A critical review of literature, presented in Chapter 2, covers modelling methods for phase change processes, existing phase change material storage tanks models, possible applications in building energy systems and current experimental data on real phase change material storage tanks. Chapter 3 describes the objectives of the thesis as well as its organisation.

Chapter 4 presents the first article entitled “Assessment of T-History Method Variants to Obtain Enthalpy-Temperature Curves for PCMs With Significant Subcooling” and published in the Journal of Thermal Science and Engineering Applications. The article details the classic experimental method used to characterize heterogeneous phase change materials, named the T-History Method, and describes the various variants on the data analysis methodology proposed by previous researchers. The article uses these different variants to analyse results from experimental tests of a phase change material and discusses each variant’s advantages and disadvantages. A proposition is made as to which variant should be adopted to characterize phase change materials with significant supercooling so as to provide all the necessary information to modellers looking to simulate their behaviour.

Chapter 5 presents the second article entitled “Experimental assessment of a phase change material storage tank” submitted to the Journal of Applied Thermal Engineering. The paper is currently in the reviewing process, revisions were required and the version presented in the thesis includes the changes that were made at the reviewer’s request. The article succinctly describes the Semi-Virtual Laboratory which was designed and constructed to test hydronic HVAC equipment and the adaptations made to it so that it could test phase change material storage tanks. One PCM capsule was instrumented with thermocouples so the PCM behaviour could be measured in addition to that of the PCM tank as a whole. Several melting and solidification cycles were completed using different inlet fluid temperatures, flowrates and load profiles. At least three repetitions were made in each test condition so repeatability could be assessed. A thorough analysis of test results is provided.

Chapter 6 presents the third article entitled “Modeling Horizontal Storage Tanks With Encapsulated Phase Change Materials for Building Performance Simulation” and submitted to the Journal of Building Performance Simulation. The numerical model developed to simulate the behaviour of horizontal storage tanks containing flat, rectangular PCM capsules is presented. A numerical analysis of modelling assumptions is made and the corrections made to the model following these results are documented. Model results are compared to the experimental data from the previous article to validate the model’s accuracy.

Chapter 7 presents a general discussion of the results and Chapter 8 presents the project conclusions and recommendations for future work.

Two appendices present additional information. Appendix A provides the thermal and physical properties of the tested PCM and describes the methodology used to obtain them. Appendix B presents the procedure used to calibrate the temperature sensors and its results. Additionally a conference paper by MacDonald et al. (2014) describes the Semi-Virtual Laboratory used to obtain the experimental results presented in Chapter 5 and Chapter 6 for model validation.

CHAPTER 4 ARTICLE 1: ASSESSMENT OF T-HISTORY METHOD VARIANTS TO OBTAIN ENTHALPY-TEMPERATURE CURVES FOR PHASE CHANGE MATERIALS WITH SIGNIFICANT SUBCOOLING

D'Avignon, K., Kummert, M., (2015). Assessment of T-History Method Variants to Obtain Enthalpy-Temperature Curves for Phase Change Materials With Significant Subcooling. Journal of Thermal Science and Engineering Applications, 7(4), 041015-041015-9. doi: 10.1115/1.4031220

Note: The article version transcribed here is the one published with a few minor corrections recommended by the jury.

4.1 Abstract

To assess the potential of thermal energy storage systems using phase change materials (PCMs), numerical simulations rely on an enthalpy-temperature curve (or equivalent specific heat curve) to model the PCM's thermal storage behavior. The so-called "T-history method" can be used to obtain an enthalpy-temperature curve (h vs T) through conventional laboratory equipment and a simple experimental procedure. Different data processing variants of the T-history method have been proposed yet no systematic comparison between these versions exists in the literature nor is there a consensus as to which should be used to obtain reliable enthalpy-temperature curves.

In this paper, an inorganic salt hydrate is tested in both heating and cooling. Four different data processing variants of the T-history method are used to characterize the PCM and produce enthalpy-temperature curves for this original experimental data set. Differences in the results produced by the different methods are discussed, the issues encountered are indicated and possible approaches to overcome these problems are provided.

Zhang et al.'s original data processing method does not provide sufficient information to produce complete enthalpy-temperature curves. The method provided by Marín et al. (2003) is promising but lacks detailed instructions on how to treat subcooling behaviour of the PCM. An interpretation is provided using an absolute temperature interval, which illustrates this behaviour and can reproduce an enthalpy-temperature curve from simulated data. The method proposed by Sandnes and Rekstad (2006) uses a correlation to determine the heat transfer to apply to the PCM

sample which leads to sporadic errors of significant magnitude. Results from the method put forth by Kravvaritis et al. (2010) closely resemble those of Marin et al.'s method using the absolute temperature interval detailed in this paper but relies on inaccurate thermodynamic assumptions and show increased sensibility to test conditions.

The use of the version introduced by Marín et al. is recommended when using the T-history method to determine enthalpy-temperature curves. For PCMs that exhibit subcooling, the alternative interpretation using an absolute temperature interval should be used so that the subcooling phase is taken into account in the enthalpy-temperature curve.

4.2 Introduction

Active thermal energy storage using phase change materials (PCMs) is frequently proposed as a method to shift building peak heating and cooling loads (Khudhair & Farid, 2004) and increase the availability of solar thermal energy (Kenisarin & Mahkamov, 2007). Recent efforts have focused on delivering simplified models of phase change material storage tanks both accessible to designers and compatible with available building energy performance simulation tools (Bony & Citherlet, 2007b; D'Avignon & Kummert, 2012; Tabares-Velasco, Christensen & Bianchi, 2012). Those models rely upon either an enthalpy-temperature curve or an apparent specific heat curve to calculate the thermal behaviour of the storage tank. These curves are difficult to derive from manufacturer data and additional experiments are often required.

Various methods have been proposed to obtain and process experimental data to produce these enthalpy-temperature curves, but no clear consensus has emerged regarding which methods to use. PCM Gütegemeinschaft eV has attempted to rectify this shortfall by defining quality criteria (RAL Gütezeichen, 2013) for the results and by limiting the approved characterization methods. One such method is differential scanning calorimetry (DSC), which has been studied extensively for PCM characterization. Authors have compared the accuracy of the isothermal step mode to that of the dynamic mode (Castellón, Günther, Mehling, Hiebler & Cabeza, 2008; Günther, Hiebler, Mehling & Redlich, 2009), measurements and calibration procedures have been put forth specifically for PCM characterization using DSC (Lázaro et al., 2013), and DSC uncertainty is well documented (Richardson, 1997; Rudtsch, 2002).

The T-history is another method often used in practice and authorized by RAL Gütezeichen (2013) but fewer authors have performed a critical assessment of its data processing methodology. Lázaro et al. (2006) verified an installation for T-history testing of PCMs, comparing the resulting enthalpy-temperature curves to DSC results. The experimental procedure and set-up used provided consistent results over multiple tests but no details are given as to the data processing variant of the T-history method which was used. Solé et al. (2013) summarized the alternative experimental setups, data processing methods and result presentation formats which have been proposed since the original T-history method was introduced (Zhang, Jiang & Jiang, 1999) and concluded on the importance that a consensus be reached. Yet, the authors offered no critical analysis of the different data processing methods nor did they recommend which should be used and which should be discarded.

None of the references found provides enough details to apply the proposed method unambiguously to a new experimental data set. For example, the treatment of subcooling is not described in Jose M. Marín et al. (2003) and the accuracy of the regression used is not quantified in Sandnes & Rekstad (2006). The papers also omit to describe the treatment of experimental variability, often altogether neglecting to display such variability. Though at times multiple samples of the same PCM were tested (Hong, Kim & Kim, 2004; Kravvaritis, Antonopoulos & Tzivanidis, 2011; Lázaro et al., 2006; Peck, Kim, Kang & Hong, 2006; Solé et al., 2013), none of these references presents the raw experimental T-history data for more than one sample and only partial results are given without explaining how the selected samples were chosen (Kravvaritis et al., 2011; Zhang et al., 1999).

Variations, imprecisions and uncertainties in the enthalpy-temperature curves cannot be ignored when assessing the potential of PCMs for various applications. Arkar and Medved (2005) determined that the PCM's apparent specific heat curve significantly affects the simulated thermal response of PCM storage tanks. Günther et al. (2009) stated a 1 K change in the estimated melting temperature of the PCM can lead to an error of 11% in the calculation of the heat transfer rate from the material. Yet, variations of the T-history method have not been critically analysed and compared after their initial publication. No study has assessed which of these methods, if any, is sufficiently reliable to provide adequate enthalpy-temperature curves for different types of PCMs.

This paper presents the results obtained by applying four data processing variants of the T-history method to original experimental data from a commercially available PCM of unknown composition. Experimental data from all samples tested are presented, illustrating the variability amongst samples, particularly relating to subcooling. Different data analysis methods are applied to the experimental data and the difficulties encountered in applying the methodologies based on their description in the literature are presented. The enthalpy-temperature curves obtained for each sample by applying the methods are analyzed and critically compared. Recommendations are made to select an appropriate data processing method for the production of enthalpy-temperature curves for a PCM exhibiting subcooling.

4.3 Literature review: PCM characterization methods

Though Differential Scanning Calorimetry (DSC) is commonly used to determine the apparent heat capacity of materials, issues have been identified when used with PCMs. Large heating rates can exacerbate hysteresis between heating and cooling curves, whereas lower heating rates can increase errors in calculated enthalpy change due to decreased signal-to-noise ratios (Günther et al., 2009). The small sample size increases the probability of subcooling and amplifies it, which deforms the cooling curve (Günther et al., 2009; Xie et al., 2013). These deficiencies led to the development of other techniques to characterize larger PCM samples using standard laboratory equipment.

One such technique is the T-history method developed by Zhang et al. (1999), which compares the evolution of the temperature through time (or "T-history") of a PCM sample to that of a reference sample as both are cooled in a controlled environment. The T-history curves resulting from this experimental test (thoroughly described in Section 4.4) are separated into three distinct temperature intervals representing the liquid state, phase change and the solid state, and are analyzed separately. Results provide the liquid and solid phase specific heat, latent heat of fusion and melting temperature of the PCM studied. These 4 parameters represent key aspects of the PCM enthalpy evolution with temperature, but are insufficient to define a complete enthalpy-temperature curve.

Marín et al. (2003) proposed to analyze the T-history curves over very small intervals of temperature, without any changes to the method applied whether the interval falls within the

solid, liquid or phase change period. This formulation produces a complete enthalpy-temperature curve over the whole temperature range tested and, as proven by Lazaro et al. (2006), the method can be directly applied to both cooling and heating processes, allowing the assessment of the presence of hysteresis, or lack thereof.

Hong et al. (2004) proposed two modifications to the original method in order to improve its accuracy: to consider variations of sensible heat occurring during phase change and to use the first derivative of the T-history curve to determine the transition from the end of the phase change to the solid phase. Peck et al. (2006) later used this method for heating processes, indicating it could determine whether the solidification temperature is different from the melting temperature. Though it contains more information than the original T-history method, this version again provides an incomplete enthalpy-temperature curve and is therefore not studied in this paper.

Sandnes and Rekstad (2006) proposed to test the reference and PCM samples in separate trials and to express heat transfer as a function of the temperature difference between the surroundings and the sample. The enthalpy change in the PCM is then determined as a function of its temperature, resulting in an enthalpy-temperature curve which can include subcooling.

Kravvaritis et al. (2010) chose to compare the time delay between the PCM and reference sample over a specified time interval. The so-called “thermal delay method” introduces the concept of an effective specific heat which varies following the PCM temperature and provides all the required information to recreate an enthalpy-temperature curve for the PCM tested.

The methods proposed by Zhang et al. (1999), Marín et al. (2003), Sandnes and Rekstad (2006) and Kravvaritis et al. (2010), hereafter respectively referred to as methods Z, M, SR and K, have been applied to our experimental data and are described in more detail in upcoming Section 4.5.

4.4 Experimental test

4.4.1 Setup

The original "T-history" method presented in (Zhang et al., 1999) was based upon a simple experimental set-up. Though methods that subsequently evolved from it made some modifications to the set-up (Solé et al., 2013), the underlying principle remains unchanged. At least one test tube is filled with the PCM and one test tube is filled with a reference material of

known thermophysical properties (e.g. water or mercury). Both samples are equipped with a temperature sensor linked to a data acquisition system and placed inside a controlled environment (water bath or insulated air chamber) whose temperature is also recorded.

In all variations, the methodology assumes the temperature distribution inside the samples can be regarded as uniform. The sample size must ensure that the lumped capacitance method can be used to evaluate the sample behavior (i.e. the Biot number should be less than 0.1), so test tubes of a small diameter are typically used as containers. Glass test tubes are preferred as they guarantee that the container will not chemically interact with the sample and that tube thermophysical properties are known and homogeneous. The reference material must also be chosen so that it does not change phase in the test temperature interval.

4.4.2 Procedure

Before the experimental test begins, an initialization period takes place where samples are heated to the test start temperature, above the PCM's melting temperature (see Figure 4-1). Once all samples have stabilized at the test start temperature and are completely liquid, a cooling test begins where samples are rapidly exposed to an environment at a temperature, below the PCM's melting temperature. From the common starting temperature the evolution of the PCM sample temperature through time (i.e. T-history curve) is measured continuously as well as that of the reference material sample (see Figure 4-1). The cooling test is completed after all samples have stabilized at the controlled environment temperature and the PCM sample is completely solid. The samples are then exposed to an environment at the original temperature, until all samples have stabilized at that temperature and the PCM sample is completely liquid, completing the heating test. A complete cycle, including both cooling and heating tests, is required if one wishes to fully characterize the PCM and verify whether hysteresis occurs. This experimental procedure is common to all variations of the T-history method except for the fact that Sandnes & Rekstad (2006) do not test both the reference and PCM samples at the same time but in subsequent experiments. The T-history curves resulting from the above mentioned experimental procedure are illustrated in detail on Figure 4-1. The hot/cold/hot cycle is often repeated several times to obtain separate data sets for the same samples.

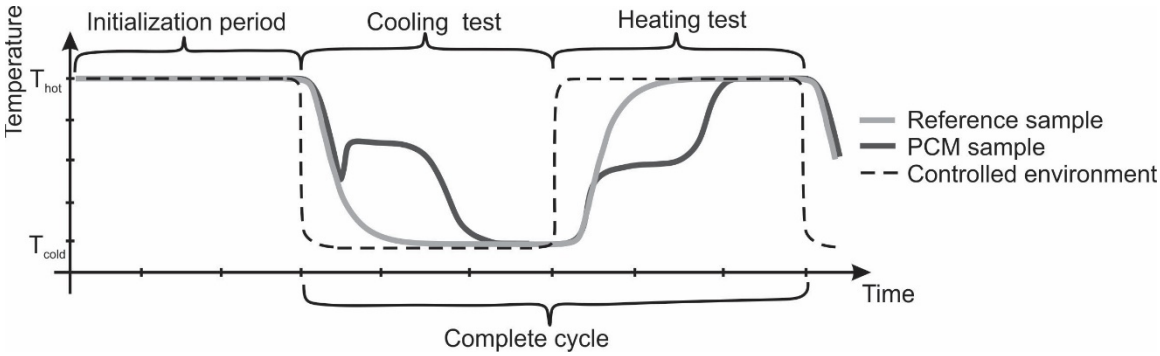

Figure 4-1: Temperature evolution during a full cycle of the T-history experimental procedure

4.4.3 Experiment

This paper analyzes a commercially available PCM (S27) whose properties, as supplied by the manufacturer (PCM Products Ltd, 2015), are detailed in Table 4.1. Twelve samples are taken from a capsule of the PCM and distilled water is used as a reference material. Each sample is weighed and placed in a glass test tube of 16 mm in diameter and 125 mm in length (Biot number < 0.1). Type-T thermocouples, previously calibrated using a water bath and a Class A Pt-100 sensor, are placed along each sample tube's central axis. Data acquisition is done at a sampling rate of 1 Hz by using the isothermal thermocouple input module NI 9214, equipped with several cold-junction compensation sensors (National Instruments Corporation). Samples are held in place by their caps in a vertical position, with additional sensors measuring the ambient air temperature in the center and on the exterior of the sample layout.

Table 4.1: PCM properties specified by manufacturer[2]

Phase change temperature	27 °C
Density	1530 kg/m^3
Latent heat of fusion	183 kJ/kg
Volumetric heat capacity	280 MJ/m^3
Specific heat capacity	2.20 kJ/kg-K
Thermal conductivity	0.540 W/m-K

[2] The properties listed have been copied exactly as found in manufacturer data.

As recommended in the RAL testing regulations (RAL Gütezeichen, 2013), three successive heating and cooling tests were performed, by switching between two environmental chambers. All PCM samples were tested at the same time, exposed to the same ambient conditions and generally showed a similar temperature evolution (see Figure 4-2). The PCM studied displayed significant subcooling during cooling tests and some samples were lost due to breakage. This paper presents the results obtained by analyzing the third cooling and heating test of the 6 PCM samples that withstood all three heating/cooling cycles.

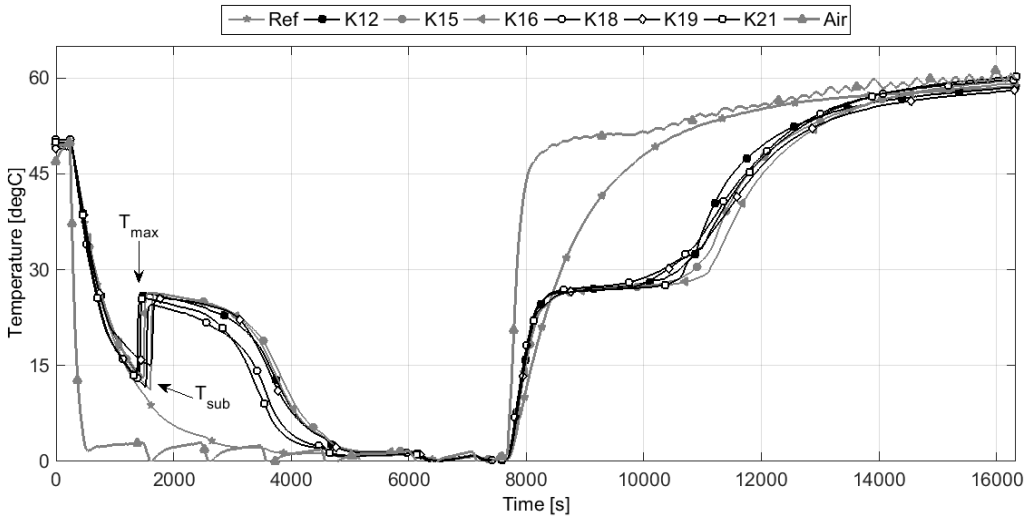

Figure 4-2: T-history data from six of the PCM samples tested for the third cooling and heating cycle

For t=[3350;3500s] on Figure 4-2, the oscillating chilled room air temperature caused by compressor on/off cycling leads to measurements of ambient air temperature being higher than the reference sample temperature. This is relatively common and can be seen in other published results (Lázaro et al., 2006; Sandnes & Rekstad, 2006). Improved control of the environmental chamber temperature delays and attenuates this effect without eliminating it completely. Placement of the samples and ambient air temperature sensor in insulating polystyrene as in (Sandnes & Rekstad, 2006) can attenuate this effect, slowing down variations in temperature.

As the PCM tested is heterogeneous and contains small grains to enhance nucleation, care was taken to use representative samples by rendering the PCM completely liquid, thoroughly mixing it and collecting an equal volume for each sample. Yet, differences exist in the experimental

results. For example, the minimum temperature reached during subcooling by PCM samples, T_{sub}, varies from 11.2 °C to 15.0 °C and is much higher for K19, than for all other samples. The maximum temperature reached during phase change, T_{max}, varies amongst samples from 24.5 °C to 26.4 °C. These differences can be partially attributed to variations in sample composition due to PCM heterogeneity, as confirmed by variations in the weight of the samples for the same sample volume. The maximum difference amongst studied samples is 2.1 g, a 10% variation. The presence of nucleation agents is known to have an impact on the degree of subcooling (Günther et al., 2009; Lázaro et al., 2006; Xie et al., 2013), which may have affected the evolution of PCM temperature through time measured during the test. All data analysis methods referenced in this article correct for variations in mass and so all results are analyzed.

4.5 Results

4.5.1 T-history method – Z

The original T-history method developed by Zhang et al. (1999) will be referred to as Z in this paper. It determines the melting point, heat of fusion, specific heat and thermal conductivity of phase change materials (PCMs) from experimental temperature curves obtained during cooling tests. The method uses measured data to solve the PCM thermal balance, represented by Equation (4-1) when the PCM is in liquid or solid state and Equation (4-2) during phase change, and thus determine PCM properties.

$$\left(m_{pcm} \cdot c_{p,pcm} + m_t \cdot c_{p,t}\right) \cdot \Delta T_{pcm} = h_g \cdot A_g \cdot \int \left(T_{pcm} - T_a\right) dt \tag{4-1}$$

$$m_{pcm} \cdot H_x \cdot \Delta T_{pcm} = h_g \cdot A_g \cdot \int \left(T_{pcm} - T_a\right) dt \tag{4-2}$$

The integral in these equations is determined from the area under the T-history curve so the only unknown terms are the PCM properties to be determined ($c_{p,pcm}$ and H_x) and the global heat transfer coefficient, h_g. Zhang et al. avoid calculating this coefficient by assuming that the coefficient which applies to the reference sample also applies to the PCM sample. The difficulty in the analysis then resides in separating the T-history curve into three parts ($A_{l,pcm}$, $A_{x,pcm}$ and $A_{s,pcm}$) on Figure 4-3b) associated respectively with the PCM's liquid state, phase change and solid state, and either Equation (4-1) or (4-2). Two key moments in the PCM's T-history curve

need to be defined: 1) the transition from liquid state to phase change and 2) the transition between phase change and the solid state.

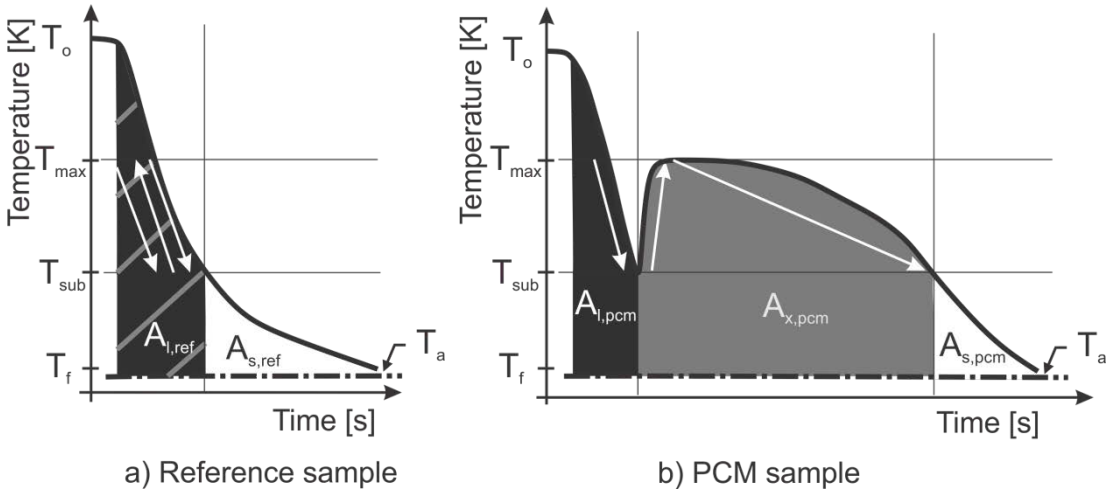

Figure 4-3: Division of the T-history curves following the method Z for a) the reference sample and b) the PCM sample

As seen on Figure 4-3b, in the case of PCMs with a significant degree of subcooling, the method uses the lowest temperature attained during subcooling, T_{sub}, as the first delimiter, marking the transition between the liquid state and phase change. On Figure 4-3a, the moment when the reference material reaches T_{sub} is also identified in order to delimit the area under the reference material T-history curve, $A_{l,ref}$, used to determine the heat transfer coefficient associated with the PCM's liquid state, $A_{l,pcm}$. The transition between phase change and the solid state is delimited by the moment when the PCM temperature reaches T_{sub} again. This delimits the area under the reference sample T-history curve, $A_{s,ref}$, used to determine the heat transfer coefficient associated with the PCM's solid phase, $A_{s,pcm}$. The remaining area under the PCM T-history curve, $A_{x,pcm}$, on Figure 4-3b is associated with phase change.

The liquid phase specific heat is obtained using the energy variations in both the reference material and PCM over temperature interval $[T_o; T_{sub}]$:

$$c_{p,l} = \frac{m_{ref} \cdot c_{p,ref} + m_t \cdot c_{p,t}}{m_{pcm}} \cdot \frac{A_{l,pcm}}{A_{l,ref}} - \frac{m_t}{m_{pcm}} \cdot c_{p,t} \tag{4-3}$$

The solid phase specific heat is obtained from Equation (4-4) below using the energy change in both samples over temperature interval $[T_{sub}; T_f]$.

$$c_{p,s} = \frac{m_{ref} \cdot c_{p,ref} + m_t \cdot c_{p,t}}{m_{pcm}} \cdot \frac{A_{s,pcm}}{A_{s,ref}} - \frac{m_t}{m_{pcm}} \cdot c_{p,t} \quad (4\text{-}4)$$

This analogy cannot be applied to phase change. As seen on Figure 4-3a, the temperature delimiting the PCM's phase change $[T_{sub}; T_{sub}]$ is a single point on the T-history curve of the reference material. The area under the T-history curve for that interval is null and so no heat transfer coefficient can be calculated for the reference material. Yet, the PCM sample travels through the temperature interval over which phase change occurs $[T_{max}; T_{sub}]$ on three occasions (see the white arrows on Figure 4-3b), all of which are encompassed in the liquid state and phase change parts (represented by areas $A_{l,pcm}$ and $A_{x,pcm}$ of the T-history curve. Equation (4-5), uses the energy variation in the reference material for the liquid phase (represented by area A_1') to determine the heat transfer coefficient to apply to the PCM over the temperature interval $[T_o; T_{sub}]$ encompassing phase change[3]:

$$H_x = \frac{m_{ref} \cdot c_{p,ref} + m_t \cdot c_{p,t}}{m_{pcm}} \cdot \frac{A_{x,pcm}}{A_{l,ref}} \cdot (T_o - T_{sub}) \quad (4\text{-}5)$$

4.5.2 Time-delay method – M

The method of Marín et al. (2003), hereafter called method M , analyses the T-history curve over small intervals of temperature, ΔT_i, without changing the method whether the interval falls within the solid, liquid or phase change period. For the same temperature interval, it is assumed the heat transfer for both samples can be characterized by the same heat transfer coefficient. This coefficient is determined using the experimental data from the reference material sample for each temperature interval studied. Thus the issue of choosing the temperature delimiting the beginning and end of phase change is eliminated. This leads to Equation (4-6) expressing the PCM enthalpy variation as a function of sample temperature from which the enthalpy-temperature curve is determined with the data normalized at a chosen temperature.

[3] There is an error in this equation in Zhang et al's paper. The denominator is indicated as m_t, the tube mass, when it should be m_{pcm}, the PCM mass.

$$\Delta H_i(\overline{T}_{pcm,i}) = \left(\frac{m_t c_{p,t}(\overline{T}_{ref}) + m_{ref} c_{p,ref}(\overline{T}_{ref})}{m_{pcm}}\right)\frac{A_{pcm,i}}{A_{ref,i}}\Delta T_{pcm,i} - \frac{m_t}{m_{pcm}} c_{p,t}\Delta T_{pcm,i} \quad (4\text{-}6)$$

The methodology described in (Jose M. Marín et al., 2003) is not explicit on the treatment of PCMs with significant subcooling. Analysing the PCM T-history curve strictly in a "cooling" mindset leads to a single temperature interval encompassing nearly all of phase change (see $\Delta T = -0.1℃$ on Figure 4-4). Subcooling is not illustrated on the enthalpy-temperature curve, where a single point defines phase change (see $\Delta T = -0.1℃$ on Figure 4-4).

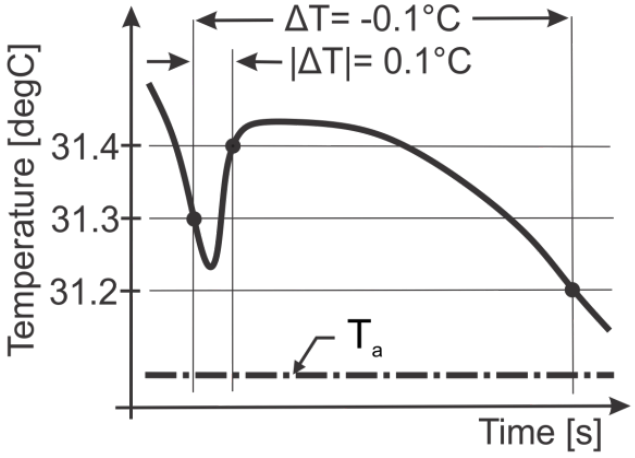

Figure 4-4: T-history curve of PCM sample indicating two alternate ways of treating subcooling in method M

Alternatively, both positive and negative variations in temperature can be considered (see $|\Delta T| = -0.1℃$ on Figure 4-4), leading to subcooling and phase change being defined by a greater number of data points. In this case, while the PCM is increasing in temperature after subcooling, the reference material sample is still cooling, so the two terms of the temperature variation, ΔT_i, in Equation (4-6) have a different sign. Other researchers have presented results illustrating subcooling behaviour using method M (Lázaro et al., 2006; Rathgeber, Miró, Cabeza & Hiebler, 2014), without explicitly mentioning their methodology.

To illustrate this issue, Figure 4-5 shows the enthalpy-temperature curve of a theoretical PCM (plain grey line) whose response to a cooling process was simulated numerically. The T-history curve resulting from this simulation was processed by method M following both interpretations mentioned above, resulting in the two dotted curves. Option 1 represents the case where the

sample temperature variation is presumed to be negative as the PCM is been cooled. The resulting enthalpy-temperature curve adequately displays the overall enthalpy variation of the process, yet it fails to illustrate the subcooling behaviour of the PCM. Using $|\Delta T| = -0.1℃$ is shown as Option 2, where the subcooling effect is clear yet portions of the enthalpy curve are inaccurate. The lowest temperature reached during subcooling does not appear on the enthalpy-temperature curve; rather the subcooling peak is rounded off as a function of the temperature interval chosen for the analysis. The overall change in enthalpy is accurate but the enthalpy-temperature curve is inaccurate during subcooling. Method M therefore results in an enthalpy-temperature curve that is useable for numerical simulation, but the PCM's behaviour during subcooling is inaccurate.

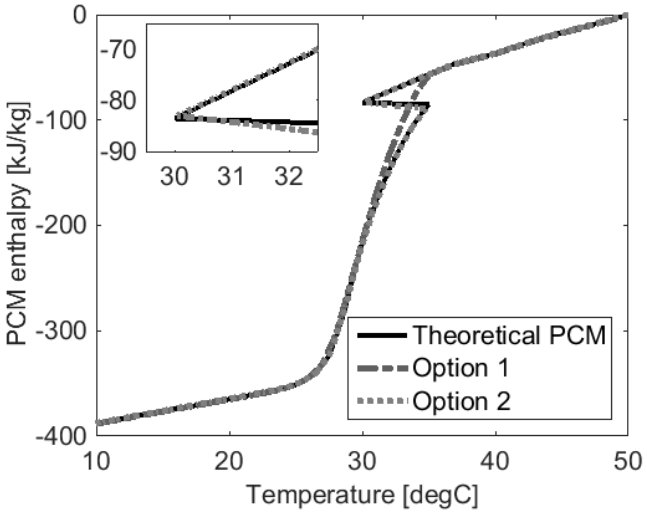

Figure 4-5: Enthalpy-temperature curves resulting from the method presented by method M according to the way subcooling is treated

The enthalpy-temperature curves resulting from the treatment of our experimental data through Method M using $|\Delta T| = -0.1℃$ are illustrated in Figure 4-6 for a temperature interval of 0.1 °C. Both cooling and heating processes are illustrated with all curves normalized to a value of 0 kJ/kg at 50 °C. The greatest cumulative difference in overall enthalpy change between 50 °C and 5 °C amongst the heating and cooling curves is 81.4 kJ/kg or 25.5%. For most samples, hysteresis of 2.6 to 3.2 °C is present between the heating and cooling processes but sample K18 displays a more pronounced hysteresis of approximately 6.4 °C. Due to the ambiguity introduced by the

method's treatment of subcooling mentioned previously, these values likely include slight errors in the portrayal of subcooling behaviour.

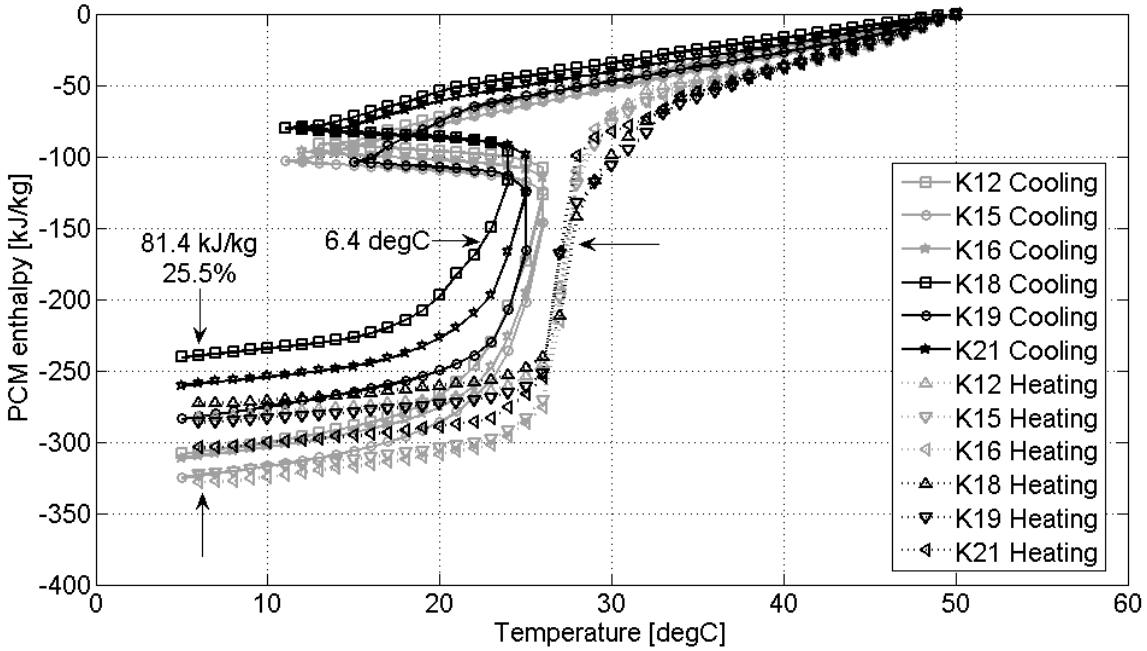

Figure 4-6: Comparison of enthalpy-temperature curves for every PCM sample, for both heating and cooling for method M

4.5.3 Sandness & Rekstad's Method – SR

Sandnes and Rekstad (2006) propose to test the reference samples in a separate trial. Their method, herein referred to as method SR, finds a polynomial to represent heat transfer from the reference sample as a function of the temperature difference between the surroundings and the sample which is latter used to calculate heat transfer from the PCM sample.

First, heat lost from the reference sample during the time interval between successive data measurements, q_{ref}, is calculated accounting for the thermal mass of the sample itself, the tube and the sensor through Equation (4-7).

$$q_{ref} = \left(m_{ref}c_{p,ref} + m_t c_{p,t} + m_{sen}c_{p,sen}\right)\frac{\Delta T_{ref,i}}{\Delta t_i} \tag{4-7}$$

A second degree polynomial is then used to express the heat lost by the reference sample for each time interval, q_{ref}, as a function of the temperature difference between the reference sample, T_{ref}, and ambient air, T_a, for that time interval. The same polynomial is used to determine the heat lost by each PCM sample, q_i, for every time interval of the experiment based upon the temperature difference between the PCM sample and ambient air. The heat lost by the PCM alone is then isolated from that lost by the tube and sensor, so the enthalpy change in the PCM, $\Delta H(\overline{T}_{pcm,i})$, can be determined as a function of the average PCM temperature, $\overline{T}_{pcm,i}$, from Equation (4-8).

$$\Delta H(\overline{T}_{pcm,i}) = \frac{q_i - (m_t c_{p,t} + m_{sen} c_{p,sen})(-\Delta T_{pcm,i})}{m_{pcm}} \tag{4-8}$$

Choosing an arbitrary reference point, the cumulative sum of the enthalpy changes is calculated for each temperature interval, resulting in an enthalpy-temperature curve. The enthalpy-temperature curves resulting from the treatment of our original PCM sample data by method SR are illustrated in Figure 7 for a time interval of 10 s between measurements (as used in Sandnes & Rekstad (2006)), for both cooling and heating process data.

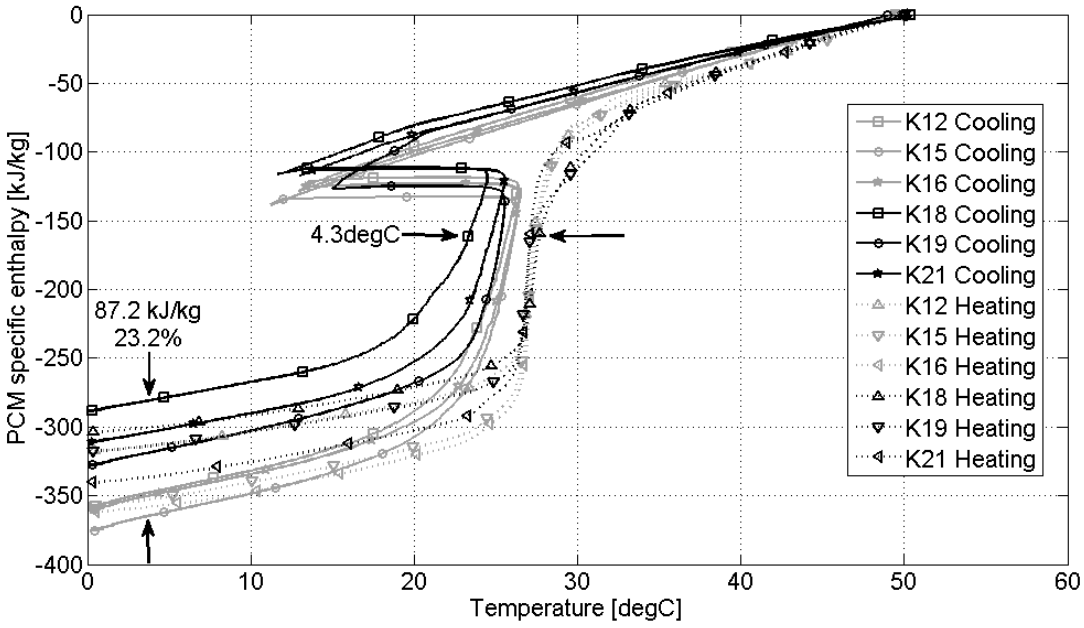

Figure 4-7: Comparison of enthalpy-temperature curves for every PCM sample by method SR

All samples display some level of hysteresis, ranging from 1.4 to 2.0 °C for most samples, up to 4.3 °C for sample K18. For samples K12, K15 and K19, the enthalpy values for the solid phase

(around 0-10 °C) are lower for the cooling process than for the heating process data. The greatest cumulative difference in the total phase change enthalpy between the cooling and heating curves of the same sample is of approximately 40.4 kJ/kg or 11.3% for sample K12. While for samples K16, K18 and K21 the opposite is true, the phase change enthalpy is greater for the cooling process and the greatest cumulative difference is of about 29.1 kJ/kg or 8.5% for sample K21. Over all the samples, the greatest cumulative difference in overall enthalpy change between 50 °C and 5 °C is about 87.2 kJ/kg or 23.2% between the cooling curves of samples K15 and K18.

The real gain provided by explicitly accounting for sensible heat changes in the sensor is questionable. Determining the adequate c_p value to use for the temperature sensor including for both the sensor wire and coating can be difficult. Determining the portion of the sensor mass contained inside the sample is also problematic and can lead to increased errors rather than improved accuracy.

Measurement errors and experimental uncertainties were thoroughly discussed in Sandnes & Rekstad (2006) but no comment on the error introduced by the polynomial in reproducing the correct heat loss for each sample was presented. Though the polynomial in Sandnes & Rekstad (2006) was generated from the average of sample heat losses, q_i, over 10 °C intervals of the temperature difference $T_{ref} - T_a$, the fit of the regression to the raw data was not quantified, nor was the use of a 10 °C interval of temperature explained or evaluated. The present authors chose a polynomial which fit the raw data for the reference sample reasonably (R2 value of 0.985). Yet data points for great temperature differences ($T_{ref} - T_a$) were quite spread out (standard deviation of 0.66 W for $T_{ref} - T_a = [10℃ \text{ to } 34℃]$) which leads to as much as a 14.2% relative difference between the measured heat transfer rate and that calculated by the polynomial. This inaccuracy is much greater than any uncertainty reported in Sandnes & Rekstad (2006) and can cause significant errors in the enthalpy-temperature curve at moments when large temperature differences exist in the test (i.e. in the liquid part of the cooling tests and the solid phase of the heating tests).

4.5.4 Thermal-delay method – K

Kravvaritis et al. (2010) suggested to assume the global heat transfer coefficient is the same for both reference and PCM samples over the same time interval studied. This is significantly different from the M and SR approaches described above, as the heat transfer coefficient is assumed to vary essentially with time and not the temperature difference. As illustrated on Figure 4-8, the T-history curve is analysed over successive time intervals of a specific duration (from t_i to t_{i+1}), where the temperature varies between the PCM ($T_{pcm,i}$ to $T_{pcm,i+1}$) and reference sample ($T_{ref,i}$ to $T_{ref,i+1}$). Method K uses the thermal delay, or temperature variation ($T_{ref,i}$ to $T_{ref,i+1}$), in the reference sample over each time interval of the test to define the heat transfer coefficient for that time interval and applies this coefficient to the PCM sample at the same time interval.

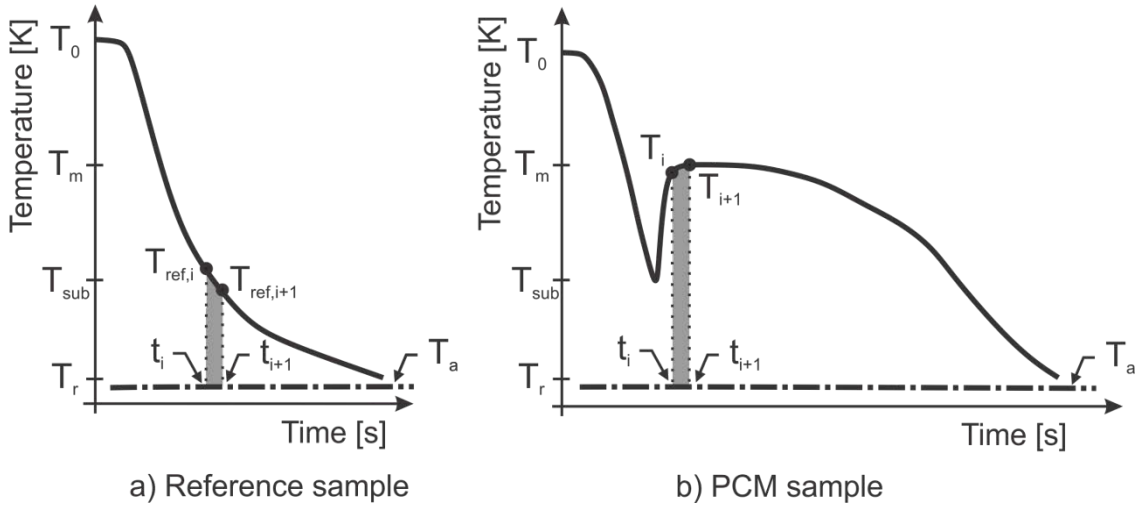

Figure 4-8: Method K for a) the reference sample and b) the PCM sample

This leads to Equation (4-9), a function expressing the PCM's effective thermal capacity, $c_{p,eff}$, as a function of the mean PCM temperature, $\overline{T_i}$, for that time interval.

$$c_{p,eff}(\overline{T_i}) = \frac{(m_{t,ref}c_{p,t,ref} + m_{ref}c_{p,ref})A_{c,pcm}}{m_{pcm}A_{c,ref}} * \frac{(T_{ref,i} - T_{ref,i+1})(T_{pcm,i} + T_{pcm,i+1} - 2T_a)}{(T_{pcm,i} - T_{pcm,i+1})(T_{ref,i} + T_{ref,i+1} - 2T_a)} - \frac{m_{t,pcm}c_{p,t,pcm}}{m_{pcm}} \quad (4\text{-}9)$$

Applying an identical heat transfer coefficient to both PCM and reference samples during the same time interval, neglects the dependency of natural convection and radiation on the temperature difference between the ambient air and sample tube. In subsequent work (Kravvaritis et al., 2011), the authors calculated a convection coefficient for both the PCM and reference samples from a correlation proposed by Popiel, Wojtkowiak, & Bober (2007). A ratio of these coefficients, $h_c/h_{c,ref}$, calculated at every time step was then applied to the first term in Equation (4-9). The authors claimed using $h_c/h_{c,ref} \approx 1$ in their calculations introduced less than a 3% error in the effective specific heat curve as a function of temperature and recommended neglecting the correction factor. Calculating convection coefficient ratio $h_c/h_{c,ref}$ for our data, resulted in values as low as 0.23 and as high as 6.20 for some time steps. Across all samples, an average relative difference in the effective specific heat values calculated was found to be 32.8%, indicating that the coefficient's relation to temperature cannot be neglected without introducing significant errors.

A comparison between the effective specific heat curves calculated from heating and cooling process data for sample K19 shown in Figure 4-9 illustrates that each process leads to significantly different behaviour. The heating process data results in a distinct peak in $c_{p,eff}$ at the estimated phase change temperature, while the cooling process data results in multiple peaks over a wide range of temperatures and the phase change temperature interval is lower in the cooling data.

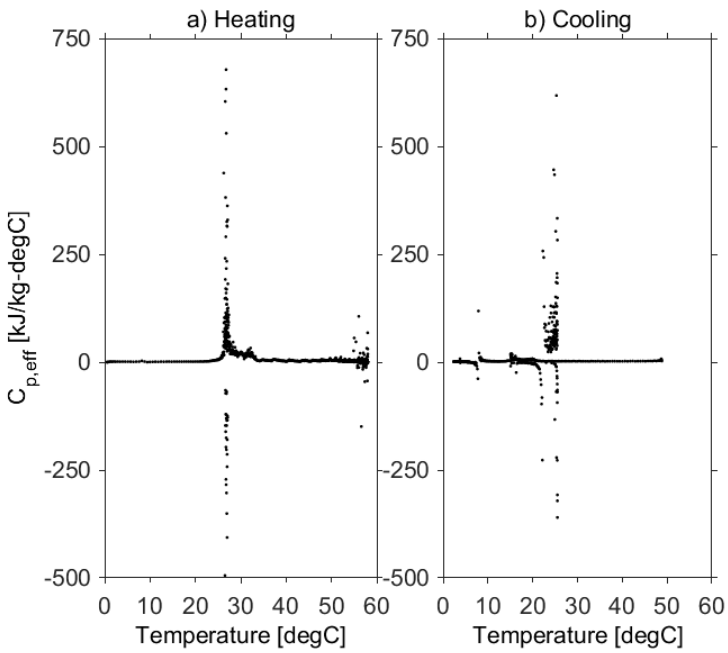

Figure 4-9: Effective specific heat curves as a function of temperature for sample K19, calculated with method K using a 10 s time interval for a) heating and b) cooling process data

In Kravvaritis et al. (2011), the authors also specify how to recreate an enthalpy-temperature curve from the effective specific heat curve for the PCM tested and how to evaluate the enthalpy of phase change. This method uses the measured data directly rather than an interpolation between measurement points as in Marín et al. (2003). Issues arise from the choice of the time interval duration. For short time intervals, the signal-to-noise ratio is low and, as can be seen on Figure 4-9, can lead to negative values of $c_{p,eff}$ which are both physically unrealistic and misguiding. Rapid dynamic effects are lost with longer time intervals which can change the coolest temperature recorded during subcooling and alter the calculated value of the latent heat of fusion.

Figure 4-10 illustrates enthalpy-temperature curves constructed for heating and cooling processes using a 10 s interval and calculating the heat transfer coefficient ratio, $h_c/h_{c,ref}$, for each time step. For most samples, heating and cooling curves differ by 1.6 to 2.4 °C during phase change while sample K18 again displays greater hysteresis of about 5.4 °C. All curves having been normalized to 0 kJ/kg at 50 °C, the solid state values are significantly different for the cooling and heating curves due to a sudden increase in enthalpy around 20 °C. The oscillating chilled

room air temperature shown on Figure 4-2 led to some measurements of ambient air temperature being higher than the reference sample temperature. The ensuing negative values of $c_{p,eff}$ caused a sudden, physically-unrealistic gain in enthalpy which explains the abnormal behaviour seen in the solid phase on Figure 4-10, between 18 and 23 °C. The "thermal-delay" method is the only one affected by this phenomenon, which is amplified by the rather large controller dead band in our experimental set-up. Methods M and SR both avoid using the reference sample data when its temperature has reached the ambient temperature, but this cannot be avoided with method K.

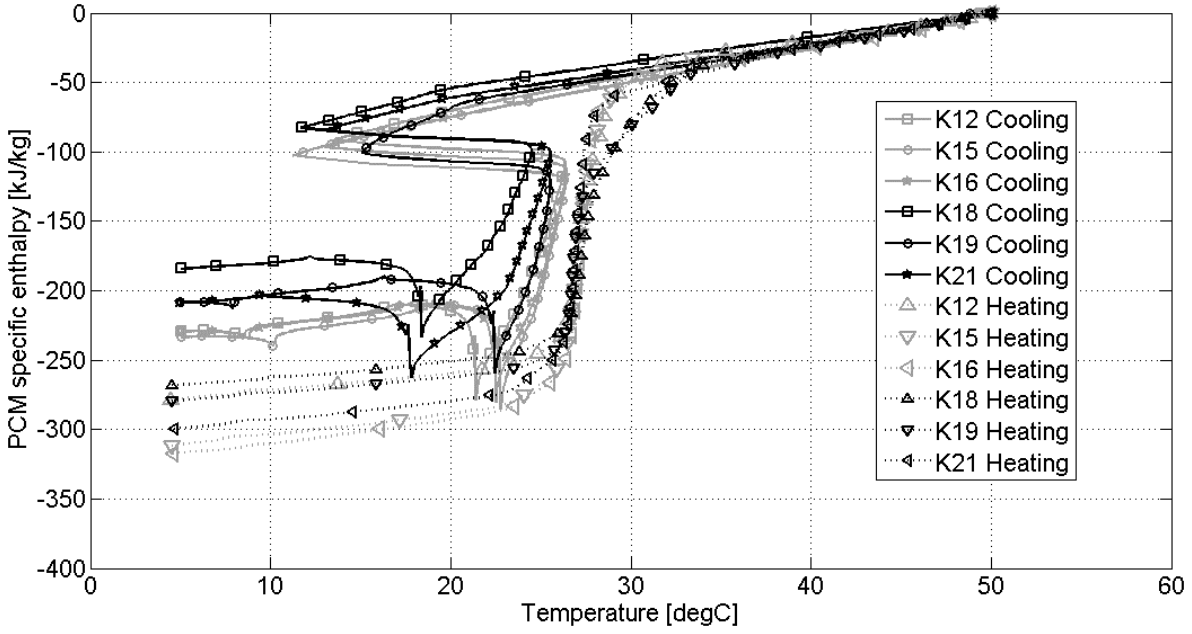

Figure 4-10: Enthalpy as a function of temperature for all samples, as per method K, for both heating and cooling processes

4.6 Discussion and recommendations

The first objective of this study was to determine which of the data processing methods could provide adequate enthalpy-temperature curves for the PCM tested. Constructing an enthalpy-temperature curve solely from the data given by the Z version neglects an important part of the PCM's behavior during phase change. For example, T_{sub}, is not the phase change temperature, yet the latent heat of fusion is calculated between two instances of this temperature. The method offers no information on the enthalpy at the melting temperature, T_m hindering a complete

representation of what occurs during phase change. Method Z does not allow for a full characterization of a PCM's behavior.

Only the methods M, SR and K provided complete enthalpy-temperature curves presented on Figure 4-11 for both cooling and heating processes. Method SR consistently yields lower enthalpy values over the whole temperature range, which also leads to lower specific heat values. For heating data, methods K and M are close for the whole temperature range. In cooling, methods K and M again display similar behaviour until the former's abnormal enthalpy peak around 20 °C. Nonetheless, the maximum cumulative difference in the overall enthalpy change between 50 °C and 5 °C amongst data treatment methods for any sample (excluding K cooling data) remains below 11.4%, which is lower than the maximum cumulative difference amongst samples when using the same data treatment method.

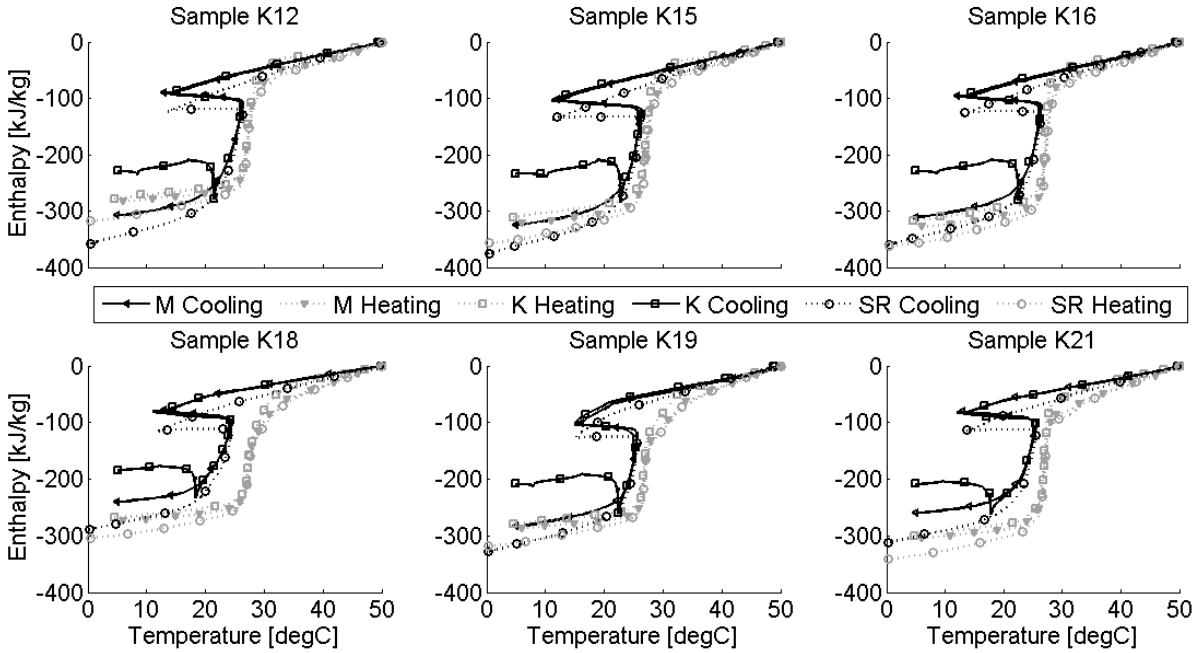

Figure 4-11: Enthalpy-temperature curves produced by method M (with absolute temperature interval), method K and method SR for all PCM samples, from both cooling and heating test data

Method M has sound thermodynamic bases and has shown to adequately portrait the overall enthalpy variation of a PCM according to its temperature. The original methodology described in (Jose M. Marín et al., 2003) lacks a detailed explanation of how to treat subcooling and only the

data processing alternative described in this paper as using an absolute temperature interval should be used for PCMs which undergo subcooling. Method K requires environmental chambers with a more precise temperature control than those that were used in this paper, or dynamic control of environmental test temperature. Moreover, we do not believe that the same heat transfer coefficient can be used for both reference and PCM samples over the same time interval. If that assumption is not valid, the thermodynamic basis for comparing the reference sample to the PCM sample over the same time interval is lost and, though results closely resemble those of method M, method K cannot be recommended. Finally, based on the results shown in this paper, the use of a polynomial to quantify the heat transfer based upon the temperature difference used in method SR introduces significant errors. Those effects are more significant than possible gains obtained by accounting for sensible heat changes in the sensor, so method SR cannot be recommended.

4.7 Conclusion

Twelve samples of a commercially available PCM were put through heating/cooling tests, as prescribed by the T-history method. The PCM, a heterogeneous salt hydrate, experienced significant subcooling and multiple samples broke; only six samples withstood all three heating/cooling cycles. The experimental data shows clear variations in the T-history curves amongst the six samples of the PCM studied; the minimum subcooling temperature varied from 11.2 to 15.0 °C and the maximum temperature reached during phase change varied from 24.5 to 26.4 °C. All samples were analyzed using four data processing variants of the T-history method.

Only three of the four data processing methods could provide adequate enthalpy-temperature curves for the PCM tested. The methodology of the “time-delay” method proposed by Marín et al. (2003), denoted as method M in this paper, lacks details on how to treat subcooling. Using the absolute temperature interval alternative presented in this paper provides an enthalpy-temperature curve where the temperature interval chosen is directly linked to the precision of the results. Potential users of the method proposed by Sandnes and Rekstad (2006) (referred to as SR) should be warned that modeling heat transfer with a polynomial can lead to significant sporadic errors. The “thermal delay” method proposed by Kravvaritis et al. (2010), referred here as method K, relies on assumptions that were not verified in our tests.

The results presented in this paper indicate that the use of the “time-delay” method, or method M, should be recommended above other variants, provided that the absolute temperature interval is used as detailed in this paper.

4.8 Acknowledgements

This work was funded by the National Science and Engineering Research Council of Canada (NSERC) through the second author’s Discovery Grant and through the Smart Net-Zero Energy Building Strategic Research Network (SNEBRN). The authors also thank the Laboratoire des Technologies de l’Énergie (LTE) of Hydro-Québec for providing laboratory facilities and personnel to perform experimental tests.

4.9 Nomenclature

A : Area [K-s] if measured under the T-history curve and [m^2] if related to heat transfer,

Bi : Biot number [-],

c : Specific heat [kJ/kg-K],

h : Heat transfer coefficient [W/m2-K],

H : PCM specific enthalpy [kJ/kg],

ΔH : Variation in PCM specific enthalpy [kJ/kg],

H_x : Latent heat of fusion [kJ/kg],

m : Mass [kg],

Δt : Time variation [s],

T : Temperature [K],

$\overline{T}$: Average temperature over time or temperature interval [K],

ΔT : Variation of temperature [K],

4.9.1 Subscript

a : Relating to the ambient,

c : Relating to the convective heat transfer coefficient,

eff : Effective,

f : Relating to the test end,

g : Relating to the global heat transfer coefficient,

i : Relating to an interval (time or temperature),

l : Relating to the liquid state of the PCM,

max : Relating to the maximum reached during phase change,

o : Relating to the test starts,

p : Pressure constant,

pcm : Relating to the phase change material,

ref : Relating to the reference sample,

s : Relating to the solid state of the PCM,

sen : Relating to the sample sensor,

sub : Relating to subcooling,

t : Relating to the sample tube,

x : Relating to phase change.

4.10 References

Arkar, C., & Medved, S. (2005). Influence of accuracy of thermal property data of a phase change material on the result of a numerical model of a packed bed latent heat storage with spheres. *Thermochimica Acta, 438*(1-2), 192-201. doi: 10.1016/j.tca.2005.08.032

Bony, J., & Citherlet, S. (2007). Numerical model and experimental validation of heat storage with phase change materials. *Energy and Buildings, 39*(10), 1065-1072. doi: 10.1016/j.enbuild.2006.10.017

Castellón, C., Günther, E., Mehling, H., Hiebler, S., & Cabeza, L. F. (2008). Determination of the enthalpy of PCM as a function of temperature using a heat-flux DSC - A study of different measurement procedures and their accuracy. *International Journal of Energy Research, 32*(13), 1258-1265. doi: 10.1002/er.1443

D'Avignon, K., & Kummert, M. (2012). *Proposed TRNSYS model for storage tank with encapsulated phase change materials*. Paper presented at the 5th National Conference of IBPSA-USA, Madison, Wisconsin.

Günther, E., Hiebler, S., Mehling, H., & Redlich, R. (2009). Enthalpy of Phase Change Materials as a Function of Temperature: Required Accuracy and Suitable Measurement Methods.

International Journal of Thermophysics, 30(4), 1257-1269. doi: 10.1007/s10765-009-0641-z

Hong, H., Kim, S. K., & Kim, Y.-S. (2004). Accuracy improvement of T-history method for measuring heat of fusion of various materials. *International Journal of Refrigeration, 27*(4), 360-366. doi: 10.1016/j.ijrefrig.2003.12.006

Kenisarin, M., & Mahkamov, K. (2007). Solar energy storage using phase change materials. *Renewable and Sustainable Energy Reviews, 11*(9), 1913-1965. doi: 10.1016/j.rser.2006.05.005

Khudhair, A. M., & Farid, M. M. (2004). A review on energy conservation in building applications with thermal storage by latent heat using phase change materials. *Energy Conversion and Management, 45*(2), 263-275. doi: 10.1016/S0196-8904(03)00131-6

Kravvaritis, E. D., Antonopoulos, K. A., & Tzivanidis, C. (2010). Improvements to the measurement of the thermal properties of phase change materials. *Journal of Measurement Science and Technology, 21*(4). doi: 10.1088/0957-0233/21/4/045103

Kravvaritis, E. D., Antonopoulos, K. A., & Tzivanidis, C. (2011). Experimental determination of the effective thermal capacity function and other thermal properties for various phase change materials using the thermal delay method. *Journal of Applied Energy, 88*(12), 4459-4469. doi: 10.1016/j.apenergy.2011.05.032

Lázaro, A., Günther, E., Mehling, H., Hiebler, S., Marín, J. M., & Zalba, B. (2006). Verification of a T-history installation to measure enthalpy versus temperature curves of phase change materials. *Journal of Measurement Science and Technology, 17*(8). doi: :10.1088/0957-0233/17/8/01

Lázaro, A., Peñalosa, C., Solé, A., Diarce, G., Haussmann, T., Fois, M., Zalba, B., Gshwander, S., Cabeza, L. F. (2013). Intercomparative tests on phase change materials characterisation with differential scanning calorimeter. *Applied Energy, 109*(0), 415-420. doi: http://dx.doi.org/10.1016/j.apenergy.2012.11.045

Marín, J. M., Zalba, B., Cabeza, L. F., & Mehling, H. (2003). Determination of enthalpy-temperature curves of phase change materials with the temperature-history method:

improvement to temperature dependent properties. *Journal of Measurement Science and Technology, 14*(2). doi: 10.1088/0957-0233/14/2/305

National Instruments Corporation. Retrieved 10-29-2014, from www.ni.com

PCM Products Ltd. (2009). Phase Change Materials Products Ltd. Retrieved 2015-11-02, from http://www.pcmproducts.net

Peck, J. H., Kim, J.-J., Kang, C., & Hong, H. (2006). A study of accurate latent heat measurement for a PCM with a low melting temperature using T-history method. *International Journal of Refrigeration, 29*(7), 1225-1232. doi: 10.1016/j.ijrefrig.2005.12.014

Popiel, C. O., Wojtkowiak, J., & Bober, K. (2007). Laminar free convective heat transfer from isothermal vertical slender cylinder. *Experimental Thermal and Fluid Science, 32*(2), 607-613. doi: http://dx.doi.org/10.1016/j.expthermflusci.2007.07.003

RAL Gütezeichen. (2013). Phase Change Material Quality Assurance *RAL-GZ 896*. Sankt Augustin, Germany: German Institute for Quality Assurance and Certification e.V.

Rathgeber, C., Miró, L., Cabeza, L. F., & Hiebler, S. (2014). Measurement of enthalpy curves of phase change materials via DSC and T-History: When are both methods needed to estimate the behaviour of the bulk material in applications? *Thermochimica Acta, 596*(0), 79-88. doi: http://dx.doi.org/10.1016/j.tca.2014.09.022

Richardson, M. J. (1997). Quantitative aspects of differential scanning calorimetry. *Thermochimica Acta, 300*(1-2), 15-28. doi: 10.1016/S0040-6031(97)00188-3

Rudtsch, S. (2002). Uncertainty of heat capacity measurements with differential scanning calorimeters. *Thermochimica Acta, 382*(1-2), 17-25. doi: 10.1016/S0040-6031(01)00730-4

Sandnes, B., & Rekstad, J. (2006). Supercooling salt hydrates: Stored enthalpy as a function of temperature. *Journal of Solar Energy, 80*(5), 616-625. doi: 10.1016/j.solener.2004.11.014

Solé, A., Miró, L., Barreneche, C., Martorell, I., & Cabeza, L. F. (2013). Review of the T-history method to determine thermophysical properties of phase change materials (PCM).

Renewable and Sustainable Energy Reviews, 26(0), 425-436. doi: 10.1016/j.rser.2013.05.066

Tabares-Velasco, P. C., Christensen, C., & Bianchi, M. (2012). Verification and validation of EnergyPlus phase change material model for opaque wall assemblies. *Building and Environment, 54*(0), 186-196. doi: 10.1016/j.buildenv.2012.02.019

Xie, J., Li, Y., Wang, W., Pan, S., Cui, N., & Liu, J. (2013). Comments on Thermal Physical Properties Testing Methods of Phase Change Materials. *Advances in Mechanical Engineering, 2013*, 1-9. doi: 10.1155/2013/695762

Zhang, Y., Jiang, Y., & Jiang, Y. (1999). A simple method, the T-history method, of determining the heat of fusion, specific heat and thermal conductivity of phase-change materials. *Journal of Measurement Science and Technology, 10*(3), 201-205.

CHAPTER 5 ARTICLE 2: EXPERIMENTAL ASSESSMENT OF A PHASE CHANGE MATERIAL STORAGE TANK

D'Avignon, K., Kummert, M., (2015). Experimental assessment of a phase change material storage tank. Submitted to the *Journal of Applied Engineering* on September 6th, 2015. Currently under review following a revision submitted on November 11th, 2015.

Note: The article version transcribed here is the revised version submitted with a few minor corrections recommended by the jury.

5.1 Abstract

This paper describes the experimental study carried out to assess the performance of a Phase Change Material (PCM) storage tank in various operating conditions in a dynamic test bench. The studied horizontal PCM tank contains stacks of slab-like PCM capsules between which heat transfer fluid can circulate. The commercially available capsules were instrumented so the PCM behaviour could be measured in addition to that of the PCM tank as a whole. Numerous melting and solidification cycles were completed with different inlet fluid temperatures, flowrates and load profiles for which at least three repetitions were made. Analysis of test results shows significant variations in the PCM behaviour under the same tests conditions including varying degree of supercooling and differing phase change temperature. The outlet fluid temperature from the tank can however be predicted accurately from operating conditions and the initial state of the PCM. Interrupting phase change processes before the PCM is completely melted or solidified affects the temperature at which the PCM changes phase as well as the degree of supercooling measured. Results from this investigation will be especially useful for researchers developing and validating numerical models for use in various building energy systems as the complete experimental data set is made available as an online companion to this paper.

5.2 Keywords

Phase change material storage tank; experimental testing; interrupted phase change

5.3 Introduction

Design, automated control and fault diagnostics in building energy systems increasingly rely on modelling and performance simulation of Heating, Ventilation and Air-Conditioning (HVAC) equipment. As HVAC equipment is significantly influenced by its surroundings and the operating conditions it experiences, data encompassing the whole operating range of each component is required for proper simulation. Unfortunately, standardized data provided by manufacturers are often limited to a few number of operating points.

Heat pumps are a good example of HVAC components that present a performance which is highly dependent on the variation of its operating conditions. Novel components such as phase change material (PCM) storage tanks are another example where the nominal capacity is insufficient for designers to assess their correct dynamic operation. As shown by Liu et al. (2011), something as critical as the rate at which heat can be stored or extracted can vary significantly with operating conditions.

Moreno et al. (2014) experimentally compared the performance of a water storage tank to that of a PCM storage tank to shift the daytime cooling load of a small space when coupled to a water-to-water heat pump and air handling unit. Both thermal energy storage (TES) tanks were horizontal and had identical dimensions but the PCM tank included stacks of a commercially-available PCM supplied in plastic rectangular capsules. Results indicate that for the same footprint, the PCM tank could on average supply 14.5% more cooling energy than the water tank, at the expense of a charging time which was 4.6 times longer. Results such as these are promising but thorough testing of such PCM capsules and tank configuration are required for HVAC system designers to consider installing them in their projects.

Thorough model validation of PCM storage tanks also requires testing multiple operating conditions for a specific PCM tank configuration so that the model can truly be validated for use in various applications. Dutil et al. (2011) indicate that most recent studies have relied on numerical results from previous researchers to validate their models and that experimental data is scarce for most recent geometries. Dolado et al. (2011) performed such thorough testing of a PCM-air heat exchanger which included metal-encapsulated PCM slabs positioned vertically. The impact of varying the fluid flowrate and inlet fluid temperature on the thermal power produced by the unit was evaluated. Detailed figures provide the evolution of the temperature

through time measured at the surface of all the PCM capsules inside the unit as well as the fluid inlet and outlet temperatures. Other such tests exist for PCMs encapsulated in plastic pouches (Saied Mohammad Vakilaltojjar, 2000; Zukowski, 2007), in plastic vertical slabs (Lázaro et al., 2009; B. Zalba et al., 2004), as well as spherical (Bedecarrats et al., 2009; I. W. Eames & Adref, 2002; Nallusamy et al., 2007) and cylindrical capsules (J. Wei et al., 2005). Such thorough analysis of thermal energy system behaviour has not been done for the commercially available capsule type described in Moreno et al.'s work.

This paper describes the experimental tests carried out to evaluate the behaviour of a real-scale PCM storage tank in varying operating conditions. For this purpose, the Semi-Virtual Lab at Polytechnique Montreal was adapted to the study of single inlet/outlet storage tanks where small flowrates were required. A horizontal tank was designed to contain stacks of commercially available slab-like PCM capsules between which heat transfer fluid could circulate. The capsules containing the PCM, a salt hydrate, were instrumented to allow measurement of the material behaviour in addition to that of the PCM tank as a whole. Numerous melting and solidification cycles were completed with different inlet fluid temperatures, flowrates and load profiles for which the results are presented here. Detailed analysis of test results allows to draw conclusions regarding the phase change material itself, the PCM capsule and overall tank behaviour. The complete experimental data set is made available to readers as an online companion to this paper in order to assist in the development and validation of PCM tank models.

5.4 Experimental set-up

As illustrated in Figure 5-1, the commercially available PCM objects tested in this project are rectangular HDPE capsules which are 0.25 m wide, 0.5 m long and 0.032 m thick. Two rows of protrusions are present on their upper and lower faces which interlock when stacked to hold the capsules at a distance of 0.007 m away from one another (see Figure 5-1 and 5-3).

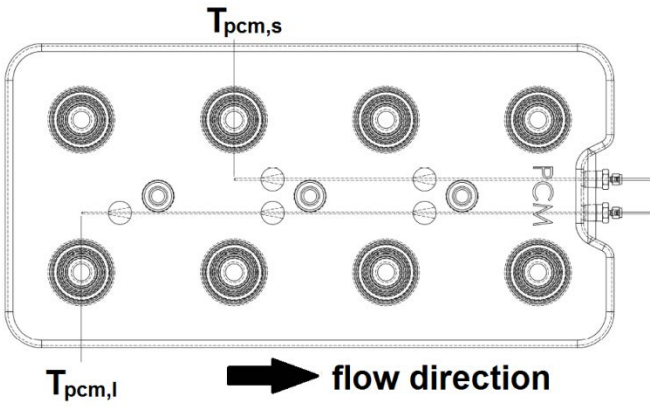

Figure 5-1: Instrumented PCM capsule

A series of holes along the central axis of the capsule penetrate to the capsule center and one lateral face includes a depression where the sealed filling orifice is located. In this study, the PCM contained in the capsules is a heterogeneous salt hydrate named S27 (PCM Products Ltd, 2015) whose properties as supplied by the manufacturer are detailed in Table 5.1.

Table 5.1: PCM properties of S27 as specified by the manufacturer[4]

Property name	**Property value**
Phase change temperature	27 °C
Density	1530 kg/m3
Latent heat of fusion	183 kJ/kg
Volumetric heat capacity	280 MJ/m3
Specific heat capacity	2.20 kJ/kg-K
Thermal conductivity	0.540 W/m-K
Mass	5.81 kg / capsule

As can be seen on Figure 5-2, PCM capsules were installed inside a horizontal insulated cylindrical tank in a 2 stacks wide by 2 stacks deep formation, for a total of 32 capsules. The PCM tank is equipped with perforated plates at its inlet and outlet to allow uniform fluid flow across the capsule faces. This results in an entry-exit volume of 81 L, located between the fluid entry/exit and the perforated plate, which is filled with fluid and exempt of any PCM capsules. The zone located between the two perforated plates has a diameter of 0.762 m and length of 1.05

[4] The properties listed have been copied exactly as found in manufacturer data.

m and is where the capsules were installed. A section made of expanded polystyrene was used to support the capsules inside the tank and insulate them from ambient conditions. This support section held the capsules in an opening 0.5 m wide and 0.37 m in height. An additional layer of insulation (in light purple on Figure 5-2 and Figure 5-3), 0.013 m in height, was added to fill the gap between the capsule stack and the capsule support. One of these commercially-available PCM capsules is instrumented by the researchers with two Type-K thermocouples, installed at two positions along the capsule's length, near its central axis (see Figure 5-1). As shown in Figure 5-3, the instrumented capsule is installed in the "downstream" stack of capsules (second row in direction of flow) about mid-way in the capsule stack.

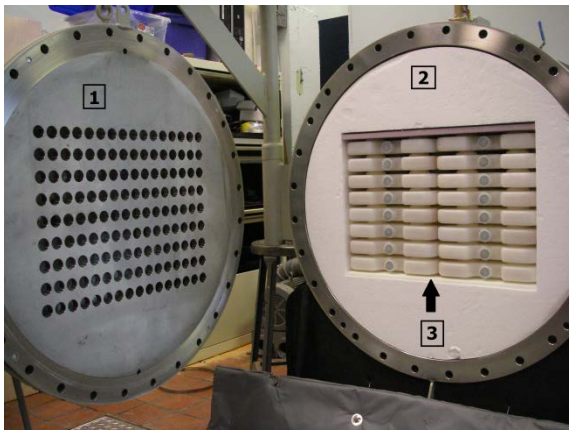

Figure 5-2: PCM tank viewed from the inlet, including 1) perforated plate, 2) capsule support and 3) PCM capsules

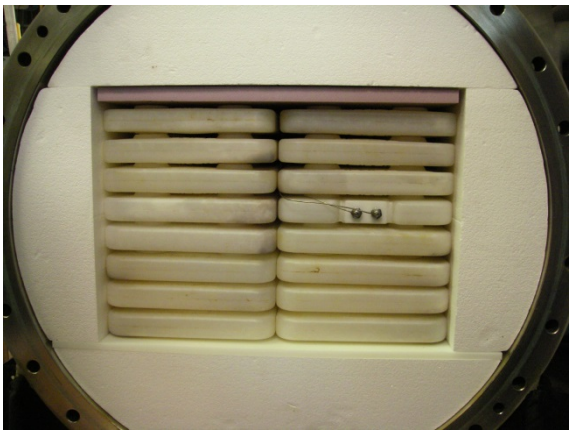

Figure 5-3: Position of the instrumented PCM capsule in the tank as viewed from the outlet

The PCM tank was tested in the Semi-Virtual Lab (MacDonald et al., 2014) at Polytechnique Montreal. It is designed to reproduce any and all conditions under which small commercial-size hydronic equipment are expected to operate. The main components of the test bench are illustrated in Figure 5-4. When the tested equipment features two inlets and two outlets as in the case of a heat pump, the two test loops (in green and yellow) supply adequate operating conditions to each side of the equipment. In the case of the PCM tank (1), these loops were used in series to service the sole inlet and outlet to the PCM tank. Each test loop is equipped with its own variable-frequency-drive and pump (2) permitting flowrates of up to 7.6 L/s. In this case, balancing valves (3) were used so part of the flow would by-pass the tested equipment in order to reduce the flow rate imposed to the PMC tank without affecting the pump's performance.

Turbine flow meters (4) with magnetic pick-up were installed to measure the exact flowrate inside the PCM tank to a precision of ± 1% of the reading. A set of calibrated PT-100 platinum resistance sensors (5) and a custom-made thermopile (6) were installed at the tank's inlet and outlet to accurately measure the fluid temperature imposed on the equipment and its response. The uncertainties on their measurements are ± 0.165 °C for the platinum sensors and ± 0.04 °C for the thermopile.

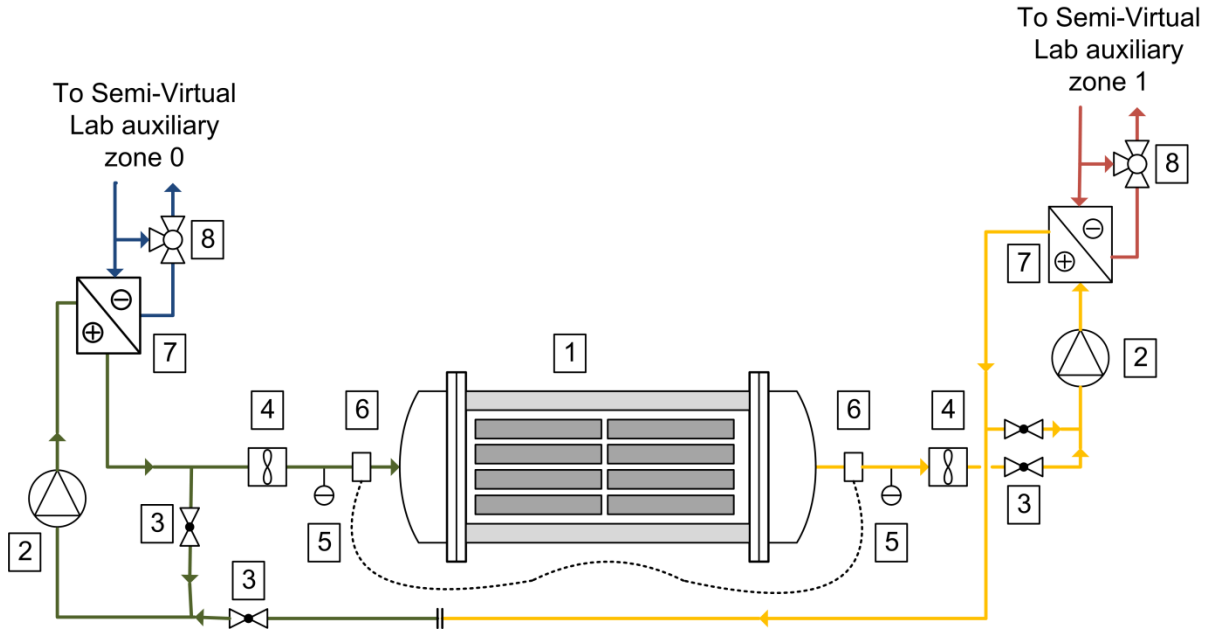

Figure 5-4: Schematic representation of the PCM tank testing zone of the Semi-Virtual Lab

The temperature of each test loop is controlled by two heat exchangers (7) linked to the two auxiliary loops of the Semi-Virtual Lab in red and blue on Figure 5-4. Depending on the operating conditions required, a series of heating and/or cooling units may be connected to either auxiliary loop if needed. This includes a non-reversing water-to-water heat pump with scroll-type tandem compressors with a nominal capacity of 100 kW, an electric boiler with a capacity of 54 kW and a heat exchanger connected to the university's chilled water loop. Multiple 3-way valves allow each of the units to be used individually, in series or completely avoided. Likewise, 3-way valves (8) are used to control the flow rate sent to the heat exchanger (7) linking each auxiliary loop to its respective test loop, allowing a precise control of the operating conditions imposed upon the equipment being tested. A reconfigurable embedded control and acquisition

system, provides high-speed signal acquisition and control of the Semi-Virtual Lab. In the present article, the data acquisition and control sampling times were set to 1 second.

5.5 Test methodology

Experimental data intended for the development and validation of numerical models should evaluate the behaviour of the system under transient/dynamic and steady-state conditions of interest. A review of existing PCM tank models and their intended uses allowed to identify relevant questions to be answered and their associated test mechanisms.

Firstly, a basic understanding of the PCM's behaviour inside the capsule is essential. Measures of PCM temperature inside the capsules can confirm the complete charge/discharge of the PCM (I. W. Eames & Adref, 2002; Nallusamy et al., 2007). T-history tests of the studied PCM (D'Avignon & Kummert, 2015a) presented a marked hysteresis between heating and cooling processes. Some DSC runs (Barreneche et al., 2013) indicated a displaced peak from the theoretical phase change temperature. Tests by Moreno et al. (2014) also indicated the presence of varying degrees of subcooling. With measurements made inside the capsules, the phase change temperature given by the manufacturer as well as the claimed absence of any hysteresis or supercooling can also be investigated. By varying the fluid flowrate and temperature differential one can assess whether these behavioural traits are constant or depend on operating conditions (Solomon et al., 2013). Using a methodology inspired by the T-history method (Günther et al., 2009), the analysis of the measured data from inside the PCM capsule allows a general characterization of the "PCM object" (i.e. the PCM in this particular encapsulation geometry) as done by Zalba et al. (2004).

The use of PCM storage tanks in HVAC systems requires a thorough knowledge of the tank's storage profile. More than the simple storage capacity, this includes understanding the power output profile that can be expected from the PCM tank, the time required to fully charge/discharge the tank (Bruno, Tay & Belusko, 2014; Nallusamy et al., 2007; Yamaha & Misaki, 2006), as well as any effects the flowrate or fluid temperature could have on these parameters (Dolado et al., 2011; Lázaro et al., 2009; Zukowski, 2007). The various step tests undertaken under differing operating conditions will also serve in answering these questions.

Knowing that a certain time is required to fully charge the PCM tank under specific operating conditions leads to the question of what happens when discharge begins before charging is completed (Bedecarrats et al., 2009). Authors have discussed the way the PCM's behaviour changes in these conditions (Bony & Citherlet, 2007b; Chandrasekharan, Lee, Fisher & Deokar, 2013; Delcroix, Kummert & Daoud, 2015) but no definite answer has been provided. This question is investigated here by a set of step tests where operating conditions toggle between charging and discharging processes before either is completed.

Operating conditions in HVAC systems are far from those of typical step tests where the inlet temperature suddenly changes to a value above or below the phase change temperature and then remains constant for a prolonged period. Instead, past research (Arkar, Vidrih & Medved, 2007; Ming Liu et al., 2011; Moreno et al., 2014) indicates that storage tanks are more likely to be used to offset a constant power load over a specific period of time. To reflect these applications tests at constant power and fixed temperature change rates are also undertaken.

Previous characterization of the studied PCM through DSC (Barreneche et al., 2013) and the T-history method (D'Avignon & Kummert, 2015a) showed that the notable level of supercooling in the material often caused a marked variability between repeated tests. Thus the present test methodology does not rely on individual tests to conclude on PCM-object or tank behaviour. Instead, each test mechanism has undergone three repetitions to assess the repeatability of results.

5.6 Results and discussion

5.6.1 Step tests

This series of tests studies the melting and solidification process within the tank after a step change in the inlet temperature, with a constant flowrate. At the beginning of the test, the tank is allowed to reach a steady-state regime with a given inlet temperature. The inlet temperature is then quickly increased (for a melting process) or decreased (for a solidification process). The operating temperatures (beginning and end of the step) were selected to ensure that the phase change would occur between these two limits. The manufacturer-provided phase change temperature, $T_{trans} = 27\ °C$, was used as a reference and the starting and ending temperature for the test were selected to provide a desired temperature differential, ΔT, above and below that

temperature. For example, a melting test with $\Delta T = 10\,°C$ would start at $T_{trans} - 10 = 17\,°C$ and reach a final temperature of $T_{trans} + 10 = 37\,°C$.

An example of such a test is illustrated in Figure 5-5 and Figure 5-6 for a flowrate $\dot{v} = 0.3$ L/s and a temperature differential $\Delta T = 10$ °C. Both Figures show the temperature data measured at the tank outlet, T_{out}, as well as inside the PCM by the short and long sensors, $T_{pcm,s}$ and $T_{pcm,l}$ respectively, following a step change in the inlet temperature, T_{in}, from 10 °C below T_{trans} to 10 °C above T_{trans} and vice versa.

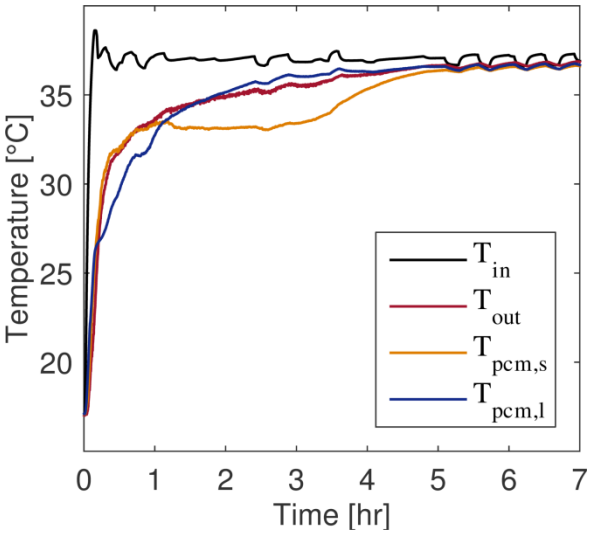

Figure 5-5: Temperature profiles for a heating test at $\dot{v} = 0.3$ L/s and $\Delta T = 10$ °C

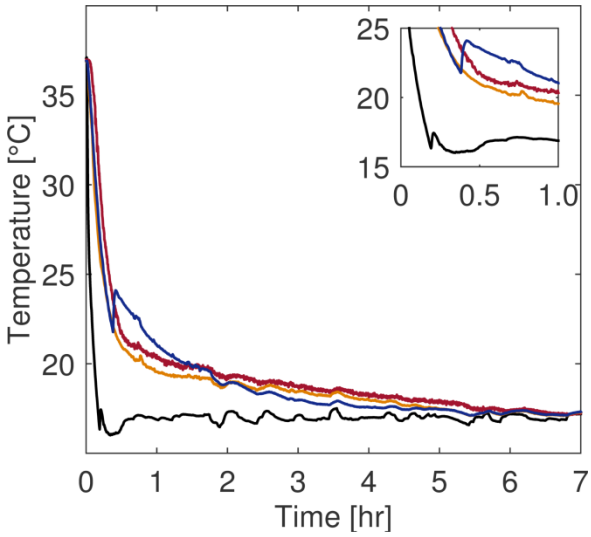

Figure 5-6: Temperature profiles for a cooling test at $\dot{v} = 0.3$ L/s and $\Delta T = 10$ °C

Figure 5-5 and Figure 5-6 indicate that the inlet fluid temperature entering the PCM tank was not perfectly controlled and exhibits an initial overshoot (0.8 to 1.6 °C) as well as small oscillations ($\simeq$ 0.5 °C). Upon closer inspection, one can see these oscillations reflected in the outlet fluid temperature, albeit with the expected delay and attenuation due to the tank's thermal mass. Temperature profile at the long sensor's position, $T_{pcm,l}$, displays little to no phase change plateau either in cooling or in heating. Rather, the PCM at that position displays a certain thermal delay with regards to the inlet temperature as well as a significant degree of supercooling (approximately 2.3 °C) in the case of Figure 5-6. The evolution of temperature at the short sensor position, $T_{pcm,s}$, exhibits a clear phase change plateau in heating while in the cooling process

only mild supercooling (approximately 0.2 °C) is present as well as a somewhat inclined phase change plateau.

In order to study the effect of different inlet fluid temperatures and flowrates on melting and solidification processes, similar step tests were repeated for all possible combinations of two flowrates ($\dot{v} = 0.3$ L/s and $\dot{v} = 0.45$ L/s) and temperature differentials ($\Delta T = 5\,°C$ and $\Delta T = 10\,°C$). In each case, three repetitions of the test were made. To allow for quick comparison, all repetitions of tests made for every flowrate and differential temperature combination are illustrated on subplots in the same figure. Figure 5-7 and Figure 5-8 illustrate the time evolution of the PCM temperature measured by the “long” and “short” sensors respectively while Figure 5-9 compares the tank outlet fluid temperature time evolution of all repetitions of the step tests. In the interest of clarity, these figures only illustrate the data from the first 5 hours of the tests though the test themselves lasted much longer.

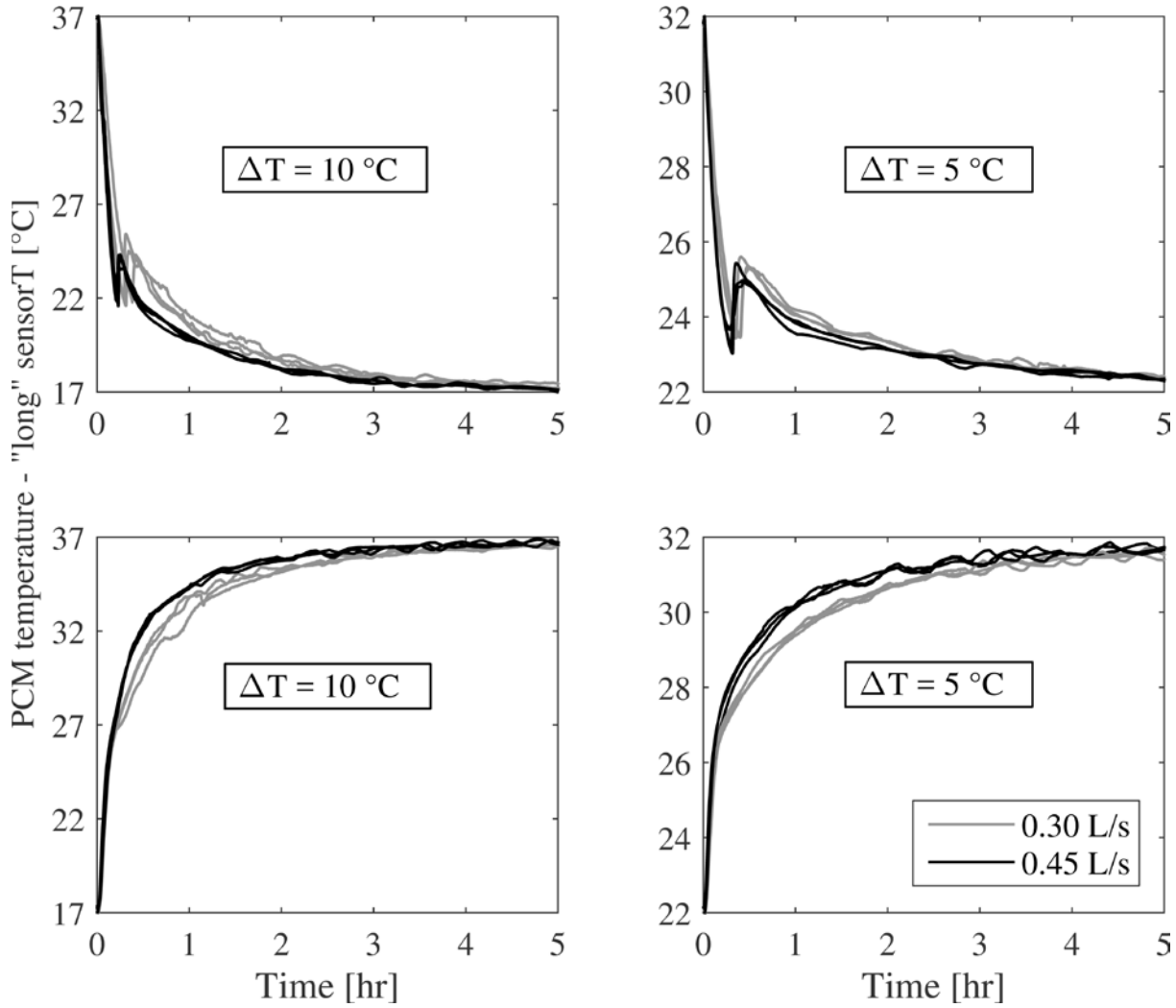

Figure 5-7: PCM temperature measured by "long" sensor as a function of time for all cooling and heating test repetitions

Figure 5-7 and Figure 5-8 indicate that the behaviour observed for each PCM sensor position in the heating and cooling tests previously analyzed (see Figure 5-5 and Figure 5-6) apply to all inlet temperature and flowrate combinations tested. The PCM behaviour at the long sensor position (see Figure 5-7) is quite constant amongst test repetitions and through test conditions: little or no phase change plateau is visible but significant supercooling occurs. It is also apparent that the PCM at this position has completely changed phase and almost reached the inlet temperature in the first 5 hours of the tests illustrated on Figure 5-7. On Figure 5-8, the PCM behaviour at the short sensor position shows greater variation amongst repetitions of the same test conditions but in all cases a clear phase change plateau is present in both heating and cooling.

The striking differences between the behaviour captured by the two sensors can be explained by the inhomogeneity of the PCM material and the inhomogeneity of heat transfer conditions (e.g. due to different liquid flowrate and temperature close to the sensor). Such differences have for example been observed by Dolado et al. (2011) who witnessed longer phase change plateaus at sensors placed further downstream from the tank inlet. Solomon et al. also reported that the effect of supercooling was more prominent in capsules closer to the fluid entry than those further downstream.

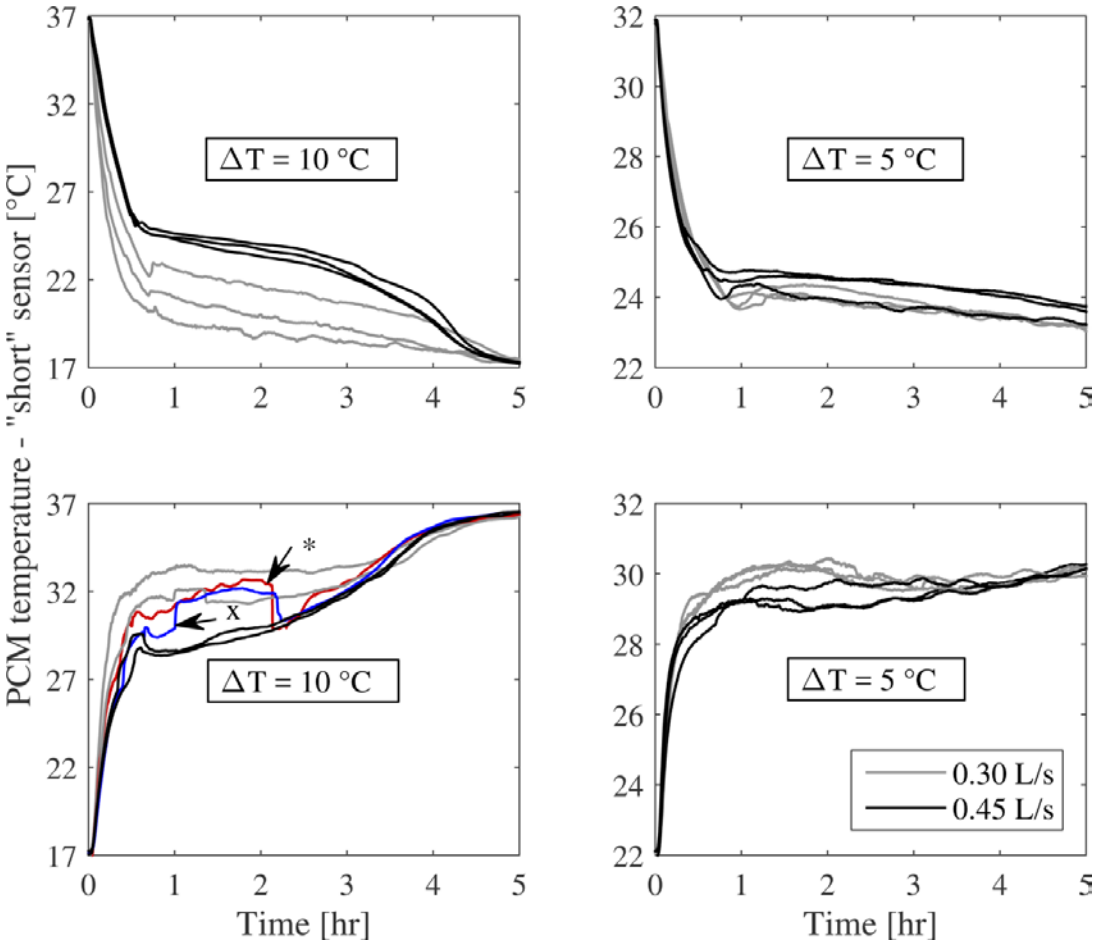

Figure 5-8: PCM temperature measured by the "short" sensor as a function of time for all heating and cooling test repetitions

The plateaus visible on Figure 5-8 allow for the assessment of the phase change temperature in all conditions tested. Comparing the heating and cooling tests held in the same conditions indicates hysteresis is present. Phase change occurs at temperatures below 27 °C in cooling and above 27 °C in heating, regardless of the flowrate or temperature differential imposed. Test

results also indicate increasing the flowrate brings the phase change plateau closer to 27 °C, reducing the hysteresis between the cooling and heating processes. The flowrate has a milder effect on the phase change plateau for the smaller temperature differential as the hysteresis was also less important for those cases. In most cases, for the same temperature differential, $T_{pcm,s}$ appears to be the same after 5 hours, no matter what the value of the flowrate is. At this location, for tests with $\Delta T = 5$ °C, the PCM has barely completed its phase change in the first 5 hours of the tests. So, a higher temperature differential imposed on the tank decreases the time required for the PCM at this position to reach the inlet fluid temperature.

Analysing Figure 5-8 further, the second repetition of the heating test with $\dot{v} = 0.3$ L/s (in red and identified by arrow "*") exhibits a sharp drop in temperature approximately 2.2 hours after the beginning of the test, before the PCM temperature begins to increase once more. The same phenomenon is visible twice for the first repetition of the heating test with $\dot{v} = 0.45$ L/s (in blue and identified by arrow "x"); once around one hour after the test began and the second at around 2.2 hour mark. It is unclear whether such readings were caused by the sudden movement of solid PCM clumps around the sensor or by a real "superheating" of the solid PCM as described by Tartaglino et al. (2005). As will be discussed in Section 5.6.4, these were not the only occurrences where such effects were visible.

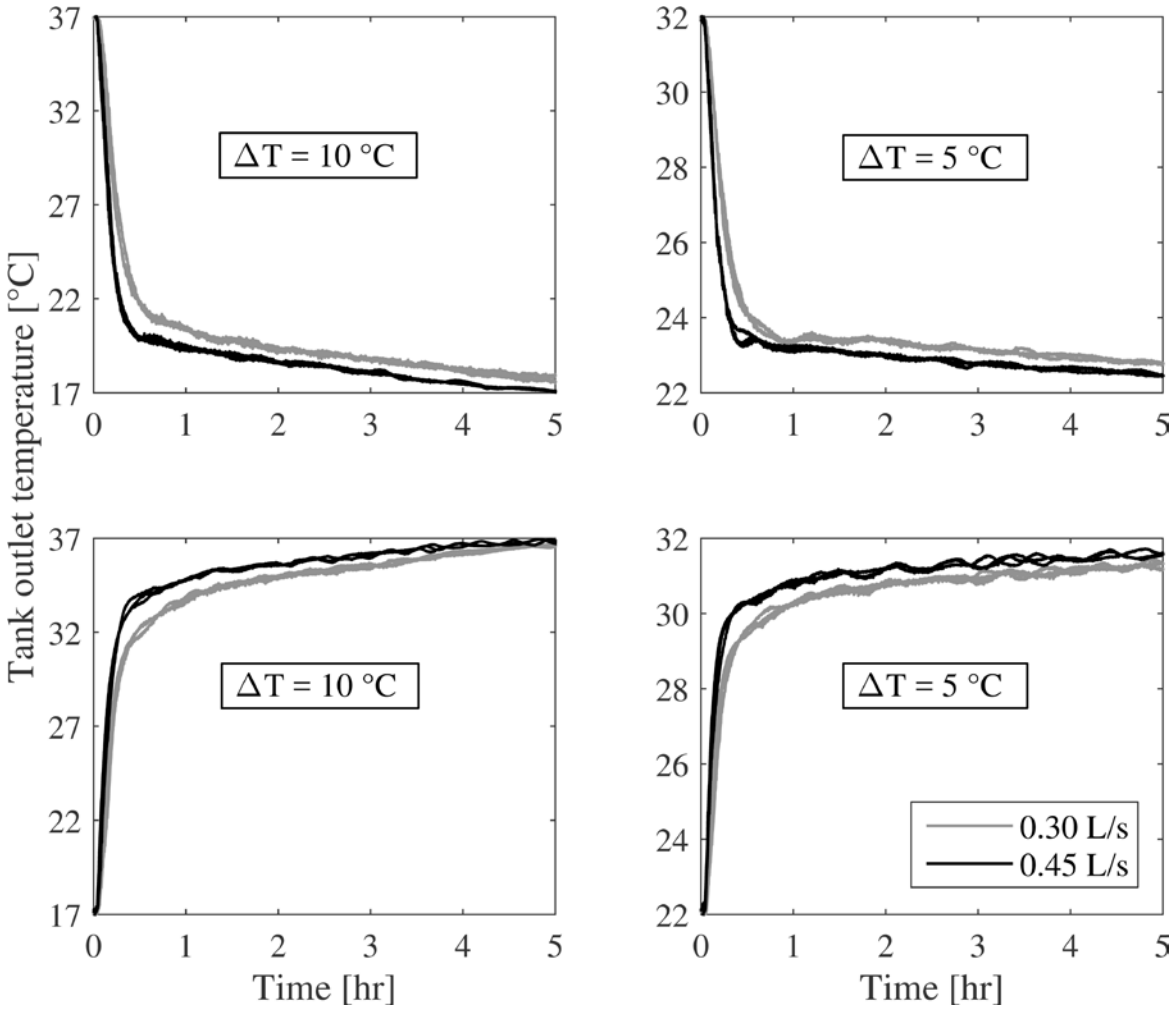

Figure 5-9: Outlet fluid temperature from PCM tank as a function of time for all heating and cooling test repetitions

Figure 5-9 illustrates the time evolution of the tank outlet fluid temperature for all step tests. For each flowrate and temperature differential tested, the three repetitions are barely distinguishable. A rapid and dramatic change in temperature occurs within the first 30 minutes of the test after which the outlet temperature slowly reaches the inlet temperature over many hours. The time profile of the outlet fluid temperature resembles an exponential curve without a clear phase change plateau which, according to Bedecarrats et al. (2009) is indicative of PCM displaying a strong degree of supercooling. The time required for the outlet fluid temperature to reach the inlet temperature is also affected by operating conditions; it appears reduced for increased ΔT and increased flowrates. All these factors indicate that no matter the observed variations in the PCM

behaviour, tests under same conditions lead to predictable thermal behavior for the PCM tank as a whole.

The power output from the PCM tank is defined as:

$$P = \dot{m}\, c_{p,w}(T_{out} - T_{in}) \tag{5-1}$$

where P is the power output [kW], $\dot{m}$ is the fluid mass flowrate [kg/s], $c_{p,w}$ is the water specific heat capacity [kJ/(kg*K)], T_{out} is the tank outlet temperature tank [°C] and T_{in} the inlet tank temperature [°C]. Using the area under the curves from the top two graphs of Figure 5-9 (and the area over the curves in the two bottom graphs) as a quick indicator, operating conditions have an effect on the profile of the power output from the tank. For further analysis, the instantaneous output power from the tank evaluated through Equation (5-1) is illustrated on Figure 5-10 for all operating conditions in both heating and cooling processes.

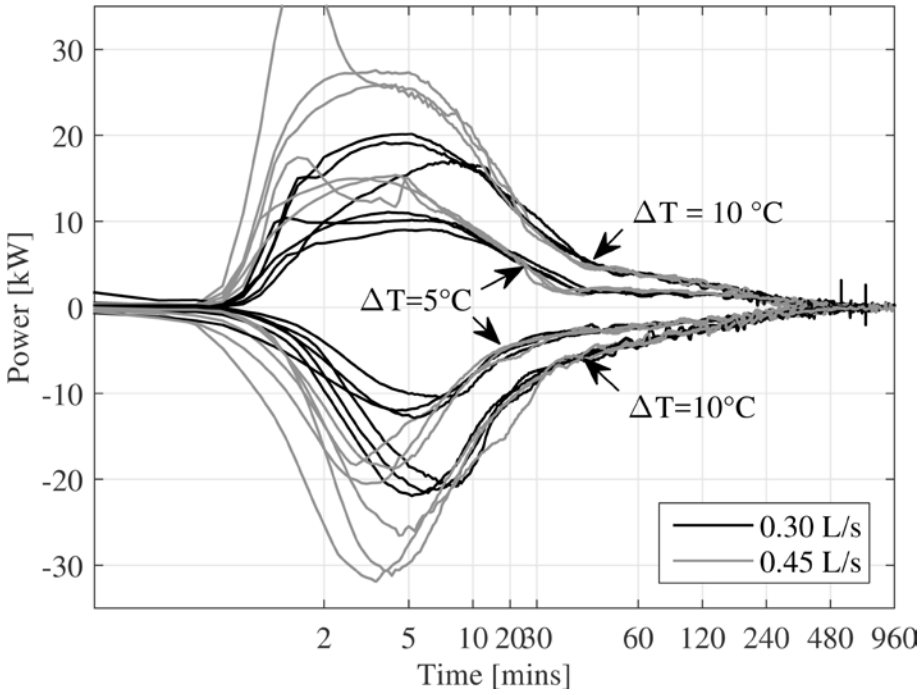

Figure 5-10: Evolution of instantaneous tank power output through logarithmic time

On Figure 5-10, the tank output power for tests previously referred to as “heating tests” (where T_{in} evolves from 17 °C to 37 °C for example) is negative as the outlet fluid temperature, T_{out}, is lower than the inlet fluid temperature, T_{in}. For all tests, the power output undergoes a significant peak over the first 15 minutes and is then reduced at a constant rate until the end of the test. The

fluid flowrate appears to affect the maximum power output reached during the first 15 minutes of the test but after that, its effect on the power output is negligible. The main differences in the maximum power output values are affected by short-term transients in the inlet temperature, which are caused by the laboratory's control system. These differences have a negligible impact on the integrated energy after a few minutes. If these very short transients (not caused by the tank itself) are ignored, the repeatability between tests is very good. Instantaneous power illustrated on Figure 5-10 is limited to 35 kW for a better view, partially omitting some initial peaks.

Though Figure 5-10 extends to 960 mins, only the first 180 mins of the tests are of interest. After that point, the output power from the tank is less than 1.9 kW for $\Delta T = 10\,°C$ and less than 1.15 kW for $\Delta T = 5\,°C$ so any useful effect it may have in most HVAC applications is negligible. The temperature differential, ΔT, affects the tank power output much longer than the flowrate, impacting the power output over the first 180 mins while the latter only affects the maximum power output attained during the initial peak.

Another important aspect to consider in evaluating the usefulness of the power emitted from the tank is the temperature differential produced. Given the accuracy of most temperature sensors implemented in real buildings and controller deadbands, a temperature differential of at least 2 °C is necessary to be useful in most thermal applications in HVAC systems. The moment when the temperature difference between the tank inlet and outlet becomes smaller than 2 °C is listed in Table 5.2 for every test operating conditions. Results indicate that lower flowrates significantly prolong the usefulness of the tank power output, as do greater temperature differentials. It also appears that for greater ΔT, the cooling processes produce a longer useful effect than the heating processes. The significant difference between the two processes hints at supercooling being the likely cause. Previous researchers (Günther et al., 2007; Solomon et al., 2013) explained that the increase in PCM temperature after supercooling requires the absorption of energy from the surrounding material. Depending on the speed of crystallization relative to the rate of heat transport in the material, this can either inhibit or accentuate the formation of a temperature plateau. Thus supercooling can prolong or shorten the time required for the PCM temperature to reach the fluid temperature.

Table 5.2: Duration of the useful power output

ΔT	v̇	Duration of useful power output	
		Heating	Cooling
10 °C	0.3 L/s	120 mins	150 mins
	0.45 L/s	70 mins	95 mins
5 °C	0.3 L/s	40 mins	30 mins
	0.45 L/s	20 mins	20 mins

To analyze the power output from the tank and its useful effect in an HVAC system, the time required to fully charge/discharge the PCM tank must be known. Authors Zalba et al. (2004) and Bedecarrats et al. (2009) have used the outlet fluid temperature as a metric to evaluate the moment at which the PCM tank is fully charged or discharged and evaluated the impact of operating conditions on this charge/discharge time. In this paper, total melt/freeze time was defined as the time required for temperature T_k to reach the inlet temperature. Temperature T_k was taken as either one of three possible metrics: the tank outlet temperature, T_{out}, the temperature measured at the short PCM sensor, $T_{pcm,s}$ or at the long PCM sensor, $T_{pcm,l}$. Considering the imprecise control of the inlet temperature discussed previously and thermopile uncertainty (± 0.04 °C), the tank was considered completely melted/frozen when temperature T_k got to within ± 0.3 °C of the inlet temperature. Average total melt and freeze time (identified by letters “M” and “F” respectively) for all operating conditions tested are presented in Figure 5-11, with error bars corresponding to the standard deviation amongst the three repetitions.

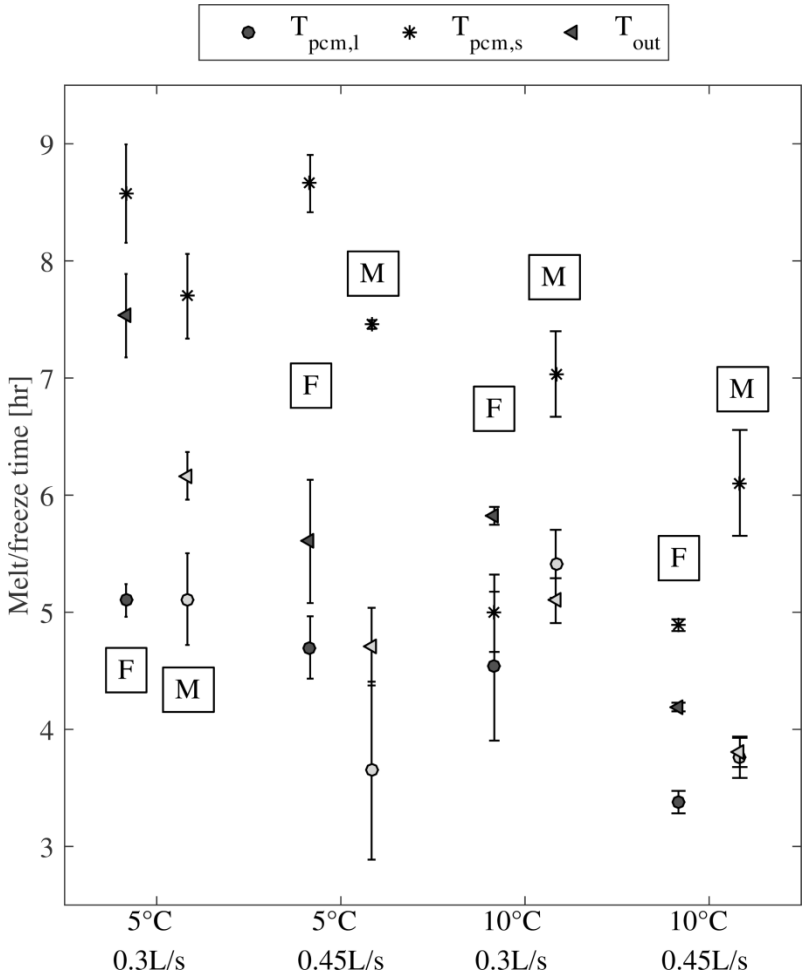

Figure 5-11: Melt (in grey) and freeze time (in black) associated with every flowrate and temperature differential combination calculated through the short, $T_{pcm,s}$, and long PCM sensors, $T_{pcm,l}$, as well as the tank outlet temperature, T_{out}.

Figure 5-11 shows that in most cases average melt and freeze times established through the outlet fluid temperature, T_{out}, are shorter than those calculated with the PCM temperature at the short sensor position, $T_{pcm,s}$. In fact, in some cases (such as both melting and freezing processes with $\Delta T = 10$ °C and $\dot{v} = 0.45$ L/s, for example), T_{out} reaches T_{in} while $T_{pcm,s}$, is still more than 4 °C warmer or colder than T_{in}. In those cases, the output power from the tank is essentially useless for most HVAC applications due to the small temperature difference produced by the tank ($|T_{in} - T_{out}| < 0.3$ °C) but heat exchange between the fluid and the PCM is still taking place. Therefore, control systems should not rely on the outlet fluid temperature from PCM tanks as an indicator that the PCM is fully charged or discharged. Rather, the PCM temperature measured furthest

from the inlet appears to be the most reliable metric and should be used to estimate the average charge/discharge time. Another alternative is for control systems to include a model of the tank estimating the PCM temperature and associated state of charge of the tank from the outlet and inlet temperature history.

Using the melt and freeze time established through the temperature measured at the short sensor as T_k, it appears that an increased temperature differential significantly reduces both melt and freeze times. However, contrary to previous findings (B. Zalba et al., 2004), increasing the flowrate has little impact for this geometry. For $\Delta T = 5$ °C, the average melt and freeze times for $\dot{v} = 0.45$ L/s are within the bounds of the standard deviation of those for $\dot{v} = 0.3$ L/s. For $\Delta T = 10$ °C, the same is true for the freeze time, while only the average melt time does actually decrease with the increase in flowrate. Counterintuitively, supercooling does not result in a solidification time longer than the melting time in all cases. Freezing occurs faster than melting for $\Delta T = 10$ °C even though significant supercooling is present (see Figure 5-7). To further analyse the effect of supercooling on tank behaviour, the degree of supercooling measured at the long and short sensor positions are illustrated in Figure 5-12 for all operating conditions.

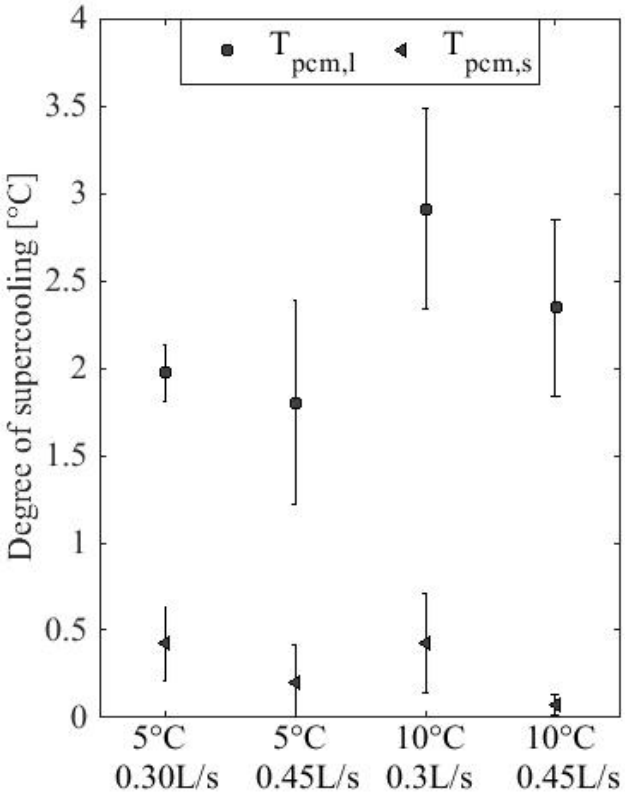

Figure 5-12: Degree of supercooling for all v̇ and ΔT combinations

Supercooling occurs for all combinations tested, but its magnitude and timing differs even within a single PCM capsule. Given the thermocouple uncertainty, supercooling measured by the short temperature sensor is essentially negligible while that measured by the long temperature sensor is significant enough to be further analysed. The rate of heat removal is known to be a significant factor in the supercooling of pure materials (Kozlowski, 2009); magnified thermal shock is said to increase the occurrence and magnitude of super-cooling. Knowing that the PCM located further upstream in the tank will experience sharper changes in fluid temperature, the PCM behaves as expected and a higher degree of supercooling is measured at the long sensor position. Again, when comparing the degree of supercooling at the long sensor across tests, the higher the thermal shock provided by the increased temperature differential heightens the average degree of supercooling measured. However, increasing the flowrate appears to have the opposite effect, slightly decreasing the average degree of supercooling. Solomon et al. (2013) found similar

effects, beyond a certain fluid velocity, their research showed that any further increases had negligible effects on supercooling.

Though the similarity of test conditions amongst repetitions is representative of the accuracy of most building control systems, the variability of the degree of supercooling measured is significant. This variance in the degree of supercooling across repetitions of the same test is however not transposed to the total freeze time; Figure 5-11 indicates total freeze time displays the same spread as total melt time. In summary, the erratic nature of supercooling does not appear to significantly impede the repeatability of the tank output.

5.6.2 Interrupted tests

Numerical modelling of PCMs is often accomplished using an enthalpy-temperature curve (or equivalent specific heat curve) to define the thermal storage behavior. For most PCMs, hysteresis is present between the enthalpy-temperature (h-T) curves followed by the PCM for heating and cooling processes. Various authors have discussed which h-T curve best represents the phase change process when melting is interrupted before phase change is complete (see point 1 on Figure 5-13) and solidification begins again. Bony and Citherlet (2007b) proposed that, after a short transition period, the PCM will begin to behave as it usually does in cooling processes. Its behaviour will be defined by the h-T curve for cooling processes leading to point 2a. Chandrasekharan et al. (2013) instead proposed that the PCM continues to behave as it does during heating, continuing to respect the defined h-T curve for heating processes leading to point 2b. Recent experimental tests by Delcroix et al. (2015) showed an organic PCM adopted an intermediate h-T curve situated between the heating and cooling h-T curves, leading to point 2c. This latter paper also showed the intermediate curve differs for the same PCM according to the operating conditions imposed.

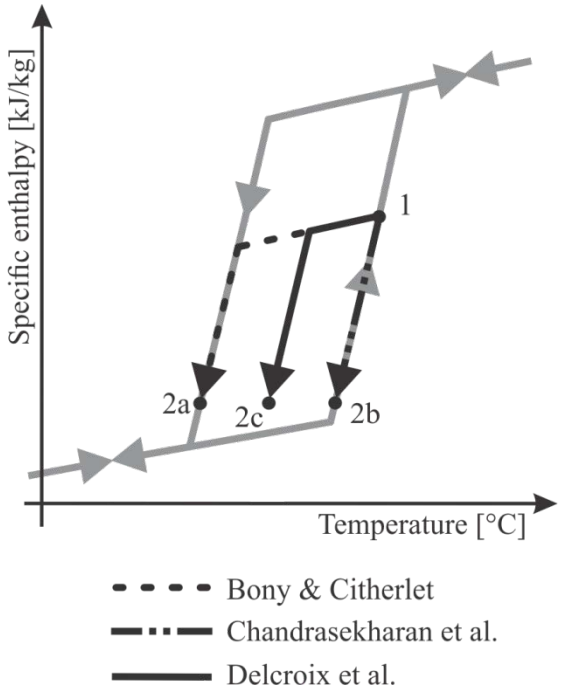

Figure 5-13: Enthalpy-temperature curve followed by PCM according to different authors

In the studied PCM, the presence of strong supercooling renders this question all the more complex if the cooling process is interrupted. Additional tests were undertaken in order to study the dynamic effects of toggling between charging and discharging processes before either is completed. An example of such a test is illustrated in Figure 5-14 for $\dot{v} = 0.3$ L/s and $\Delta T = 10$ °C. The test begins with an initialization period (not shown) during which the entire PCM tank reaches 37 °C, followed by 1 hour of cooling with the inlet temperature at 17 °C. The cooling process is then interrupted before the PCM has completely solidified and heating is resumed. This toggling is repeated until the test includes four interrupted cooling sequences (hours 0 to 1, 2 to 3, 4 to 5 and 6 to 8) and four interrupted heating sequences (hours 1 to 2, 3 to 4, 5 to 6 and 7 to 8).

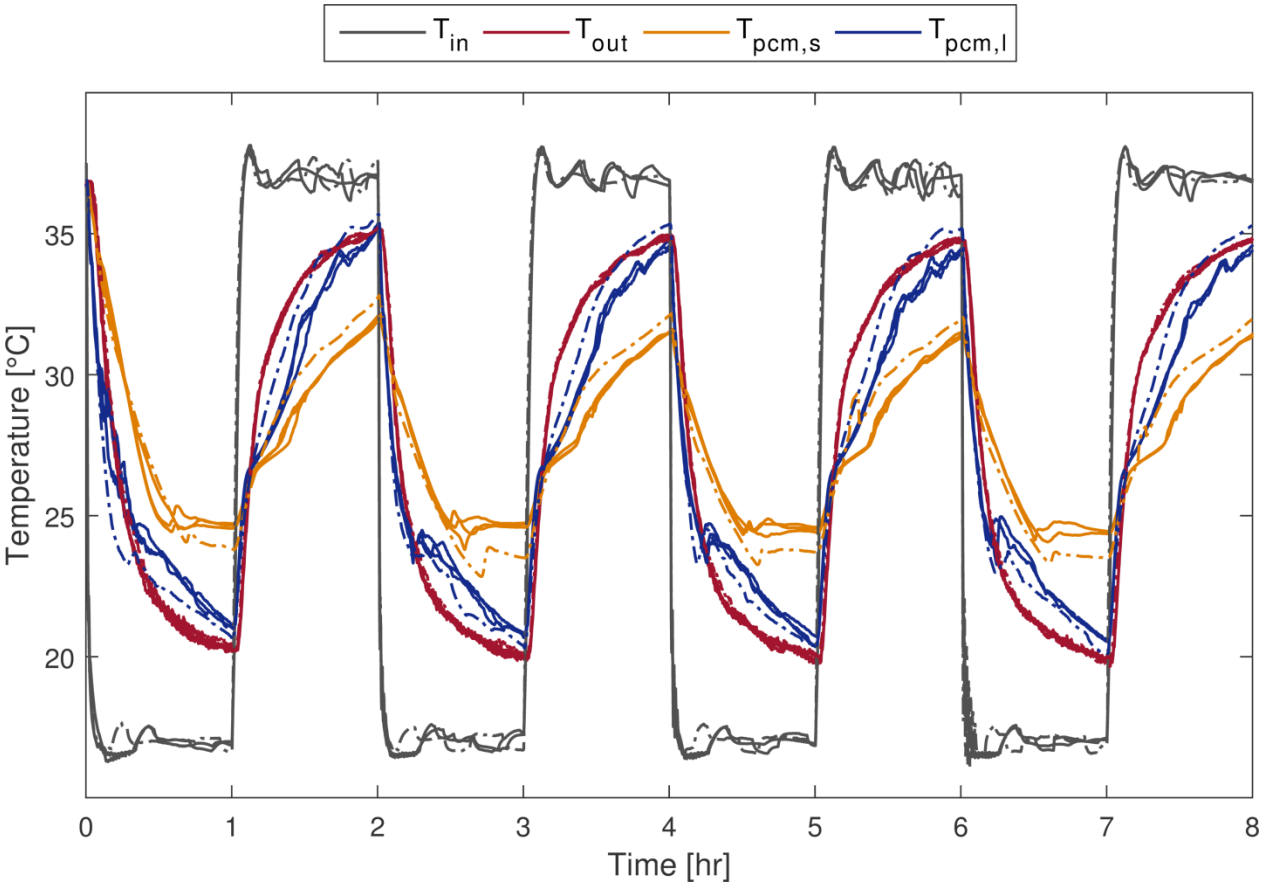

Figure 5-14: Interrupted heating and cooling tests, $\dot{v} = 0.3$ L/s, $\Delta T = 10$ °C, with the fourth repetition indicated by dash-dotted lines

Figure 5-14 displays results from four repetitions of the same 8 hour test, "toggling" between cooling and heating operating conditions. Results are quite similar from one sequence to the next. Even the first cooling sequence (hours 0 to 1) resembles the three later cooling sequences (hours 2 to 3, 4 to 5 and 6 to 8) though it started with the PCM in a fully liquefied state and the others began with the PCM still in transition. The long sensor position indicates supercooling is still present, albeit at a higher temperature of $\simeq 23.5$ °C compared to $\simeq 21.7$ °C for the uninterrupted tests (see top right on Figure 5-7). As expected, since the PCM is not completely solidified when heating begins, the maximum temperature reached at the tank outlet after 1 hour of heating is higher than for the step tests after the same duration; the same logic applies to the cooling tests.

Temperatures measured at the short sensor indicate the PCM is in phase change when conditions toggle from cooling to heating. A plateau is clearly visible at approximately 24.5 °C, the phase

change temperature in these conditions. This is significantly higher than for the step tests held in the same operating conditions (see $\dot{v} = 0.3$ L/s, $\Delta T = 10$ °C on top left of Figure 5-8) where the phase change plateau occurred between 19.8 and 22.8 °C. In heating, only a short plateau is visible at this sensor position, centered at approximately 27 °C. Again, this differs significantly from the results of uninterrupted tests under the same operating conditions (see $\dot{v} = 0.3$ L/s, $\Delta T = 10$ °C on bottom left of Figure 5-8) where the phase change plateau was situated between 30.5 and 33.5 °C. In both heating and cooling processes, the phase change plateau from the interrupted test were closer to those from uninterrupted tests at higher flowrates (see $\dot{v} = 0.45$ L/s, $\Delta T = 10$ °C on top and bottom left of Figure 5-8). These results would indicate hysteresis between heating and cooling h-T curves is reduced for the interrupted tests in comparison to uninterrupted tests in the same conditions. This appears to substantiate Delcroix et al.'s findings that the PCM follows an intermediate h-T curve, situated between its usual heating and cooling curves. Further work on this question is necessary before any final conclusions can be made.

The first three test repetitions all followed one another over a period of 48 hours while the fourth repetition occurred 10 days later. Though not shown here, a stabilization period of 4 hours preceded the toggling process in order to ensure the PCM began in the same state for all repetitions. Nonetheless, the PCM's behaviour during the fourth repetition (identifiable by the dash-dotted lines) clearly stands out. In cooling, greater supercooling is displayed at the short sensor position as well as a lower phase change plateau. In heating, both the temperatures at the long and short sensor positions increase to a higher value than for the other repetitions, even though the PCM at the short sensor began the heating process from a colder state. These results are presented here to highlight the variability of PCM behaviour, indicating that perhaps the "thermal history" of a PCM can influence its future behaviour. Nonetheless, as in the case of the previous step tests, the behaviour of the PCM tank as a whole remains consistent between repetitions.

5.6.3 Fixed temperature change rate tests

Previous sections indicated that operating conditions such as the flowrate, $\dot{v}$, and overall temperature differential, ΔT, as well as the PCM's initial state have an impact on its behaviour. Additional tests were performed to study the effect of milder changes in temperature by imposing

to the PCM tank a specific inlet temperature change rate of 1.25 °C/hr. Results are illustrated in Figure 5-15.

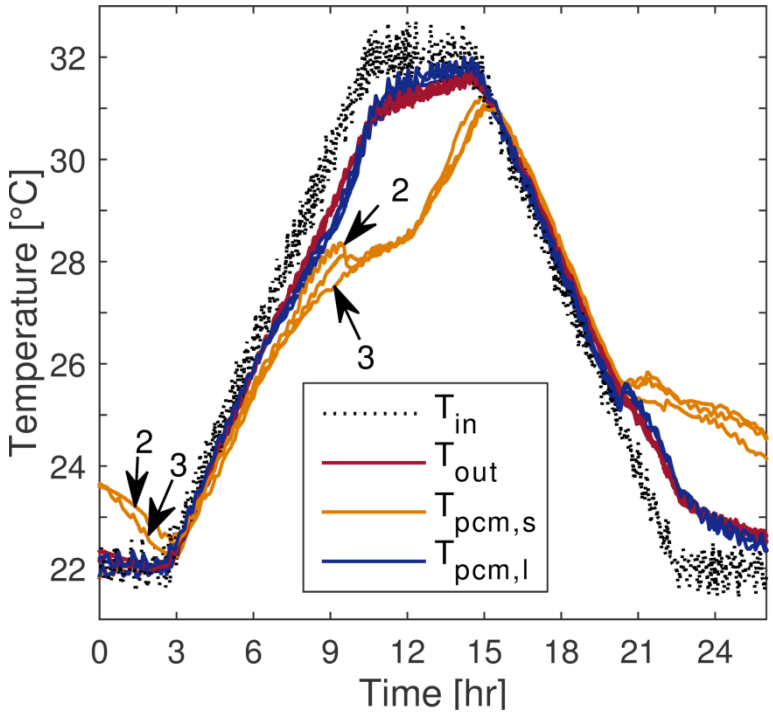

Figure 5-15: Test results for inlet temperature change rate of 1.25 °C/hr, $\dot{v} = 0.3$ L/s

Though the temperature measured at the short sensor position indicates the PCM did not have sufficient time to fully stabilize at 22 °C before the second and third test repetitions began (indicated with arrows “2” and “3” on the Figure), the behaviour measured is still quite similar amongst repetitions. The outlet temperature from the tank and long sensor temperature are indistinguishable between repetitions. It appears that as most of the PCM was completely solid before tests began, the state of the PCM at the short sensor position did not significantly influence the tank outlet temperature.

In heating, although the outlet fluid temperature is initially indistinguishable from the inlet fluid temperature, after 6 hours the two begin to separate. This is likely the moment when the PCM begins to change phase, at least in the first upstream capsule, as the inlet fluid reaches 27 °C at that moment. The sensors measuring the PCM temperature in the downstream capsule indicate it only begins to change phase around 9 hours after the beginning of the test. The same effect is present in cooling where the inlet and outlet temperature begin to separate around 19 hours into

the test when the inlet temperature again reaches the manufacturer specified phase change temperature of 27 °C. The maximum temperature differential attained between the inlet and outlet is approximately 1.3 °C in heating and 1.5 °C in cooling. Both occur at the moment the inlet fluid temperature has reached the full temperature differential for the test, indicating tests limited to smaller temperature differentials around the phase change temperature might not provide suitable conditions for useful power output from the PCM tank.

The short sensor measured a phase change plateau at approximately 28 °C in heating and 25.5 °C in cooling. For step tests with the same flowrate and overall temperature differential (see Figure 5-8, both top and bottom right), the phase change plateau was approximately 30 °C in heating and 24 °C in cooling. On Figure 5-15, the long sensor position also measured an average supercooled temperature of 25.2 °C, while the average supercooled temperature was 23.6 °C at the same sensor position during step tests. Both elements indicate the attenuated change in inlet temperature affected PCM behaviour in a similar manner as the interrupted tests, namely by reducing hysteresis between heating and cooling h-T curves.

5.6.4 Constant power tests

Some potential applications of thermal storage tanks in buildings are to offset a constant load from the HVAC system. In order to assess the PCM tank's potential for such applications, additional tests were performed where the inlet temperature sent to the tank was maintained at 5 °C above or below the tank outlet temperature. Tests were made at a flowrate of 0.3 L/s, resulting in a constant heating/cooling power of 6.24 kW imposed to the tank. This regimen was maintained until the inlet temperature reached the temperature differential of $\Delta T = 10$ °C, which occurred a little after 1 hour, resulting in a rate of inlet temperature change of ~18 °C/hr. Results are illustrated in Figure 5-16 and Figure 5-17 for the heating and cooling processes, respectively.

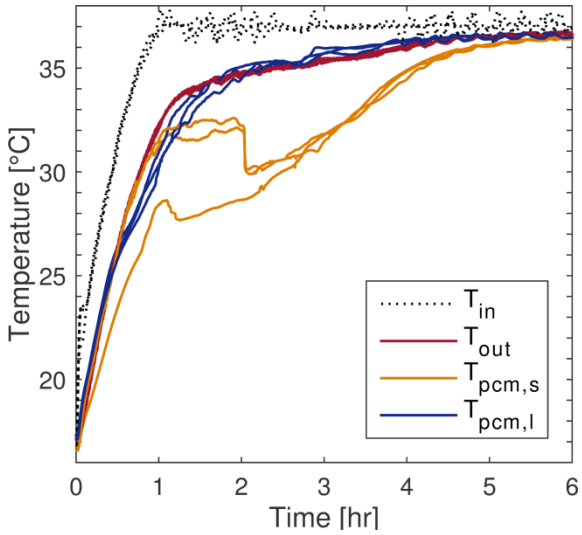

Figure 5-16: Temperature profiles for a heating test at $\dot{v} = 0.3$ L/s and constant power input

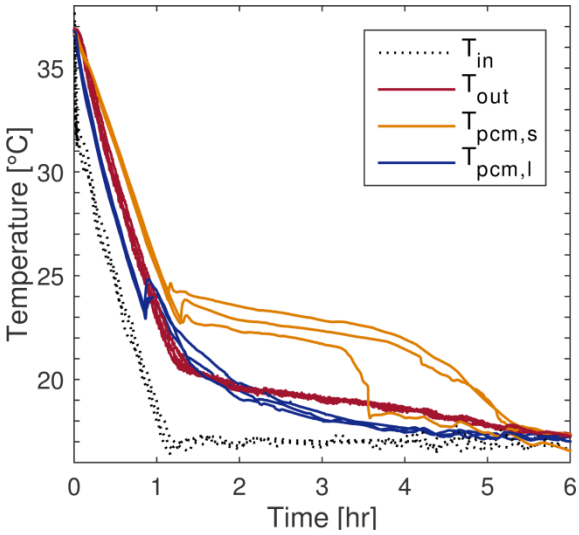

Figure 5-17: Temperature profiles for a cooling test at $\dot{v} = 0.3$ L/s and constant power input

The heating process illustrated in Figure 5-16 shows that the PCM behaviour measured at the long sensor position is again constant amongst test repetitions, as is the overall tank behaviour indicated by the outlet fluid temperature. Temperature $T_{pcm,l}$ increases steadily alongside the outlet fluid temperature for the first 30 minutes or so, until the inlet temperature reaches 27 °C, the manufacturer's specified phase change temperature. Afterwards, the temperature at the long sensor experiences a marked reduction in its slope before it resumes again and catches up to the outlet fluid temperature, eventually surpassing it. This behaviour resembles closely that measured at the same sensor for step tests under similar conditions, namely at $\dot{v} = 0.3$ L/s and $\Delta T = 10$ °C, illustrated on the bottom left graph from Figure 5-7.

In the case of the short sensor measurements, a marked phase change plateau is visible, consistent with behaviour measured in the step tests under similar operating conditions illustrated on the bottom left graph from Figure 5-8. The first and second test repetitions exhibit a sharp drop in temperature ($\simeq 2$ °C) 2 hours after the beginning of the test, shortly after having reached a phase change plateau of approximately 32 °C. These apparent "superheating" effects are similar to those measured at the short sensor in the second repetition of those step tests, identified on Figure 5-8 by "*". Again, the cause of this phenomenon is unclear. The third repetition of the heating test is different. Temperature $T_{pcm,s}$ exhibits a milder slope from the beginning of the test which

persists until a short phase change plateau is reached at 28.5 °C. At this point, the short sensor measures a small drop in temperature ($\simeq$ 1 °C) following which the $T_{pcm,s}$ resumes its increase at a similar slope to that of the two other test repetitions.

In cooling, the degree of supercooling measured at the long sensor position is much milder on Figure 5-17 (0.6 to 1.3 °C) compared to previous step tests under similar conditions ($\dot{v} = 0.3$ L/s and $\Delta T = 10$ °C on Figure 5-13); it more closely resembles the data from the short sensor for these same step tests. All repetitions exhibit a phase change plateau measured by the short sensor which occurs at approximately 24 °C, a similar temperature to those of the step tests. However, in the case of the third test repetition, the plateau ends abruptly after 3.3 hrs, a full hour before the other two repetitions. As in the previous tests analysed, these marked differences in PCM behaviour did not significantly influence the tank outlet temperature which remains constant amongst repetitions.

In both cases the maximum temperature differential attained between the inlet and outlet is significant; it is approximately 5.9 °C in heating and 5.5 °C in cooling. Both occur at the moment the inlet fluid temperature has reached the full temperature differential for the test, approximately 1 hour into the test. A significant temperature differential ($\geq$ 2 °C) remains until a little after the 3rd hour of the test. In comparison, the average duration of useful power output for step tests indicated in Table 5.2 for the same overall temperature differential, $\Delta T = 10$ °C, and flowrate, $\dot{v} = 0.3$ L/s, are 2.0 and 2.5 hrs for the heating and cooling tests respectively. This indicates the slightly milder rates of inlet temperature change (~18 °C/hr) of the constant power tests can increase the duration of useful tank power output by 30 minutes or more compared to step changes. To conclude whether the rates of temperature change expected in HVAC applications can provide the adequate conditions for sustained useful power output from the PCM tank, further analysis is performed in the following section.

5.7 Comparison of useful energy from the tank for all tests

The apparent thermal power provided by the tank is defined in Equation (5-1). To obtain the net thermal power released by the tank, the thermal losses (or gains) to (from) the environment must be taken into account. The net energy released by the tank over a given time interval between t_0 (beginning of the test) and t_e (end of the test) can be obtained by Equation (5-2) :

$$E_{exp} = \int_{t_0}^{t_e} P(t)\,dt - \int_{t_0}^{t_e} UA \cdot (T_{amb}(t) - T_{tank}(t))\,dt \quad (5\text{-}2)$$

where E_{exp} is the net energy calculated from experimental data. The second term on the right subtracts the tank thermal gains from the environment depending on the ambient temperature, T_{amb} and the tank average temperature T_{tank}, which is estimated using the average between the tank inlet and outlet temperature. Term U represents the tank's overall heat transfer coefficient and A is the overall heat transfer surface area.

In Equation (5-2), the test duration, $t_e - t_0$, is first fixed as the total melt/freeze time established as the moment the short temperature sensor, $T_{pcm,s}$, gets within ± 0.3 °C of the inlet temperature. The energy calculated is labelled the total experimental energy, $E_{exp,tot}$, supplied by the tank. A second duration, $t_e - t_0$, is used which is determined by the moment the outlet fluid temperature gets within 2 °C of the inlet temperature, leading to the useful experimental energy output, $E_{exp,use}$.

From data supplied by the manufacturer (see Table 5.1), a theoretical value of the energy contribution from the tank, E_{theo}, can be calculated through Equation (5-3).

$$E_{theo} = V_w \rho_w c_{p,w} \Delta T_{theo} + n_{cap} m_{pcm} c_{p,pcm} \Delta T_{theo} + n_{cap} m_{pcm} h_m \quad (5\text{-}3)$$

The sensible energy change in the water is accounted for by term $V_w \rho_w c_{p,w} \Delta T_{theo}$ and the sensible energy change in the PCM is accounted for by term $n_{cap} m_{pcm} c_{p,pcm} \Delta T_{theo}$. Note that with the definition used above for the temperature differential during a test, ΔT, the temperature change between the start and the end of the test, ΔT_{theo}, is equal to $2 \cdot \Delta T$. The latent energy change in the PCM is accounted for through the latent heat of fusion, h_m, number of PCM capsules, n_{cap}, and each capsule's mass, m_{pcm}.

The values of energy output determined from all three test repetitions are averaged, converted into kWh and illustrated in Table 5.3 for all operating tests. The average values of $E_{exp,use}$, $E_{exp,tot}$ and E_{theo} are respectively denoted by $\overline{E}_{exp,use}$, $\overline{E}_{exp,tot}$ and $\overline{E}_{theo}$.

Table 5.3: Total energy variation in the test for each process and operating condition

Test		ΔT [°C]	$\dot{v}$ [L/s]	$\overline{E}_{theo}$ [kWh]	$\overline{E}_{exp,tot}$ [kWh]	$\overline{E}_{exp,tot}/\overline{E}_{,theo}$	$\overline{E}_{exp,use}$ [kWh]	$\overline{E}_{exp,use}/\overline{E}_{,theo}$
Cooling	Constant power	10	0.30	16.7	15.9	95.2%	11.8	70.7%
	Step	10	0.30		16.2	97.0%	11.5	68.9%
		10	0.45		16.5	98.8%	9.5	56.9%
		5	0.30	13.1	10.9	83.2%	3.0	22.9%
		5	0.45		11.5	87.8%	2.9	22.1%
Heating	Constant power	10	0.30	-16.7	-16.7	100.0%	-9.3	55.7%
	Step	10	0.30		-17.0	101.8%	-10.9	65.3%
		10	0.45		-16.9	101.2%	-9.8	58.7%
		5	0.30	-13.1	-11.6	88.5%	-3.5	26.7%
		5	0.45		-11.8	90.1%	-2.9	22.1%

The tests with constant temperature change rate described in Section 5.6.3 are not included in Table 5.3. These tests were intended to investigate the tank behaviour under milder temperature changes, so that the "useful" energy calculated using the criterion of an inlet-outlet temperature difference larger than 2 °C are never met during the test.

Comparing the average total energy change measured during the experiment, $\overline{E}_{exp,tot}$ to that estimated theoretically, $\overline{E}_{theo}$, shows differences within 5 % for all tests at the larger temperature differential, $\Delta T = 10$ °C. The experimental results show that the full energy output theoretically available has been extracted from the tank at the moment the temperature at the short sensor reaches the inlet temperature. The difference is however significant for the smaller temperature differential, $\Delta T = 5$ °, especially for the lower flowrate where the net total energy calculated from experimental data barely reaches 83.2% of the theoretical value for the cooling process. Such a significant difference hints that the latent heat of fusion might not have been released entirely before declaring the end of the experiments. In other words, the PCM would continue to release or absorb heat, but at such a low rate that this would not result in usable (or even measurable) temperature differences. The increased difference present for tests with lower flowrates strengthens that hypothesis. Knowing these energy variations were established for test durations of 8 hours or more (see Figure 5-11), increasing the test duration to ensure the latent heat of fusion is entirely released appears unreasonable.

The ratios between $\overline{E}_{exp,use}$ and $\overline{E}_{theo}$ show similar, but exacerbated, trends. At most 70 % of the expected energy has been recovered from (or stored into) the storage tank when the inlet-outlet temperature difference drops below 2 °C. The tests with a lower ΔT even show values around 22 %. These results again highlight the importance for future installations of establishing a reliable metric to determine when the tank has been completely charged or discharged, which is a key information for control systems managing thermal storage.

Studying the different test conditions indicates that varying the overall temperature differential has the greatest impact. For step tests with the same flowrate, the larger temperature differential ($\Delta T = 10$ °C) leads to significant increases in both the magnitude of the useful energy output from the tank and its relative importance compared to the theoretical energy storage potential in those operating conditions. In comparison, varying the flowrate of the step test (keeping ΔT constant) does not have as much of an impact. The constant power tests resulted in inlet temperature change rates of approximately 18 °C/hr in heating and 17 °C/hr in cooling which are much closer to the rates of temperature change expected in HVAC applications than step changes in inlet temperature. Though less drastic than step changes, they remain relatively "sharp" changes in inlet temperature compared to the mild rates used in the constant temperature change rate tests (1.25 °C/hr). Comparing results from the constant power tests and step tests under the same conditions, it appears both sets of operating conditions lead to notable useable energy outputs. It is clear optimized use of the PCM tank should favor large temperature differential and sharp changes in inlet temperature (such as those used in Sections 5.6.1 and 5.6.4). The advantage of reducing flowrates should be further investigated.

5.8 Conclusion

This paper presents detailed results from a thorough experimental study of the behaviour of a PCM storage tank containing stacks of commercially available slab-like PCM capsules. Numerous tests were undertaken exploring a range of operating conditions: multiple flowrates and overall temperature differentials, different initial thermal states of the PCM, as well as several inlet temperature profiles.

The results demonstrate that the PCM behaviour varies greatly from the information provided by the manufacturer. Numerous tests exhibited supercooling and hysteresis that are not documented

in manufacturer literature and also showed apparent phase change temperatures different from that reported by the manufacturer.

The systematic repetition of test conditions indicated that the general PCM behaviour can be predicted for specific test conditions. Yet, finer aspects of the PCM's behaviour within the capsule can show a significant variability for repetitions of the same test. Nevertheless, experiments with the same conditions leads to similar thermal behavior for the PCM tank as a whole as proven by the nearly identical outlet temperature profiles. This confirms that the outlet fluid temperature of a latent energy storage tank (hence its energy storage rate) can be accurately predicted by modelling the average behaviour of the PCM.

The variability in the degree of supercooling measured is significant across repetitions of the same test, indicating it cannot be predicted reliably. However, it is likely that supercooling could be neglected without affecting the modelled tank outlet temperature significantly. The same cannot be said for hysteresis which cannot be ignored to model the tank thermal performance.

It has been found that interrupting the PCM's phase change before it is completed affects the apparent phase change temperature of the following test, leading to reduced hysteresis between enthalpy-temperature curves.

The duration for which useful power can be extracted from the tank is found to be significantly lower than that required to ensure the tank is completely discharged. In certain test conditions, when the tank outlet fluid temperature was used as the test stop criteria, the measured energy storage capacity was only 22% of the theoretical value. Mild rates of temperature change (1.25 °C/hr) provided no useful output power over the duration of the tests. Sharper inlet temperatures changes (~18 °C/hr or step changes) should be favored for a greater pro-portion of the theoretical potential energy of the tank to be recovered as a useful energy out-put. Large temperature differentials should also be favored with that purpose in mind.

5.9 Acknowledgments

This work was partly funded by the National Science and Engineering Research Council of Canada (NSERC) through the second author Discovery Grant and through the Smart Net-Zero Energy Building Strategic Research Network (SNEBRN). The first author was also supported by

a Fonds de recherche du Québec – Nature et technologies (FRQNT) doctoral research scholarship.

5.10 References

Arkar, C., Vidrih, B., & Medved, S. (2007). Efficiency of free cooling using latent heat storage integrated into the ventilation system of a low energy building. *International Journal of Refrigeration-Revue Internationale Du Froid, 30*(1), 134-143. doi: 10.1016/j.ijrefrig.2006.03.009

Barreneche, C., Solé, A., Miró, L., Martorell, I., Fernández, A. I., & Cabeza, L. F. (2013). Study on differential scanning calorimetry analysis with two operation modes and organic and inorganic phase change material (PCM). *Thermochimica Acta, 553*(0), 23-26. doi: 10.1016/j.tca.2012.11.027

Bedecarrats, J. P., Castaing-Lasvignottes, J., Strub, F., & Dumas, J. P. (2009). Study of a phase change energy storage using spherical capsules. Part I: Experimental results. *Energy Conversion and Management, 50*(10), 2527-2536. doi: 10.1016/j.enconman.2009.06.004

Bony, J., & Citherlet, S. (2007). Numerical model and experimental validation of heat storage with phase change materials. *Energy and Buildings, 39*(10), 1065-1072. doi: 10.1016/j.enbuild.2006.10.017

Bruno, F., Tay, N. H. S., & Belusko, M. (2014). Minimising energy usage for domestic cooling with off-peak PCM storage. *Energy and Buildings, 76*(0), 347-353. doi: http://dx.doi.org/10.1016/j.enbuild.2014.02.069

Chandrasekharan, R., Lee, E. S., Fisher, D. E., & Deokar, P. S. (2013). An Enhanced Simulation Model for Building Envelopes with Phase Change Materials. *ASHRAE Transactions, 119*(2).

D'Avignon, K., & Kummert, M. (2015a). Assessment of T-History Method Variants to Obtain Enthalpy-Temperature Curves for PCMs With Significant Subcooling. *Journal of Thermal Science and Engineering Applications, 7*(4), 041015-041015. doi: 10.1115/1.4031220

Delcroix, B., Kummert, M., & Daoud, A. (2015). *Thermal behavior mapping of a phase change material between the heating and cooling enthalpy-temperature curves.* Proceedings of IBPC 2015: the 6th International Building Physics Conference, Torino, Italy.

Dolado, P., Lazaro, A., Marin, J. M., & Zalba, B. (2011). Characterization of melting and solidification in a real-scale PCM-air heat exchanger: Experimental results and empirical model. *Renewable Energy, 36*(11), 2906-2917. doi: 10.1016/j.renene.2011.04.008

Dutil, Y., Rousse, D. R., Ben Salah, N., Lassue, S., & Zalewski, L. (2011). A review on phase change materials: Mathematical modeling and simulations. *Renewable and Sustainable Energy Reviews, 15*(1), 112-130. doi: 10.1016/j.rser.2010.06.011

Eames, I. W., & Adref, K. T. (2002). Freezing and melting of water in spherical enclosures of the type used in thermal (ice) storage systems. *Applied Thermal Engineering, 22*(7), 733-745. doi: 10.1016/S1359-4311(02)00026-1

Günther, E., Hiebler, S., Mehling, H., & Redlich, R. (2009). Enthalpy of Phase Change Materials as a Function of Temperature: Required Accuracy and Suitable Measurement Methods. *International Journal of Thermophysics, 30*(4), 1257-1269. doi: 10.1007/s10765-009-0641-z

Kozlowski, T. (2009). Some factors affecting supercooling and the equilibrium freezing point in soil–water systems. *Cold Regions Science and Technology, 59*(1), 25-33. doi: 10.1016/j.coldregions.2009.05.009

Lázaro, A., Dolado, P., Marín, J. M., & Zalba, B. (2009). PCM–air heat exchangers for free-cooling applications in buildings: Experimental results of two real-scale prototypes. *Energy Conversion and Management, 50*(3), 439-443. doi: 10.1016/j.enconman.2008.11.002

Liu, M., Bruno, F., & Saman, W. (2011). Thermal performance analysis of a flat slab phase change thermal storage unit with liquid-based heat transfer fluid for cooling applications. *Solar Energy, 85*(11), 3017-3027. doi: 10.1016/j.solener.2011.08.041

Liu, M., Saman, W., & Bruno, F. (2011). Validation of a mathematical model for encapsulated phase change material flat slabs for cooling applications. *Applied Thermal Engineering, 31*(14-15), 2340-2347. doi: 10.1016/j.applthermaleng.2011.03.034

MacDonald, F., D'Avignon, K., Kummert, M., & Daoud, A. (2014). *A TRNSYS-LabVIEW bi-directional connection for HVAC equipment testing using hardware-in-the-loop simulation.* Paper presented at the 9th International Conference on System Simulation in Buildings 2014, Liege, Belgium.

Moreno, P., Castell, A., Solé, C., Zsembinszki, G., & Cabeza, L. F. (2014). PCM thermal energy storage tanks in heat pump system for space cooling. *Energy and Buildings, 82*(0), 399-405. doi: 10.1016/j.enbuild.2014.07.044

Nallusamy, N., Sampath, S., & Velraj, R. (2007). Experimental investigation on a combined sensible and latent heat storage system integrated with constant/varying (solar) heat sources. *Renewable Energy, 32*(7), 1206-1227. doi: 10.1016/j.renene.2006.04.015

PCM Products Ltd. (2015). Phase Change Materials Products Ltd. Retrieved 2015-11-02, from http://www.pcmproducts.net

Solomon, G. R., Karthikeyan, S., & Velraj, R. (2013). Sub cooling of PCM due to various effects during solidification in a vertical concentric tube thermal storage unit. *Applied Thermal Engineering, 52*(2), 505-511. doi: 10.1016/j.applthermaleng.2012.12.030

Tartaglino, U., Zykova-Timan, T., Ercolessi, F., & Tosatti, E. (2005). Melting and nonmelting of solid surfaces and nanosystems. *Physics Reports, 411*(5), 291-321. doi: 10.1016/j.physrep.2005.01.004

Vakilaltojjar, S. M. (2000). Phase Change Thermal Storage System For Space Heating And Cooling. Ph. D., University of South Australia. Retrieved from http://arrow.unisa.edu.au:8081/1959.8/82317

Wei, J., Kawaguchi, Y., Hirano, S., & Takeuchi, H. (2005). Study on a PCM heat storage system for rapid heat supply. *Applied Thermal Engineering, 25*(17-18), 2903-2920. doi: 10.1016/j.applthermaleng.2005.02.014

Yamaha, M., & Misaki, S. (2006). The evaluation of peak shavings by a thermal storage system using phase-change materials in air distribution systems. *HVAC&R Research, 12*(Supplement 3), 861-869. doi: 10.1080/10789669.2006.10391213

Zalba, B., Marin, J. M., Cabeza, L. F., & Mehling, H. (2004). Free-cooling of buildings with phase change materials. *International Journal of Refrigeration, 27*(8), 839-849. doi: 10.1016/j.ijrefrig.2004.03.015

Zukowski, M. (2007). Experimental study of short term thermal energy storage unit based on enclosed phase change material in polyethylene film bag. *Energy Conversion and Management, 48*(1), 166-173. doi: 10.1016/j.enconman.2006.04.020

CHAPTER 6 ARTICLE 3: MODELING HORIZONTAL STORAGE TANKS WITH ENCAPSULATED PHASE CHANGE MATERIALS FOR BUILDING PERFORMANCE SIMULATION

D'Avignon, K., Kummert, M., (2015). Modeling Storage Tanks With Encapsulated Phase Change Materials for Building Performance Simulation. Submitted to the *Journal of Building Performance Simulation* on November 12th, 2015.

Note: The article version transcribed here is the one submitted with a few minor corrections recommended by the jury.

6.1 Abstract

This paper describes a model developed to simulate the performance of a horizontal storage tank filled with commercially available, slab-like macro-encapsulated phase change material (PCM). It is based on one-dimensional conduction and implemented as a component for the TRNSYS simulation program. Using the thermo-physical properties of the PCM, it maps its thermal behaviour taking into account hysteresis in the enthalpy-temperature curve.

The validity of the modelling assumptions is assessed using a detailed finite-element model. Experimentally measured thermal behaviour of a full-scale PCM storage unit is used to validate the model. A variety of flowrates, inlet temperature profiles and temperature intervals are evaluated in 13 distinct tests. Comparisons between measurements and simulations indicate the validated model can simulate the behaviour of such PCM storage tanks and be used to improve their design for specific applications.

6.2 Introduction

Phase Change Materials (PCMs) have received much attention from researchers lately. Contrary to electrical batteries and flywheels, PCM storage can address a particular clientele looking specifically for energy in the form of heat. Their high-energy storage density and capacity to store and supply energy at nearly constant temperature are advantageous compared to sensible heat storage. As heating and hot water production represented around two-thirds of global energy

consumption in 2008 (International Energy Agency, 2008), phase change materials are of great interest in the building industry.

Recent work by Moreno et al. (2014) showed that a horizontal PCM storage tank could supply an average of 14.5% more cooling energy than a water tank with an identical footprint. Their experimental tests compared the performance of a horizontal water storage tank to that of an identical tank filled with stacks of the commercially-available PCM capsules illustrated on Figure 6-1. Though such results are encouraging, the lack of thoroughly validated numerical models allowing the simulation of such tank's behaviour once inserted in a complex building energy system remains a major obstacle for Heating Ventilation and Air-Conditioning (HVAC) system designers to consider installing them in their projects.

Research has led to numerous detailed models able to trace the evolution in space and time of the phase change boundary in materials. However, these models are often too computationally-intensive to perform long-term analyses and optimization studies of complete building systems. Moreover, Dutil et al. (2011) indicated that the majority of recent studies rely on numerical results from previous researchers to validate their models. As experimental data is rare for most recent geometries, experimental validation is often replaced by experimental verification in limited specific operating conditions.

Simplified models exist for some PCM tank and encapsulation geometries but the study of encapsulated PCM of rectangular geometry has been scarce for liquid heat transfer fluid applications. Elsayed (2007) studied horizontal slab-like capsules of ice exposed to cyclic heat transfer fluid temperatures. He found that the heat transfer fluid temperature has greater impact on the heat transfer efficiency than the convection heat transfer coefficient.

Bony and Citherlet (2007b) modified a pre-existing TRNSYS model of stratified hot water storage tanks named Type 60 to include thermal effects of PCM capsules of various geometries. Results of the simulation of a vertical cylindrical storage tank containing cylindrical PCM capsules showed good agreement to experimental data once internal convection inside the PCM's liquid phase was considered. However, the model was experimentally validated solely for that geometry. Though it allows some flexibility in the definition of the tank and capsule geometries, its convection coefficient is calculated for vertical plates and other limitations inherent to Type 60 remain, indicating it might not simulate horizontal storage tanks as faithfully. Other studies

considered constant temperature boundary conditions (Costa et al., 1998; Hamdan & Elwerr, 1996; Lacroix, 2001; Silva et al., 2002) rather than convective heat transfer due to liquid flow.

A so-called “phase change processor” introduced by Halawa, Saman and Bruno (2010) has been verified against experimental data where air is used as heat transfer fluid (Saman et al., 2005). It was later used in a 1-D model produced by Liu, Saman and Bruno (2011) to simulate the behavior of horizontal PCM tanks for use in refrigerated trucks. Following two experimental tests of a complete melt/freeze cycle, results showed a close agreement between the outlet fluid temperature measured experimentally and its simulated counterpart. The capsule geometry tested is a rigid container in the form of a rectangular prism with no protrusions.

No model has yet been developed for horizontal storage tanks with PCM capsules such as the ones illustrated on Figure 6-1, and we have not found any validation attempt of a generic model for this type of storage tank. This paper presents our attempt to fill this gap and presents a new model for horizontal storage tanks with commercially-available PCM capsules of rectangular geometry. This model is to be used in whole building simulations and has been formulated as a TRNSYS component, emphasis is thus placed on computational efficiency and the accuracy of heat transfer fluid outlet temperature on the time scale of typical building system response. The mathematical model developed is based on a variant of the so-called enthalpy method introduced by Voller (1990) and used by Bony and Citherlet (2007b) for other tank and capsule geometries. As pointed out by Dutil et al. (2011), it is not advisable to use past studies to make general conclusions on what assumptions are reasonable in modelling PCMs, so detailed finite-element modelling is used in this paper to assess the modelling assumptions used. Finally, model results are compared to a series of 13 experimental tests of a real-scale unit with this specific capsule geometry, for a thorough validation using multiple flowrates, inlet temperature profiles and temperature ranges.

6.3 Mathematical model

To ensure compatibility with whole building simulation programs, a numerical model is developed and implemented as a TRNSYS component. A simplified model is built following the principles of the control-volume method (also known as the finite volume method) to ensure conservation of mass, no matter what the grid sizing is (Patankar, 1980). Looking to maximize

computational efficiency in year-long simulations, detailed tracking of the melting front is not a required output. Instead, the physics modelled are simplified as only the evolution of the outlet fluid temperature and global state of charge of the PCM tank are of interest. These outputs need be determined with sufficient accuracy on the time scale of typical building Heating, Ventilation and Air-Conditioning (HVAC) systems response. In this work, we assume that these requirements translate into an accuracy of ±1 °C over 5 min intervals.

The geometry modelled is that of a horizontal tank including horizontal slab-like HDPE capsules filled with PCM. As can be seen on Figure 6-1, the capsule's top and bottom surfaces are covered with a series of plastic protrusions that fit together to maintain a preset clearance between the capsules. This creates a small channel into which heat transfer fluid (HTF) can circulate above and below each capsule. The capsule top and bottom surfaces also have a series of holes that penetrate to its center, presumably for additional rigidity. Finally, its downstream lateral face includes a depression where the sealed filling orifice is located.

Figure 6-1: Flat slab-like PCM capsule

In the model, the complex capsule geometry is reduced to a simple rectangular prism represented in orange on Figure 6-2. Looking at the schematic latent energy storage tank from the heat transfer fluid entry point, we observe the PCM capsules are laid out in a number of columns which extend over the length (i.e. x-axis) of the PCM tank. Each column contains a certain number of rows over the width of the tank (i.e. z-axis) containing layers of capsules stacked vertically (i.e. y-axis). In this example, the layout consists of 4 layers of capsules arranged in 2 columns and 3 rows.

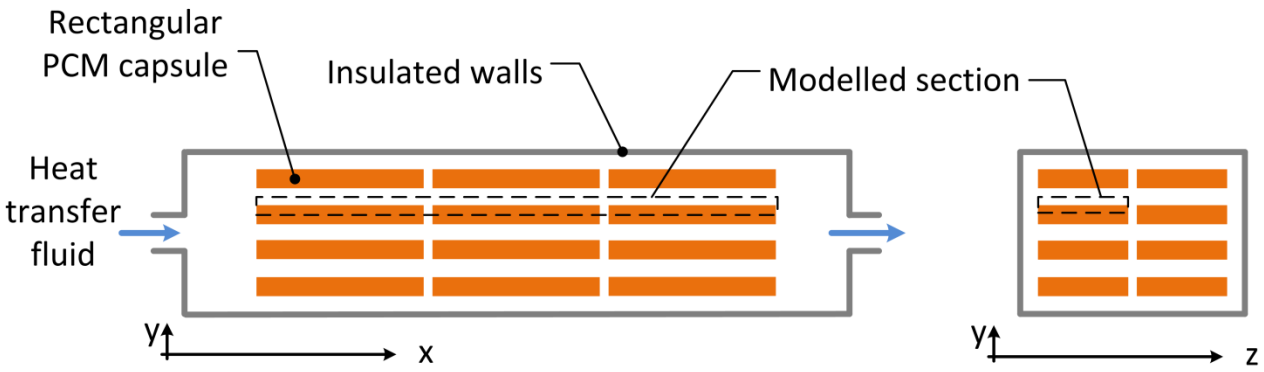

Figure 6-2: Modelled section of the PCM storage tank

As the fluid flow is considered uniformally distributed throughout the cross-section yz, the model considers the behaviour of only one layer of capsules along a single column. All the rows of that column are treated as though they were a single capsule whose results are extrapolated to represent the behaviour of the entire PCM tank. Exploiting the symmetrical nature of the PCM capsules, only the half-height of the PCM capsule and half-height of the fluid passage are modelled (see the doted area on Figure 6-2).

Heat transfer to/from the capsules is simplified by two main assumptions. Natural convection within the liquid phase of the PCM is neglected because of the thin, flat nature of the containers used and their horizontal layout (as indicated by Zivkovic and Fujii (2001)). As the capsules are tightly squeezed against one another, we also assume that the lateral capsule faces do not significantly contribute to the heat transfer within the PCM. Instead, the predominant mode of heat transfer within the PCM occurs through conduction along the y-axis so that the full width of the PCM capsule (z-axis) is represented by only one PCM control volume. The same assumption is made for the fluid control volumes where no significant thermal gradients are expected along the z-axis.

Detailed modelling of fluid flow between two PCM capsules can rapidly decrease the prospects of obtaining a reasonable computation time. So, as seen on Figure 6-3, a uniform velocity profile is assumed and the full half-height of the fluid passage can be modelled by a single fluid control volume. The simplified TRNSYS model uses a series of fluid control volumes over the length of the PCM capsule (along the x-axis), each fluid control volume encompassing the half height and

full width of the fluid passage modelled. Similarly, only the half the height of the PCM capsule is modelled, though it is discretized in several control volumes along the y-axis.

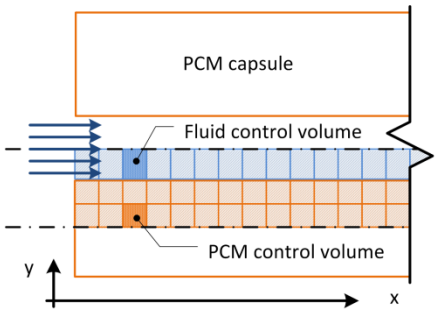

Figure 6-3: Modelled section of the PCM tank (between the two dotted lines) is discretized into several control volumes (illustrated here for 2 PCM control volumes in the y direction)

The present model uses semi-explicit time-discretization, implementing an internal time-step when necessary. TRNSYS functions in such a way that any information passed along between components during an iteration are the time-averaged values over the time step concerned. Therefore time-averaged values of the entering fluid temperature and fluid flow rate are the input data to the model no matter what time-discretization scheme is used inside the model. Implicit discretization would theoretically offer the advantage of numerical stability even with the use of the large time steps (Incropera, Dewitt, Bergman & Lavine, 2007) used in the case of yearly building simulations. A recent study indicates that it allows the use of time steps as large as 15 minutes in the simulation of PCM wall layers without compromising accuracy (Al-Saadi & Zhai, 2015). Numerical stability however does not ensure physically-plausible results. The Courant-Friedrichs-Lewy condition (de Moura & Kubrusly, 2013) indicates the small residency time of the fluid in the PCM tank (< 1 min) requires relatively small time steps or significant relaxation to ensure physically-plausible results in transient conditions. Moreover, though explicit time-discretization schemes are not unconditionally stable, they offer the advantage that a clear and easy to implement criteria exists to ensure stability (Incropera et al., 2007) which is why they were chosen as the time-discretization scheme for this model.

The model considers the three modes in which the latent energy storage tank functions. First, the storage tank must be “charged” by melting or solidifying the PCM depending on whether heat or cold is to be stored. When the demand occurs, the tank’s energy is then “discharged” as the PCM

goes through the reverse change of phase. The third mode encompasses what happens in between, that is during the period when the tank is keeping the stored energy; the “waiting” mode. The first two modes function very much in the same way; forced convection between the PCM capsule wall and the heat transfer fluid is the predominant method of heat transfer. The “waiting” mode usually implies no fluid flow coming in or out of the latent energy storage tank and natural convection in the heat transfer fluid becoming important. In order to optimize the model’s computational efficiency, separate mathematical formulations are used depending on the relative importance of advection and diffusion in the fluid, using the thermal diffusion Peclet number, Pe, as a criteria.

6.3.1 Significant flow conditions | Pe > 2

For each fluid control volume considered, the energy balance results in Equation (6-1):

$$\frac{\rho_f c_{p,f} V dT}{dt} = \dot{m} c_{p,f} (T_{in} - T_{out}) + h_{eq} S_x \left(T_{pcm} - T_f\right) \tag{6-1}$$

The term on the left represents the net rate of energy stored in the fluid control volume over a certain time step, with $\rho_f c_{p,f} V$ being the fluid’s heat capacity. The term $\dot{m} c_{p,f} (T_{in} - T_{out})$ represents the net rate of energy transport into the control volume through advection. The term $h_{eq} S_x \left(T_{pcm} - T_f\right)$ represents the net rate of energy exchanged between the fluid and the PCM through convection, with h_{eq} the equivalent heat transfer coefficient and S_x the surface area of the heat exchange between the fluid and PCM control volumes.

For cases with high Peclet number (Pe > 2), the fluid flow causes energy transfer between fluid control volumes to occur mainly in the direction of flow. In this case, the influence of downstream conditions on the fluid temperature is low and space can be considered a one-way coordinate (Patankar, 1980). Hence, the upwind scheme is used as a spatial discretization method for the fluid control volume equation. A solution is then obtained by marching through the control volumes in the direction of flow and solving for the fluid control volume temperature and the associated PCM control volumes’ state to within the limits of the convergence criteria before moving on downstream to the next fluid control volume.

Using central time differentiation to solve for Equation (6-1) results in the formulation illustrated in Equation (6-2):

$$\left\{\frac{\rho_f c_{p,f} V}{\Delta t} + \frac{\dot{m} c_{p,f}}{2} + \frac{h_{eq} S_x}{2}\right\} \cdot T_{f,(i)} = \dot{m} c_{p,f} \cdot \bar{T}_{f,(i-1)} + \left(\frac{\rho_f c_{p,f} V}{\Delta t} - \frac{\dot{m} c_{p,f}}{2} - \frac{h_{eq} S_x}{2}\right) \cdot T_{f,(i)}{}^{0} + h_{eq} S_x \cdot \bar{T}_{pcm,(i,1)} \quad (6\text{-}2)$$

Here $T_{f,(i)}$ is the temperature of a given fluid control volume and similarly, $T_{pcm,(i,1)}$ is the temperature of the adjacent PCM control volume. In this formulation, values from the previous time step are indicated with superscript "0" while values from the present time step bear no annotation and time averaged values are indicated with an overline (ex. $\bar{T}$ indicates the time-averaged temperature). The upstream control volume is indicated with subscript "(i-1)" and the control volume calculated bears subscript "(i)". More details on the method used to identify the various control volumes can be seen in Figure 6-4.

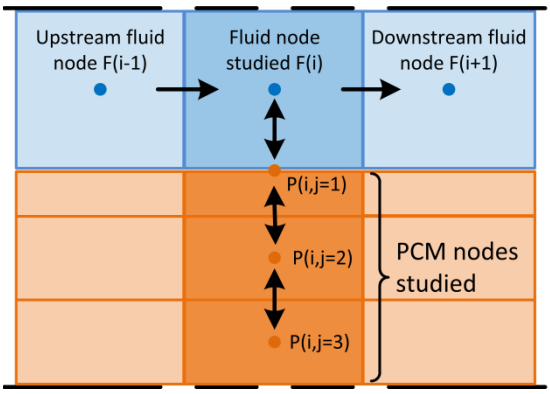

Figure 6-4: Model discretization

In the calculation of the heat transferred by convection to the PCM, the thermal mass of the capsule wall is neglected and an equivalent heat transfer coefficient, h_{eq}, is determined to account for all thermal resistances between the fluid and PCM. As the node of the PCM control volume closest against the capsule wall is situated at the capsule wall, the thermal resistance of the PCM itself is not present in the coefficient. The equivalent heat transfer coefficient used is provided by Awad's correlation for a thermally and hydraulically developing laminar flow between two plates at constant temperature (Awad, 2010). The same equivalent convection coefficient is applied to every fluid control volume, but this coefficient will change in time throughout the simulation in response to varying flow velocities.

To determine the fluid's impact on the PCM control volume, a variant of the so-called enthalpy method is used where the temperature field in the PCM is not calculated explicitly but through enthalpy-temperature correlations. Thus, the change in the state of the PCM control volume adjacent to the capsule surface is determined by calculating the change in enthalpy produced by the energy flux between the fluid and PCM control volume (see Equation (6-3)). For other PCM control volume, solely conduction heat transfer from upper and lower PCM control volumes is considered, as indicated in Equation (6-4).

For surface control volume, j = 1

$$H = H^0 + \left\{ h_{eq} S_x \left(\bar{T}_{f,(i)} - \bar{T}_{pcm,(i,j)} \right) + \frac{k_{pcm,(i,j+1\rightarrow j)} S_{pcm}}{\Delta y} \left(\bar{T}_{pcm,(i,j+1)} - \bar{T}_{pcm,(i,j)} \right) \right\} \cdot \frac{2\Delta t}{m_{pcm}} \tag{6-3}$$

For interior control volumes, j > 1

$$H = H^0 + \frac{S_{pcm}\Delta t}{\Delta y \, m_{pcm}} \cdot \left\{ k_{pcm,(i,j-1\rightarrow j)} \left(\bar{T}_{pcm,(i,j-1)} - \bar{T}_{pcm,(i,j)} \right) + k_{pcm,(i,j+1\rightarrow j)} \left(\bar{T}_{pcm,(i,j+1)} - \bar{T}_{pcm,(i,j)} \right) \right\} \tag{6-4}$$

Where H is the current PCM enthalpy and H0 is the PCM enthalpy for the same PCM control volume from the last time step. The PCM thermal conductivity, k_{pcm}, varies with temperature, hence it is different for different control volumes. Conductive heat transfer between two PCM control volumes is based on the harmonic mean of these two control volumes' thermal conductivity. An example is shown in Equation (6-5) between nodes (i,j-1) and (i,j):

$$k_{pcm,(i,j-1\rightarrow j)} = \frac{2 k_{(i,j)} k_{(i,j-1)}}{k_{(i,j)} + k_{(i,j-1)}} \tag{6-5}$$

Following the calculation of the PCM control volume enthalpy, the new PCM control volume temperature is then found through interpolation of the enthalpy-temperature curve which will be further explained in Section 6.3.3.

At every time step, a stable solution is found for each control volume through the comparison of the different temperatures in the tank at the current and past time steps. The absolute change in temperature between two iterations must be less than 10^{-3} °C for the PCM temperature and HTF

temperature for convergence to be reached. This method ensures that a minimal number of iterations are required.

6.3.2 Negligible flow conditions | Pe < 2

For cases with low Peclet number, we assume that the heat transfer between the fluid and PCM control volumes is caused solely by natural convection occurring in the fluid. Conduction between fluid control volumes becomes an important heat transfer mode and so a central-difference scheme is used for spatial discretization of the fluid control volume heat balance equation, resulting in Equation (6-6):

$$\frac{\rho_f c_{p,f} V dT}{dt} = \dot{m} c_{p,f}(T_{in} - T_{out}) + h_{eq} S_x \left(T_{pcm} - T_f\right) + \frac{k_f A_f}{\Delta x}\left(T_{f,(i-1)} - 2T_f + T_{f,(i+1)}\right) \tag{6-6}$$

where A_f is the surface area of the fluid passage, k_f is the fluid thermal conductivity and Δx the length of the fluid control volume. Using central time differentiation results in Equation (6-7).

$$\begin{aligned}\left(\frac{\rho_f c_{p,f} V}{\Delta t} + \frac{k_f A_f}{\Delta x} + \frac{h_{eq} S_x}{2}\right) \cdot T_{f,(i)} \\ = \left(\frac{\rho_f c_{p,f} V}{\Delta t} - \frac{k_f A_f}{\Delta x} - \frac{h_{eq} S_x}{2}\right) \cdot T_{f,(i)}{}^{0} + \left(\bar{T}_{f(i-1)} + \bar{T}_{f(i+1)}\right)\frac{k_f A_f}{\Delta x} + h_{eq} S_x \bar{T}_{pcm,(i,1)}\end{aligned} \tag{6-7}$$

In this case, the equivalent heat transfer coefficient is determined using Globe and Dropkin's correlation for natural convection in a horizontal cavity (Incropera et al., 2007). The new PCM control volume temperature is still found through interpolation of the same enthalpy-temperature curve referred to previously.

In this case, both the upstream and downstream fluid conditions will influence the fluid temperature and so a solution is obtained for all fluid and PCM control volumes in the tank before verifying whether the convergence criterion is satisfied. This method requires more iterations per time step than the marching-time procedure used in significant flow conditions and negatively affects calculation time.

6.3.3 Enthalpy-temperature curve and hysteresis

During phase transition, both liquid and solid phases are present in the PCM. They are separated by an interface composed of both phases (defined as a “mushy” state) that is constantly shifting position. On each side of this boundary, the properties of the material can be quite different so predicting the behaviour of a PCM during phase change is categorized as a moving boundary problem for which multiple numerical methods have been developed (Bansal & Buddhi, 1992). The method used here is a variant of Voller’s (1990) enthalpy method and does not require the boundary position to be traced throughout the domain. In fact, as this method uses the same governing equation for the two phases it avoids any sharp discontinuities at the phase change interface. Other authors have used it successfully to simulate the behaviour of PCM capsules (Bony & Citherlet, 2007b; Puschnig et al., 2005). The method relies on an enthalpy – temperature curve to calculate the temperature of each PCM control volume. Though these curves are rarely supplied by PCM manufacturers, they can be determined experimentally through the T-history method (Jose M. Marín et al., 2003). Figure 6-5 illustrates an example of such curves for a PCM with hysteresis.

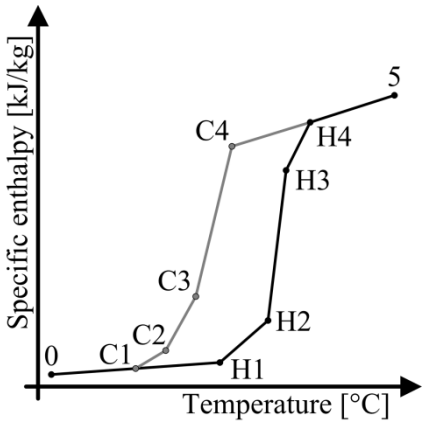

Figure 6-5: Schematic of an enthalpy-temperature curve with hysteresis

In this example, two curves relate the specific enthalpy and temperature of a material; the one annotated with “C” represents the cooling process and the other annotated with “H” represents the heating process. The model is designed to handle such a case as this, where hysteresis is present between the heating and cooling processes, provided that the supplied enthalpy-temperature curves follow certain guidelines. First, the model requires the two enthalpy-

temperature curves be built of linearly increasing functions expressed through 6 data points pairs. The two curves must share a common overall enthalpy variation over the temperature range over which they are defined (i.e. points 0 and 5 are common to both). In addition, the liquid specific heat must be the same for both processes so the slope from point C4 to 5 must be the same as that from H4 to 5. The same is true for the solid phase (common slope from point 0 to C1 and 0 to H1). In order to assess the PCM's state of charge, the PCM will be considered fully solid at any temperature below C1 and completely liquid at any temperature above H4.

The presence of hysteresis between the heating and cooling curves introduces the question of what happens when either process is interrupted. Figure 6-6 illustrates the different behaviours proposed when heating is interrupted without the PCM having completely melted (see point a).

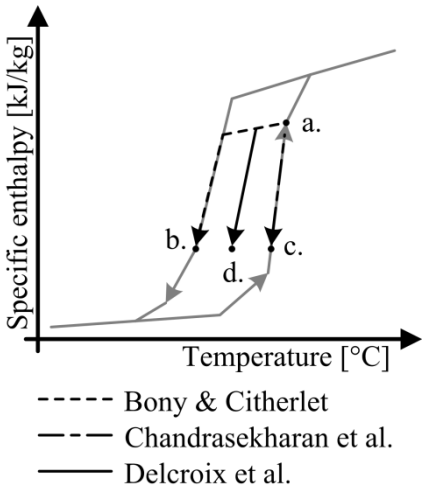

Figure 6-6: Enthalpy-temperature curve followed by PCM according to different authors

Bony and Citherlet (2007b) proposed that the PCM transitions from one curve to the next following the average slope of the liquid and solid states (i.e. average of slope C4 to 5 and slope 0 to C1 from Figure 6-5) and then simply reintegrates the appropriate h-T curve. This behaviour is defined by the h-T curve for cooling processes leading from point a to point b on Figure 6-6. Chandrasekharan et al. (2013) instead proposed that the PCM continues to follow the defined h-T curve for heating processes leading from point a to point c. Recent experimental tests by Delcroix et al. (2015) showed an organic PCM adopted an intermediate h-T curve situated between the heating and cooling h-T curves, shown schematically on Figure 6-6 as that between point a. and point d. This latter study also showed the intermediate curve differs for the same PCM according

to the operating conditions imposed, which is similar to the behaviour recorded in detailed experimental tests on the specific geometry under study (D'Avignon & Kummert, 2015b). As no theory has yet been devised to define what the intermediate curve should be, the model in this case adopts the Bony and Citherlet theory that the PCM will transition towards and then follow the cooling curve.

6.4 Preliminary study through detailed model analysis

The validity of the assumptions made in the present model was evaluated in a preliminary study. This study also permitted to assess the limitations associated with the use of such a simplified model in lieu of a more physically accurate but computationally-intensive model. Detailed finite element models built in COMSOL Multiphysics (2015) were used as a target for comparison. In these models phase change is accounted for by treating the PCM as a pseudo porous media; a solid porous matrix with a liquid media flowing through it. The time-varying proportion of the fluid to the porous matrix (a.k.a the liquid fraction) is controlled by the evolution of the domain's enthalpy along the enthalpy-temperature curve, as it is done in Brent et al's enthalpy-porosity approach (1988). The heat equation and continuity equation control the heat flow.

6.4.1 Fluid flow

In the simplified TRNSYS model, fluid velocity used in calculating the heat transfer coefficient is obtained from the fluid mass flow rate entering the tank assuming a uniform fluid velocity profile across the height of the fluid passage and full width of the tank. This assumption implies that both the real capsule geometry (namely the protrusions and holes along both its upper and lower surfaces) and real fluid flow profile can be neglected. To evaluate the validity of this assumption, different detailed finite elements models were built in COMSOL Multiphysics and compared.

The first detailed model (hereafter referred to as "Model 1") represents a finite element version of the simplified TRNSYS model. It uses the same simplified geometry as the proposed TRNSYS model; the PCM capsules and their associated fluid passages modelled as rectangular prisms and only the half height of both are considered. Model 1 is two-dimensional and imposes a boundary condition at the capsule wall to force fluid flow to "slip" along the capsule face, thus keeping the

fluid velocity profile undeveloped over the length of the capsule as illustrated on the left side of Figure 6-7.

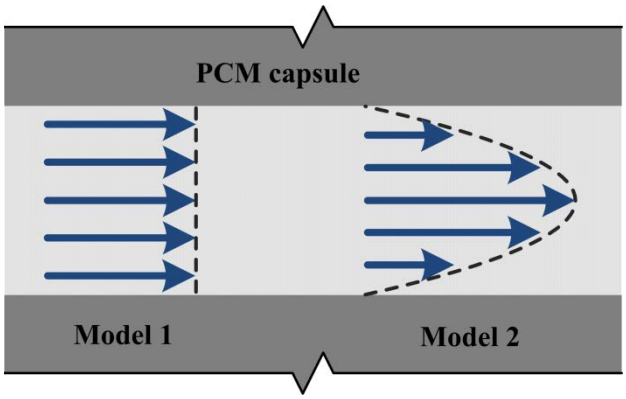

Figure 6-7: Fluid flow profiles studied

Model 2 is a duplicate of Model 1 but the boundary condition at the capsule wall is a null fluid velocity, forcing the fluid flow to develop into a boundary layer following the continuity equation and the Navier-Stokes equation, as illustrated on the right side of Figure 6-7. Lastly, a 3D model considers the impact of the real capsule geometry on the flow velocity profile. Model 3 has the same null fluid velocity condition at the capsule surface as Model 2. In this case, the series of protrusions along the capsule's top and bottom surfaces are modelled, as well as the series of holes along these surfaces that penetrate to the capsule centre. The depression and sealed filling orifice on the capsule's downstream lateral face however are not considered. The realistic geometry increases the PCM volume by only 0.025% compared to Models 1 and 2 but increases the heat transfer surface by 3.9 %.

In all COMSOL models, the evolution of the fluid flow profile over the length of the PCM capsule is simulated through the use of the continuity equation and the heat equation. A flat velocity profile condition is imposed to the fluid coming into the vertical space between two capsules. Water is used as the heat transfer fluid with thermal properties held constant at the values found in Table 6.1. The PCM modelled is a heterogeneous salt hydrate named S46 (PCM Products Ltd, 2015) whose properties are also in the Table. The PCM capsule modelled is commercially available (PCM Products Ltd, 2015) in dimensions of 0.5 m long, 0.25 m wide and 0.038 m in height, with a spacing of 0.013 m between two stacked capsules to allow fluid passage.

Table 6.1: Material characteristics

Fluid properties	**Value**	**Units**
Specific heat	4182	J/(kg-°C)
Density	988.99	kg/m^3
Thermal conductivity	0.62556	W/(m-°C)
Dynamic viscosity	$5.86*10^{-4}$	Pa*s
PCM S46 properties[5] (manufacturer data)	**Value**	**Units**
Specific heat capacity	2410	J/(kg-°C)
Volumetric heat capacity	333	MJ/m^3
Density	1587	kg/m^3
Thermal conductivity	0.450	W/(m-°C)
Latent heat of fusion	210 000	J/kg
Melting temperature	46.1	°C
Freezing temperature	45.9	°C
Initial temperature	30.0	°C

The test case detailed in Table 6.2 was used to evaluate the PCM capsule's behaviour. Results are presented for a fluid entry velocity of 0.01 m/s (different fluid velocities between 0.01 m/s and 0.05 m/s showed similar results). Results are presented for a heating case with the PCM remaining in its solid phase.

Table 6.2: Data for simulation test cases

Test Case 1 Heating, low fluid velocity		
Initial conditions	Fluid and PCM temperature	30 °C
	Fluid velocity	0 m/s
t = 0 s to 3000 s	Fluid and PCM temperature	45 °C
	Fluid velocity	0.01 m/s
Test Case 2 Alternating heating and cooling, with waiting period		
Initial conditions	Fluid and PCM temperature	30 °C
	Fluid velocity	0 m/s

[5] The properties listed have been copied exactly as found in manufacturer data.

Table 6.2 (continued): Data for simulation test cases

t = 0 s to 8 hrs	Fluid and PCM temperature	53 °C
	Fluid velocity	0.01 m/s
t = 8 hrs to 12 hrs	Fluid and PCM temperature	53 °C
	Fluid velocity	0 m/s
t = 12 hrs to 20 hrs	Fluid and PCM temperature	39 °C
	Fluid velocity	0.01 m/s
t = 20 hrs to 24 hrs	Fluid and PCM temperature	39 °C
	Fluid velocity	0 m/s

Thermohydraulic simulations of Case 1 resulted in the expected fluid velocity profile; the flow profile remains constant along the height of the fluid passage and along the length of the PCM capsule at a value of 0.01 m/s throughout the simulation. In the case of Model 2, results indicate the fluid forms a fully developed profile that reaches velocities of up to 0.0149 m/s. The flow profile evolves rapidly becoming fully developed in less than 40 s, at a distance of 0.2 m from the leading edge of the PCM capsule. As most applications studied will imply the use of more than one capsule in over the length of the tank and flow velocities will be kept constant for elongated periods of time, correlations representing hydraulically developed flow should be used.

Figure 6-8 illustrates the velocity profile of the heat transfer fluid from Model 3 at t=1500 s. In the sections behind the protrusions, flow velocity tends towards zero. Where no protrusions interfere, the flow velocity is much higher than the 0.01 m/s imposed in the simplified TRNSYS model, reaching velocities as high as 0.0275 m/s.

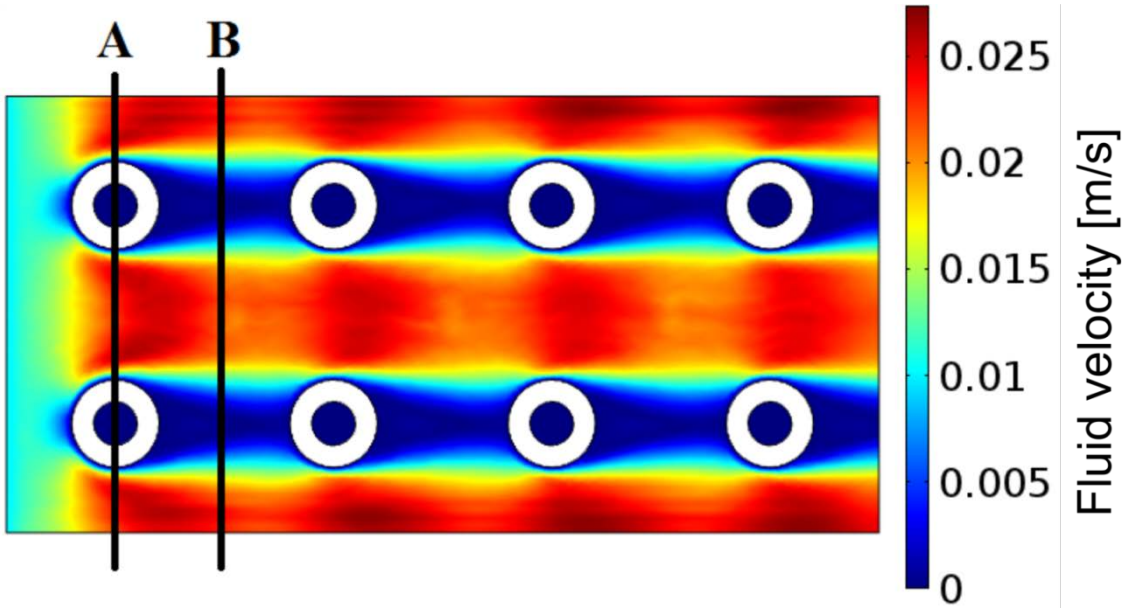

Figure 6-8: Velocity profile [m/s] at the half-height of the fluid passage for Model 3

The developed flow profile in Model 2 induces higher fluid velocities over parts of the fluid passage than that modelled through the assumption of a flat velocity profile as in Model 1. This behaviour is even more pronounced in Model 3, as the fluid only circulates over approximately two-thirds of the capsule width, leading to further increases in fluid velocities.

The different models have a negligible impact on the outlet fluid temperature over most of duration of test Case 1. The mean absolute difference between Models 1 and 2 is 0.53 °C over the length of the whole simulation and that between Models 2 and 3 is only 0.34 °C. However, the differences between the models are significant at the beginning of the simulation. The first moments of the evolution of the outlet fluid temperature through time for all three models are presented in an inset on Figure 6-9 for test Case 1.

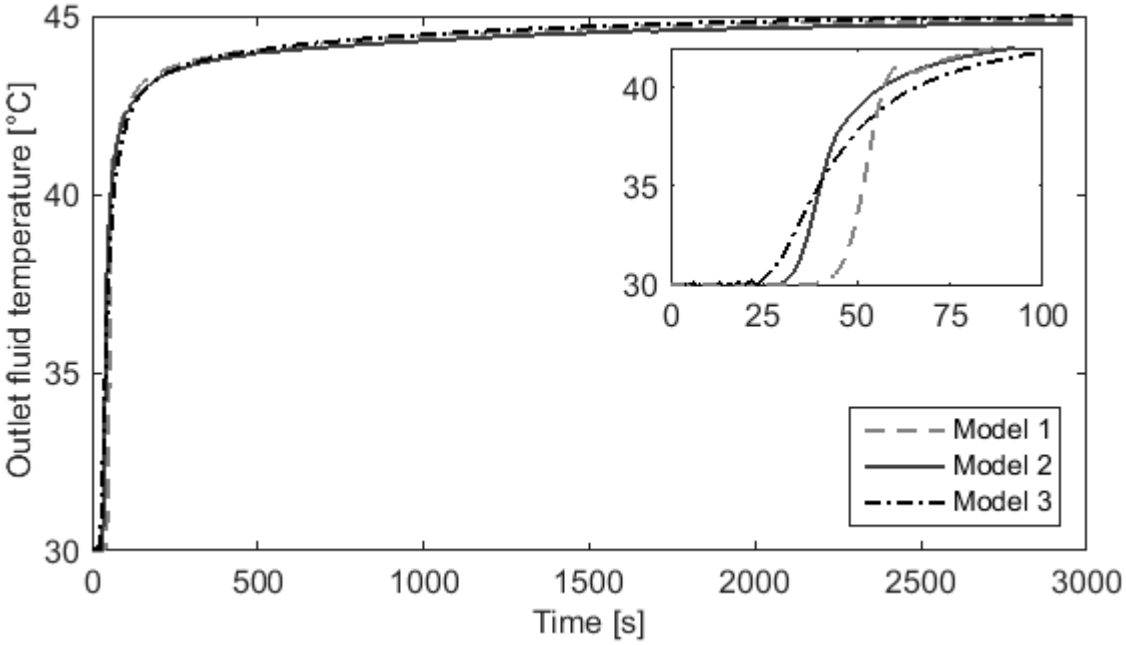

Figure 6-9: Outlet fluid temperature for Case 1

The moment when the outlet fluid temperature begins to increase above 30 °C and the time required to reach a plateau at about 45 °C are different for all three models. The outlet fluid temperature rise occurs sooner for Models 2 and 3 due to the fact that the developed flow profile allows higher fluid velocities over parts of the passage between two capsules. Some hot inlet water thus reaches the tank outlet faster than in Model 1. For each model, the timing of the increase of outlet fluid temperature is coherent with that model's fluid velocity; the temperature increase is centered at 50 s for Model 1 (fluid velocity of 0.01 m/s), and centered around 30 to 35 s for Model 2 (fluid velocity of 0.0149 m/s). This leads to a significant difference in the outlet fluid temperature between Models 1 and 2 at the beginning of the simulation (t = 36 s to 56 s), reaching a maximum difference of 7.03 °C. Model 3 has the most slanted profile, likely caused by the enhanced heat transfer from the fluid to the PCM due to an augmented capsule surface and increased fluid velocities. These results indicate inaccuracies are to be expected following rapid changes in flow velocity when using the simplified TRNSYS model, if the correct "average" fluid velocity is not estimated.

6.4.2 Heat transfer surface

Heat transfer inside Model 3 is analyzed at different sections to assess the impact of modelling the real geometry through a simplified rectangular prism. As shown on Figure 6-8, Section A cuts through the protrusions, perpendicular to the direction of fluid flow while Section B bisects the first hole along the capsule's centerline. Figure 6-10 (Section A) shows that the protrusions act as thermal barriers, impeding heat transfer to the PCM immediately below. Section B shows that the holes along the capsule center act like thermal bridges to the center of the capsule, even though fluid flow in these holes is very small. Zones in Figure 6-8 where the fluid velocity is the highest coincide with the highest PCM temperature in Figure 6-10, indicating the higher flow velocity has locally increased heat transfer to the PCM capsule.

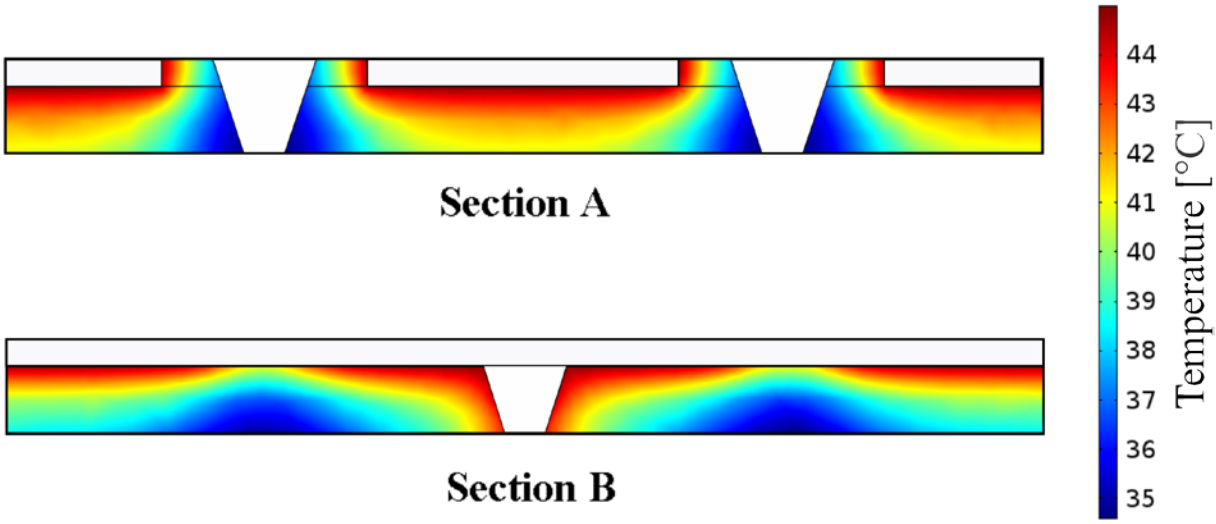

Figure 6-10: Temperature distribution at sectional cuts of the PCM capsule, 1500 s into Case 1

The temperature distribution visible on sectional cuts from Figure 6-10 also shows a significant temperature gradient over the half height of the PCM capsule. Even greater temperature gradients occur over the half height of the PCM capsule near the beginning of the simulation. Such gradients will require the use of several control volumes along the capsule half-height in the simplified model, using the discretization criteria described in Section 6.4.2. Temperature variations along the width of the PCM capsule are limited to the areas surrounding the protrusions and holes. In the TRNSYS model, these protrusions and holes are replaced by an

equivalent horizontal surface so the use of a single node over the width of the PCM capsule should be adequate.

Though the real capsule geometry's impact on the flow and temperature distribution is evident on Figure 6-8 and Figure 6-10, the maximum absolute difference between outlet fluid temperature resulting from Model 2 and Model 3 is only 1.95 °C. So it is concluded that the real capsule geometry is reasonably well represented by the simple rectangle used in Model 2 and simple TRNSYS model.

6.4.3 Lateral conduction between PCM nodes

A past comparison exercise (D'Avignon & Kummert, 2013) verified that conduction in the PCM in the direction of fluid flow (i.e. along the x-axis on Figure 6-3) can be neglected for this geometry. An analysis of the test cases previously described in Table 6.2 indicates that heat transfer between PCM nodes along the x-axis becomes increasingly important as the simulation progresses in time. However, the highest energy fluxes between PCM control volumes occur at the beginning of the simulation. Thus, when the contribution of conduction between PCM control volumes along the x-axis becomes significant in proportion, its absolute value is very small. Results indicated the maximum absolute difference in the outlet fluid temperature between Model 1 versions with and without conduction between PCM nodes in the direction of flow is less than 0.017 °C. On the scale of typical building applications, such a small temperature difference is negligible. Thus, though heat transfer between laterally adjacent PCM control volumes is definitely present, neglecting its contribution is justifiable for the simplified TRNSYS model.

6.4.4 Grid and time step analysis

Incropera et al. (2007) give stability conditions for explicit discretization schemes in the form of a maximum allowable time step as a function of the distance between adjacent control volumes and material properties. Applying the same principles to the semi-explicit schemes leads to Equation (6-8) and (6-9), two different criteria depending on the position of the PCM control volume:

PCM control volume at the capsule wall

$$Fo(1+Bi) = \left(\frac{k_{pcm}\Delta t}{\rho_{pcm}c_{p,pcm}\Delta y^2}\right)\cdot\left(1+\frac{h_{eq}\Delta y}{k_{pcm}}\right) \leq 1 \tag{6-8}$$

Interior PCM control volume

$$Fo = \frac{k_{pcm}\Delta t}{\rho_{pcm}c_{p,pcm}\Delta y^2} \leq 1 \tag{6-9}$$

Here, the Fourier number, Fo, represents the ratio of the conductive heat transfer rate to the rate of heat storage while the Biot number, Bi, is the ratio of the heat transfer resistances inside and at the surface of the material. The PCM's specific heat, $c_{p,pcm}$, varies during its change of phase so the minimum value over the expected temperature range must be used.

In the case of the fluid control volumes, physically-plausible results can be ensured by the Courant-Friedrichs-Lewy (CFL) condition (de Moura & Kubrusly, 2013) which accounts for heat and mass transfers across control volumes. The principle of the CFL condition is to ensure that the values used in calculations for a given time step are relevant for that time step. In this case, the size of the fluid control volumes must not be too small, to ensure that it cannot be completely "flushed out" by fluid from the upstream control volumes in the duration of one time step. This condition can be expressed through Equation (6-10) :

$$\Delta x > \frac{\dot{m}\Delta t}{\rho_f A_f} \tag{6-10}$$

The length of one fluid control volume, Δx, is a function of the number of fluid control volumes as well as the number and length of the PCM capsules; all parameters specified by the user but which the model will verify satisfy Equation (6-10).

Incropera's and Courant-Friedrichs-Lewy's stability conditions impose a minimum size for control volumes at a specific time step duration. Result accuracy however is dependent on the control volumes being at a uniform temperature, which requires a small control volume size. Reduced grid size and simulation time step also negatively impact computational efficiency. The necessity of striking a balance between computational costs, numerical stability and accuracy can

be visualized through the temperature distribution on sectional cuts from Figure 6-10, which illustrates a significant temperature gradient over the half height of the PCM capsule 1500 s into Case 1. Even greater temperature gradients occur at the beginning of the simulation (t < 1500 s). The temperature evaluated along a vertical line cutting through the centre of sectional cut A is presented on Figure 6-11 for various time stamps of Case 1.

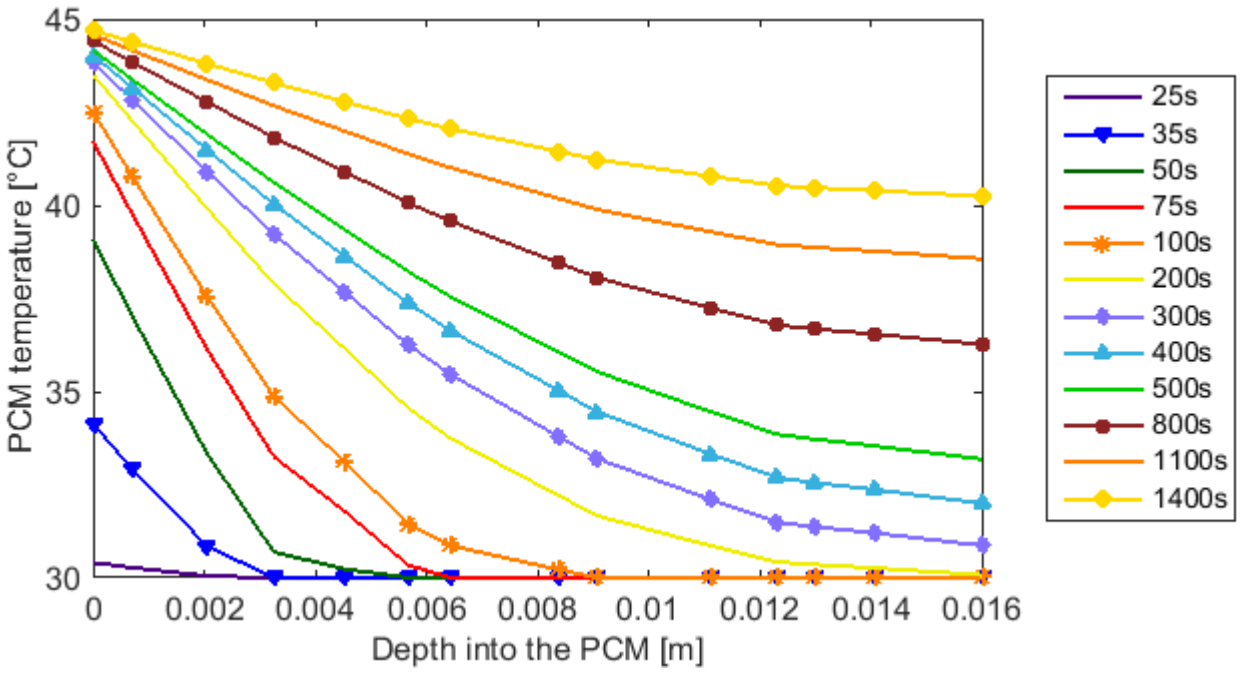

Figure 6-11: Temperature distribution at sectional cuts of the PCM capsule, 1500 s into Case 1

Figure 6-11 shows that significant temperature gradients are present. From t=75 s to t=500 s, they are greater than 10 °C, reaching a variation of as much as 13.4 °C at t=200 s. This clearly indicates that the half-height of the PCM capsule must be represented by more than one PCM control volume or significant errors in the instantaneous heat transfer between each PCM and fluid control volume could occur. These errors would be most significant after a sharp transition in the incoming fluid velocity or temperature. However, including additional PCM control volumes reduces each control volume's size, which will be limited by the criterion established previously and the objective of a reasonable computational time for annual (or multi-annual) building simulations.

A grid analysis was performed by varying the number of fluid control volumes over the length of the tank (x-axis) and number of PCM control volumes over the half-height of the capsule (y-

axis). The power delivered by the tank was evaluated over 15 mins intervals and compared to the power output calculated from Model 3. Results indicate the maximum difference in power output between models decreases with increasing number of fluid control volumes. However, for 10 to 30 fluid control volumes, the variation between the results is negligible. As for the PCM, the maximum difference increases with an increasing number of PCM control volumes over the half thickness of the capsule. The case with only one PCM control volume however is a notable exception; the maximum difference calculated in this case is actually the highest of all grids tested. Therefore, if Model 3 results are deemed reliable, a number of 3 to 5 PCM control volumes is most accurate.

A similar analysis is performed for varying time increments keeping constant the number of PCM and fluid control volumes, at 3 and 15 respectively. To ensure simulation time steps remained inferior to the residence time of the fluid in the tank, only time steps from 1 s to 45 s were tested. Results indicate the different time increments did not significantly affect the outlet fluid temperature profile, the variations in outlet fluid temperature being less than 0.01 °C throughout the simulation.

6.5 Model adjustments

Following a series of preliminary experimental tests some adjustments were made to the simplified TRNSYS model, to account for phenomena that cannot be fully represented in the simplified 1-D approach. These adjustments are related to the presence of air voids in the PCM capsules, the presence of fluid volumes that are not in direct contact with the PCM capsules, and to the heat transfer and fluid velocity impacts of geometry simplifications.

The change of phase of a material between liquid and solid is often accompanied by a change in volume. Studying the flat slab-like PCM capsules available on the market indicates they are usually not filled to capacity, leaving space in the capsule to account for changes in the material's volume. This leads to inaccuracies where the model assumes the disposition of the PCM inside the capsule illustrated on Figure 6-12A while the real situation corresponds to Figure 6-12B. If any air is present in the capsule, the latter case leads to increased thermal resistance between the fluid and PCM on the upper surface of the capsule and disrupts the capsule's symmetry. If the capsule is vacuum sealed, the encapsulation material might instead buckle following the PCM

density change and alter the capsule geometry. This phenomena is accounted for by redistributing the PCM along the capsule's centerline as in Figure 6-12C. The use of an equivalent thermal resistance, encompassing both the capsule wall and void thermal resistances is also implemented.

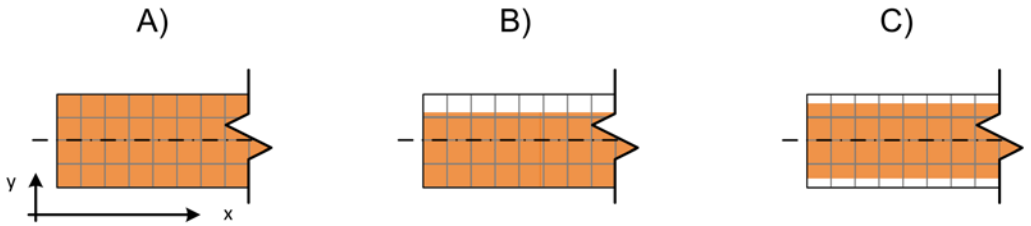

Figure 6-12: Repartition of PCM inside the capsule

In order for the heat transfer fluid flow to be evenly distributed amongst the PCM capsules, industrial tanks used for PCM storage require the use of a diffuser and/or mixing length. Both methods imply a significant volume of water, unaffected by PCM capsules, must be accounted for both at the tank entry and exit (see Figure 6-13). This additional heat transfer fluid volume is modelled as a single, perfectly mixed fluid node, which is solved outside of the PCM/fluid iteration loops.

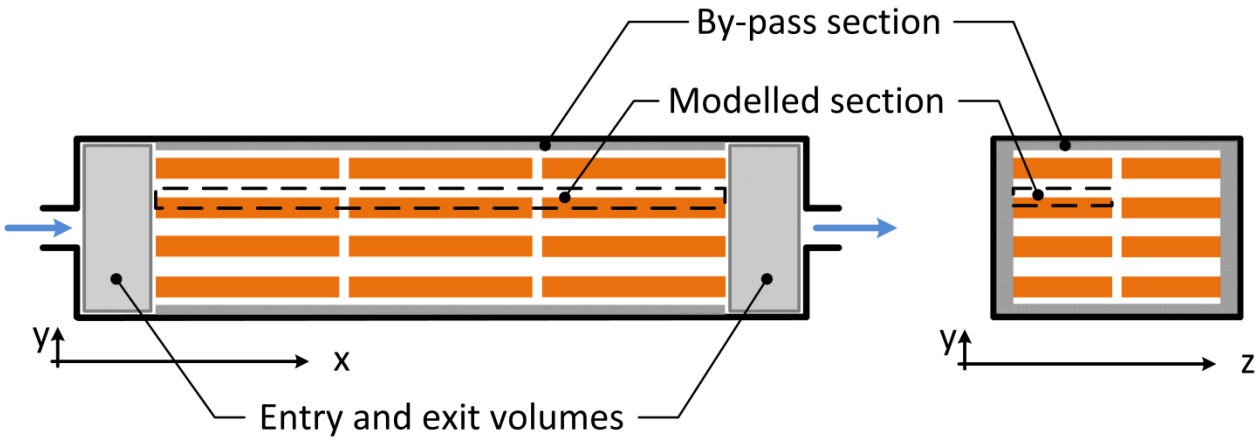

Figure 6-13: Schematic of by-pass section and entry/exit volumes

Any tank cross-section is bound to allow for some fluid to circulate outside the modelled fluid passages. Examples are illustrated on Figure 6-13 where parts of the fluid flow circulates in the lateral space between the tank wall and adjacent capsules and outside the fluid passage height modelled. In the proposed model, this phenomena is compensated by a by-pass factor which

allow parts of the heat transfer fluid to circumvent the fluid control volumes interacting with the PCM and arrive unaffected at the tank outlet.

As discussed in Section 6.4.2, the capsule protrusions increase heat transfer fluid flow which in turn impact model results following sudden changes in flowrates or inlet temperature. These same protrusions modify the surface area over which heat is exchanged between the fluid and PCM. The model therefore allows the user to separately adjust the width of the fluid flow passage and heat transfer surface to account for the real geometry.

6.6 Experimental validation

6.6.1 Experimental set-up

The objective of the model validation is to verify the model's ability to represent the behaviour of the PCM tank over the full range of operating conditions likely to happen in typical use. To achieve this, a horizontal storage tank filled with the rectangular PCM capsules of Figure 6-1 was thoroughly tested in the Semi-Virtual Lab at Polytechnique Montreal (D'Avignon & Kummert, 2015b). The referenced experimental study evaluated the performance of the tank over 13 distinct tests of melting and solidification cycles with different inlet fluid temperatures, flowrates and load profiles. At least three repetitions were made of each test to assess repeatability of results. The complete experimental data set was made available by the authors so it can be of use to other researchers developing and validating numerical models of such tanks. Results were reported and thoroughly analysed in the cited paper so only the key points relevant to the present model validation will be discussed here.

The main components of the experimental set-up are illustrated in Figure 6-14. Turbine flow meters with magnetic pick-up are installed at both the inlet and outlet of the tank so that the flowrate inside the PCM tank can be measured to a precision of ± 1% of the readings. A set of calibrated PT-100 platinum resistance temperature sensors measure the fluid temperature entering and leaving the PCM tank; the uncertainty on their measurements is ± 0.165 °C. A custom-made thermopile with a ± 0.04 °C uncertainty also provides an additional measurement of the temperature difference between the tank inlet and outlet. A configurable controller including a processor and field-programmable gate array (FPGA) offers high-speed signal acquisition and

control of the Semi-Virtual Lab. All experimental tests referred to in the present article used 10 second sampling times for data acquisition and test bench control.

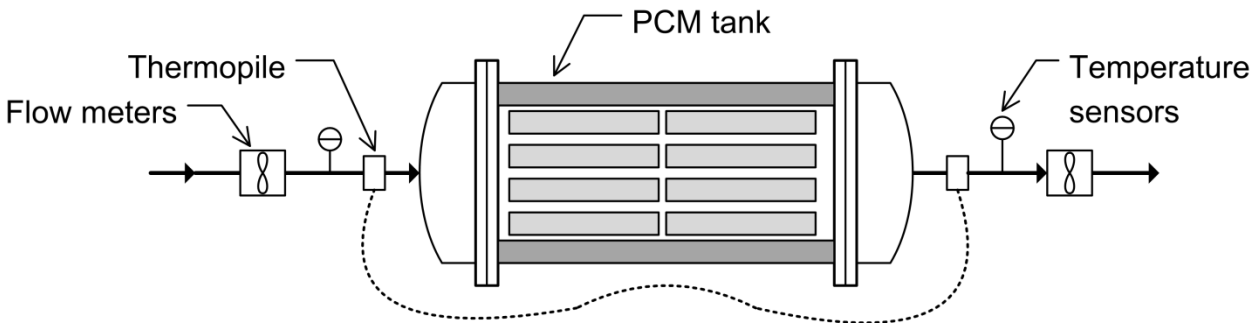

Figure 6-14: Experimental set-up schematic

The tank was submitted to a total of 13 distinct tests, listed in Table 3, and 3 repetitions were made of each test. The tests include different flowrates, $\dot{v}$, and temperature intervals, ΔT, as well as both heating and cooling processes. Various load profiles were also tested:

- Step changes: these tests take place over an interval of temperature, $[T_{trans} - \Delta T; T_{trans} + \Delta T]$, centered on the PCM's theoretical phase change temperature, T_{trans}. The tank is initially in a steady-state when a sudden change in inlet temperature is imposed and maintained until the end of the test.
- Fixed rate of temperature change: simulates conditions were a fixed rate of temperature change of the inlet fluid is imposed to the tank;
- Constant power tests: simulates conditions were a constant power load is imposed to the tank over a specific period of time;
- Interrupted tests: operating conditions are toggled between charging and discharging processes before either is completed.

The PCM objects tested in these experiments are commercially available rectangular HDPE capsules, illustrated on Figure 6-1. They are 0.25 m wide and 0.5 m long with protrusions and holes on their upper and lower faces, offering a heat transfer surface of approximately 1290 cm^2. When stacked, the capsules are a distance of 7 mm away from one another, reserving ~ 17.5 cm^2 for the passage of heat transfer fluid. Contained in the capsules is a heterogeneous salt hydrate

named S27 (PCM Products Ltd, 2015) whose properties as supplied by the manufacturer are detailed in Table 6.3.

Table 6.3: Characteristics of phase change material S27[6]

PCM S27 properties	Value	Units
Specific heat capacity	2.20	kJ/(kg-°C)
Volumetric heat capacity	280	MJ/m^3
Density	1530	kg/m^3
Thermal conductivity	0.540	W/(m-°C)
Latent heat of fusion	183	kJ/kg
Phase change temperature	27	°C

Each S27-filled capsule weighs 5.81 kg with the mass of the encapsulation itself deemed negligible. Previous characterization tests (D'Avignon & Kummert, 2015a) lead to the two functions illustrated on Figure 6-15 relating the specific enthalpy and temperature of the material which will be used in this validation; the one annotated with "C" represents the cooling process and the other annotated with "H" represents the heating process.

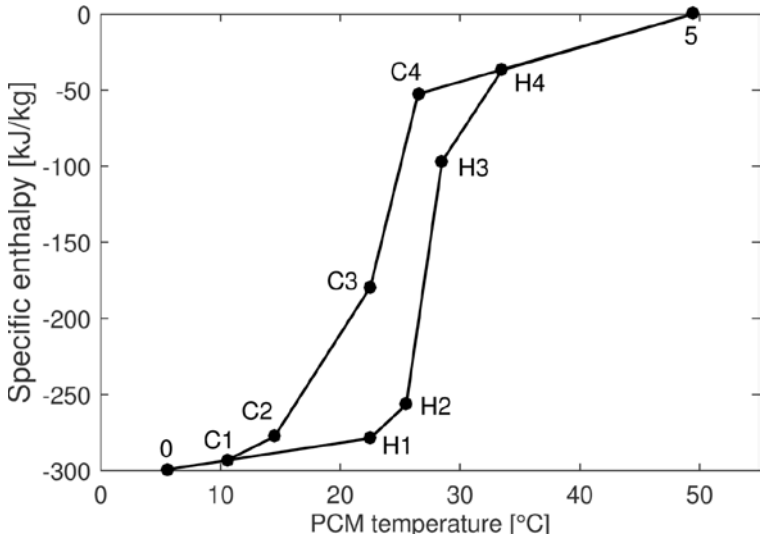

Figure 6-15: Enthalpy-temperature curve of PCM S27

[6] The properties listed have been copied exactly as found in manufacturer data.

A total of 32 capsules are installed inside the insulated tank in 4 stacks of 8 capsules, 2 stacks wide by 2 stacks deep. The PCM storage tank itself is cylindrical so a hollow shape of expanded polystyrene, which can be seen on Figure 6-17, was used to support the capsules inside the tank and insulate them from ambient conditions. Due to the capsule support design, some heat transfer fluid will by-pass the area where the PCM capsules are located, likely circulating outside the fluid passage height modelled.

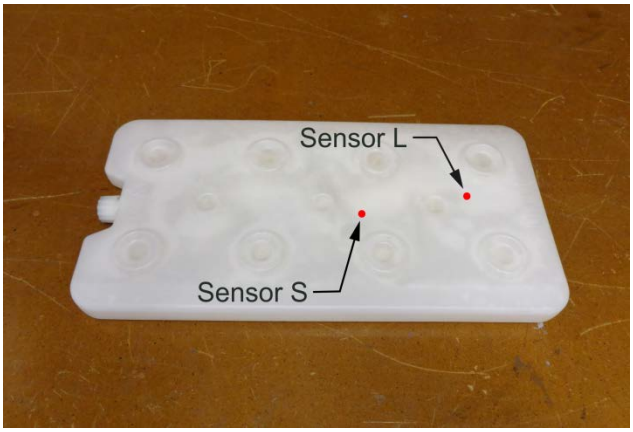

Figure 6-16: PCM capsule tested

Figure 6-17: Insulated PCM storage tank

As illustrated on Figure 6-17, one of the PCM capsules is equipped with two Type-K thermocouples, installed at different positions along the capsule's length, near its central axis. The approximate position of the sensor can be seen on Figure 6-16. The instrumented capsule's position inside the stack appears on Figure 6-17, it is installed in the "downstream" stack of capsules (second row in direction of flow) and about mid-way in the capsule stack.

6.6.2 Comparison to experimental results

The purpose of the proposed model is to adequately represent the behaviour of a horizontal PCM storage tank in year-long building performance simulations. Therefore the metric of importance in this model validation is the outlet fluid temperature exiting the PCM tank. Also of importance, the power output from the tank, $\dot{Q}$, is calculated through Equation (6-11) from the inlet fluid temperature, T_{in}, the outlet fluid temperature, T_{out}, and the fluid flow rate, $\dot{v}$.

$$\dot{Q}\ [kW] = \dot{v} \cdot c_p \cdot \rho \cdot (T_{in} - T_{out}) \tag{6-11}$$

In the case of the step tests, the comparison of the tank's outlet fluid temperature measured experimentally to that computed numerically is illustrated on Figure 6-18 for every flowrate and temperature interval tested. All step tests display short-term differences between the numerical and experimental results but overall the curves are in very good agreement.

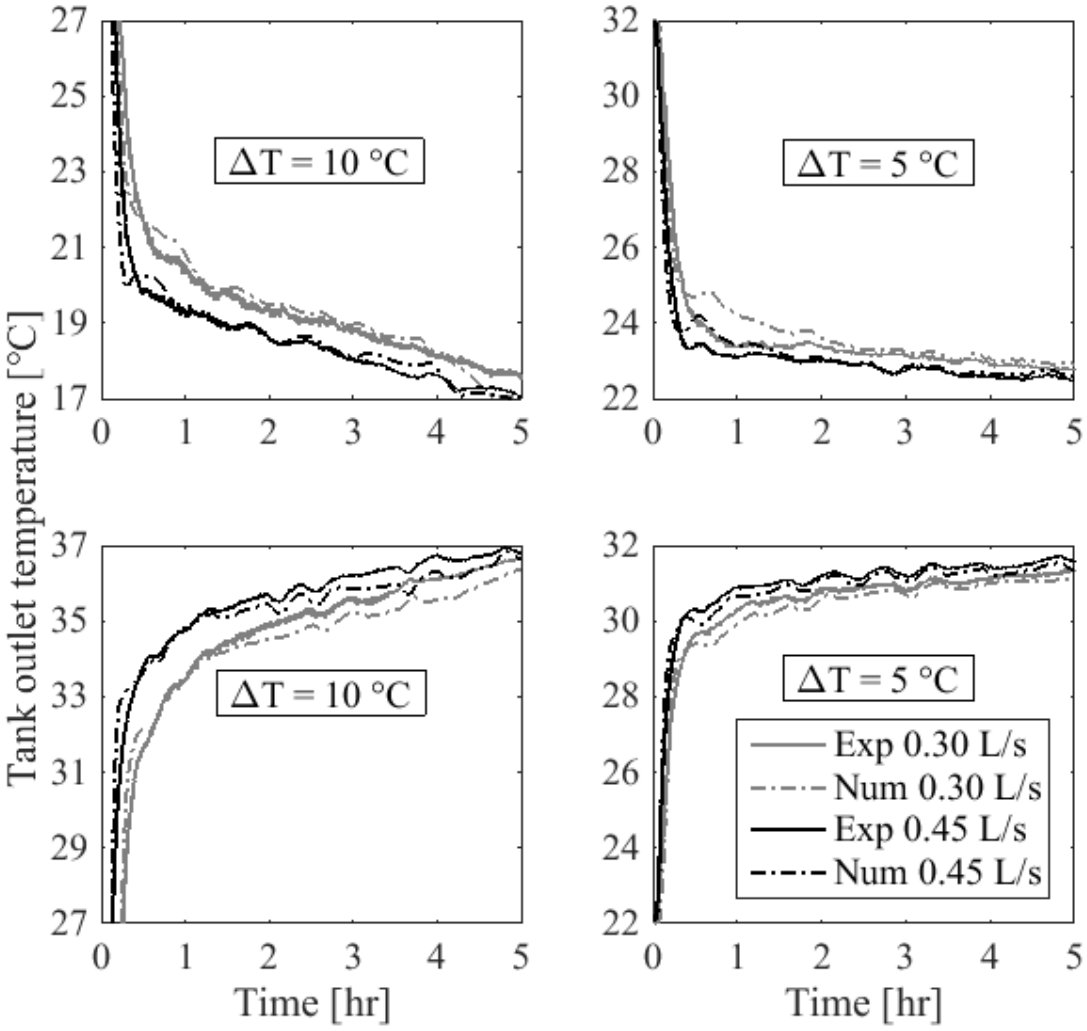

Figure 6-18: Tank outlet fluid temperature as a function of time for all step tests

To quantify the difference between the experimental data and numerical results, two indicators were used. The first is the maximum absolute difference, $maxD$, between both experimental, y_{exp}, and numerical, y_{num}, values which is calculated through Equation 11. The maximum absolute difference in the outlet fluid temperature is an imperative metric of comparison as most

building control systems would make use of the tank's outlet fluid temperature in their algorithms. Any absolute difference larger than the control system's deadband (a value of 1 °C will be used here) would impact tank control and building energy use calculations. The maximum absolute difference in power is also important in controlling such a PCM tank.

$$maxYD = \max_{1,2,\ldots,N}\{|y_{exp} - y_{num}|\} \tag{6-12}$$

The second metric considered is the coefficient of variation of the root mean square error, CV(RMSE), which is used to weigh the overall agreement between the numerical and experimental results over the entire test duration. As specified in ASHRAE's Guideline 14 (ASHRAE, 2002), it is evaluated through Equation (6-13) with $\bar{y}$ being the arithmetic mean of the sample of n readings.

$$CV(RMSE) = 100\% * \sqrt{\left\{\sum_{t=1}^{n}\left(y_{exp} - y_{num}\right)^2\right\}/\{n-1\}} * \frac{1}{\bar{y}} \tag{6-13}$$

To calculate the CV(RMSE) for the outlet fluid temperature, T_{out}, the arithmetic mean of the sample is not a representative metric so instead the overall test temperature variation will be used, or $2 \cdot \Delta T$. For the CV(RMSE) of the tank power, $\dot{Q}$, the arithmetic mean of the sample will be used. Guideline 14 requires the coefficient of variation of the root mean square error, CV(RMSE), for the power over hourly intervals to be smaller than 30% for a model to be considered reliable. In this case, though the tank power is calculated over 5 mins intervals, the same value is targeted. Values from all metrics are listed in Table 6.4 for each test.

Table 6.4: Validation metrics for all PCM tank tests

Test		Test parameters		Outlet fluid temperature		Tank power	
Process	Test type	ΔT [°C]	$\dot{v}$ [L/s]	maxD [°C]	CV(RMSE) [%]	maxD [kW]	CV(RMSE) [%]
Cooling	Fixed temperature change rate (1.25 °C/hr)	5	0.30	0.6	2.1	0.7	30.7
	Constant power	10	0.30	1.0	1.8	1.1	18.1

Table 6.4 (continued): Validation metrics for all PCM tank tests

	Step	10	0.30	2.5	1.9	2.6	28.2
		10	0.45	3.6	2.6	5.2	32.1
		5	0.30	1.2	2.9	1.3	30.3
		5	0.45	1.6	2.2	2.2	31.3
Heating & cooling	Interrupted	10	0.30	3.4	3.4	3.3	14.9
Heating	Fixed temperature change rate (1.25 °C/hr)	5	0.30	1.0	1.7	1.2	24.4
	Constant power	10	0.30	0.9	2.1	1.0	24.9
	Step	10	0.30	1.9	1.8	1.8	24.9
		10	0.45	2.4	2.0	3.8	29.4
		5	0.30	1.0	2.0	0.9	29.4
		5	0.45	1.1	1.9	1.4	27.3

The maximum difference in outlet fluid temperature momentarily exceeds 1 °C for all tests where rapid inlet temperature changes occur, namely the step tests and interrupted test. The experimental and numerical values of the fluid temperature exiting the tank are illustrated on Figure 6-18 for all step tests and on Figure 6-19 for the interrupted test. In all cases, the maximum difference in outlet fluid temperature occurs in the few minutes following the sharp change in inlet temperature indicating they are likely caused by the simplified flow profile modelled. For the reminder of the test duration, the difference between the experimental and numerical values remains well under 1 °C. The resulting coefficient of variation of the root mean square error, CV(RMSE), of the power output is 14% for the interrupted test. For step tests, the CV(RMSE) remains below 30% in heating but increases slightly beyond this limit for cooling processes.

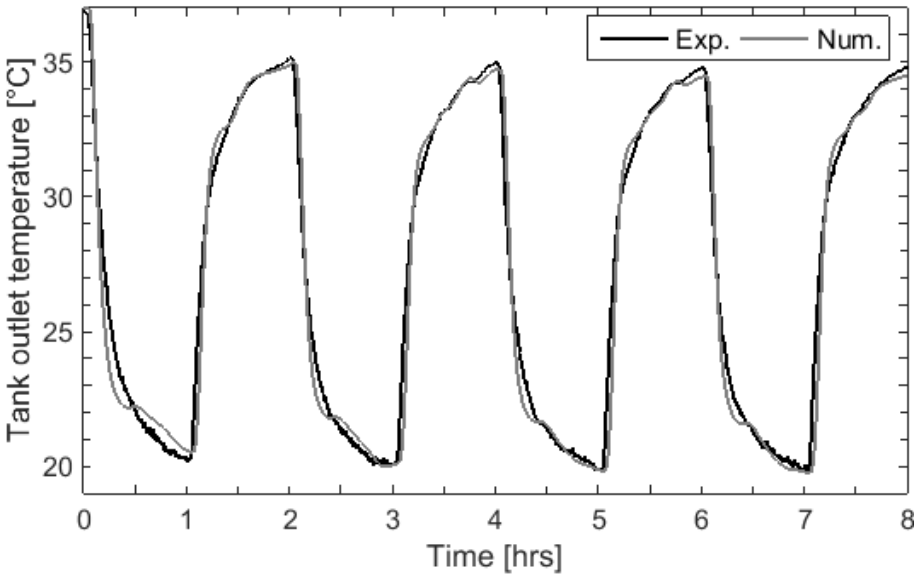

Figure 6-19: Tank outlet fluid temperature as a function of time for interrupted test

Both heating and cooling tests at a fixed temperature change rate are illustrated on Figure 6-20. The data shows a good agreement between numeric and experimental results; the maximum absolute difference is ≤ 1.0 °C for the outlet temperature and ≤ 1.2 kW for the tank power output. However, these test conditions are not likely operating conditions in real building applications. The inlet temperature change rate of 1.25 °C/hr is so mild that the difference between the inlet and outlet fluid temperatures never reaches 2 °C. Given building controller deadbands and the typical precision of temperature sensors, a difference of less than 2 °C will not be useful in most HVAC applications. Therefore, useful power output from the tank under these operating conditions is minimal. This is reflected in the coefficient of variation of the root mean square error, CV(RMSE), on the power output which 30.7% and 24.4% in cooling and heating respectively, due to the small average power output.

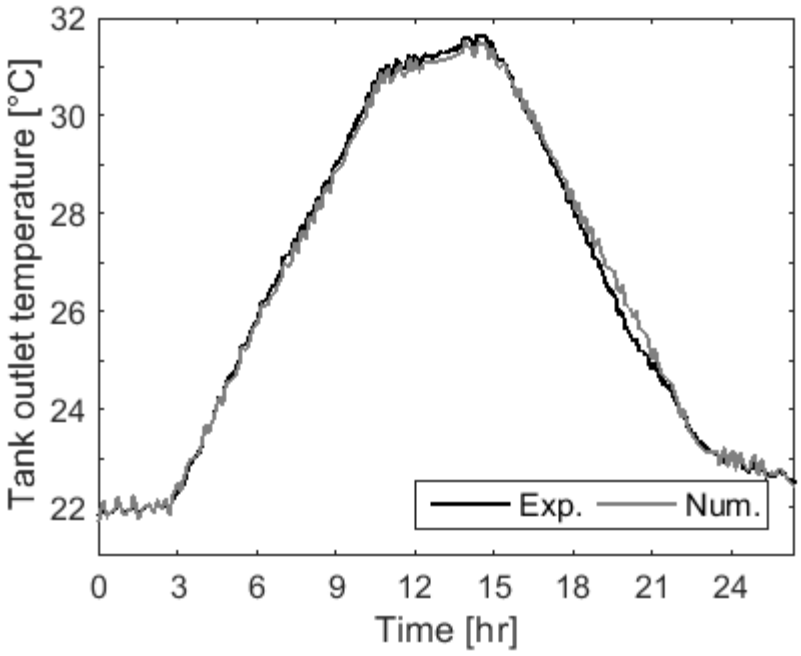

Figure 6-20: Tank outlet fluid temperature as a function of time for fixed temperature change rate tests

The constant power tests, illustrated on Figure 6-21 and Figure 6-22 below, were performed with the inlet tank temperature maintained at 5 °C above or below the tank outlet temperature, resulting in a constant heating/cooling power of 6.24 kW imposed to the tank. The outlet fluid temperature agrees quite well with the experimental data for both heating and cooling processes. This is reflected in the maximum absolute difference in outlet temperature of ~1.0 °C and CV(RMSE) of 18.1 % in heating and 24.9 % in cooling indicated in Table 6.4.

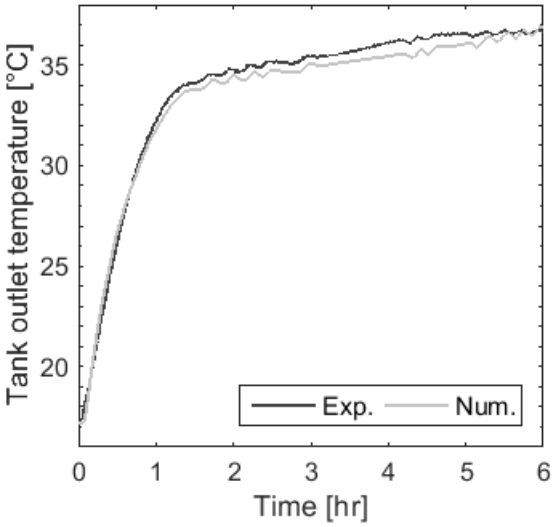

Figure 6-21: Tank outlet fluid temperature for constant power heating test

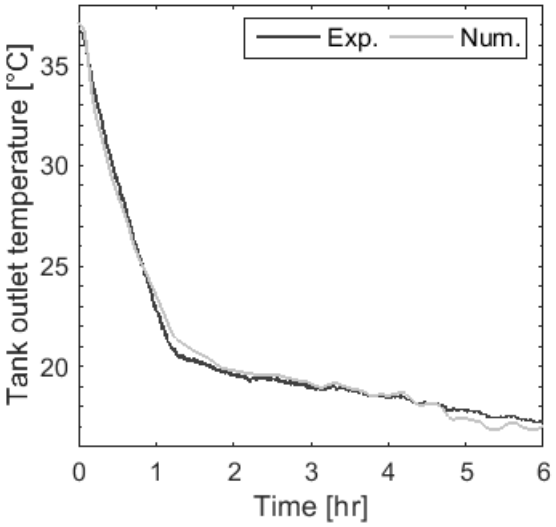

Figure 6-22: Tank outlet fluid temperature for constant power cooling test

The tests on these figures show amongst the best results of all the processes evaluated and are also most similar to the operating conditions of such PCM tanks in buildings. The constant power tests resulted in a rate of inlet temperature change of ~18 °C/hr in heating and 17 °C/hr in cooling, much closer to the rates of temperature change present in real HVAC applications than the step changes discussed previously.

6.7 Discussion

Differences between the numerical and experimental data could be caused by the PCM properties used as inputs into the model. PCM S27 manufacturer data leads to an enthalpy-temperature curve based on a pure substance assumption as defined by Tittelein et al. (2015). This curve is significantly different from results from previous characterization work through DSC (Barreneche et al., 2013) and the T-history method (D'Avignon & Kummert, 2015a) which instead indicate the PCM behaves more like a binary mixture. Moreover, though those characterization results indicated important supercooling and hysteresis between heating and cooling enthalpy-temperature curves in PCM samples of a few grams, the PCM's behaviour as a whole PCM-object could be significantly different. Temperature sensors located inside the PCM

capsules during the detailed experimental tests used in this validation indicated hysteresis was not always present and phase change appeared to occur at different temperatures according to the operating conditions (D'Avignon & Kummert, 2015b). The reduced model precision for cooling processes could be due to PCM supercooling which was present during the experimental tests but is not being modelled. The enthalpy-temperature curve of the PCM-object should be evaluated on its own using methods such as the energy-balance (José M. Marín, Zalba, Cabeza & Mehling, 2005; B. Zalba et al., 2004). Another enthalpy-temperature curve also could have led to a better agreement between experimental and numerical results and should be investigated.

6.8 Conclusion

A model was developed and experimentally validated to simulate the thermal behaviour of a horizontal energy storage unit including PCM capsules. The model is based on one-dimensional conduction and advection, utilizing control-volume method and semi-implicit temporal discretization, and it is implemented as a TRNSYS component for use in whole building analyses. The phase change process is modelled with the enthalpy method using different heating and cooling curves.

The model can be used for both fluid flowrates leading to internal forced convection and negligible flow conditions (Pe > 2). It was experimentally validated for flowrates from 0.3 to 0.45 L/s (approximately 0.1 to 0.15 m/s) and various inlet temperature profiles over the 17 to 37 °C temperature interval.

Detailed numerical modelling showed that thermal simulation of lateral conduction between PCM control-volumes was not necessary. It also indicated the simplified flow profile would lead to inaccuracies following rapid changes in inlet temperatures or flowrates. Inaccuracies due to the use of a simplified capsule geometry should be compensated by the additional parameters implemented (adjustable width of flow passage and heat transfer surface).

Comparison of numerical and experimental results indicated the proposed model was suitable for of the thermal behaviour of this type of PCM storage tank. The maximum coefficient of variation of the root mean square error on tank power was 32.1% over 5 minute intervals, indicating the model is in line with the requirements specified in ASHRAE’s Guideline 14.

6.9 Acknowledgements

This work was partly funded by the National Science and Engineering Research Council of Canada (NSERC) through the second author Discovery Grant and through the Smart Net-Zero Energy Building Strategic Research Network (SNEBRN). The first author was also supported by a Fonds de recherche du Québec – Nature et technologies (FRQNT) doctoral research scholarship.

6.10 References

Al-Saadi, S. N., & Zhai, Z. (2015). Systematic evaluation of mathematical methods and numerical schemes for modeling PCM-enhanced building enclosure. *Energy and Buildings, 92*(0), 374-388. doi: 10.1016/j.enbuild.2015.01.044

ASHRAE. (2002). ASHRAE Guideline 14-2002 *Measurement of Energy, Demand and Water Savings*. Atlanta, GA, USA: American Society of Heating, Refrigerating and Air-Conditioning Engineers.

Awad, M. M. (2010). *Heat transfer for laminar thermally developing flow in parallel-plates using the asymptotic method*. Paper presented at the 3rd International Conference on Thermal Issues in Emerging Technologies Theory and Applications, Cairo, Egypt.

Bansal, N. K., & Buddhi, D. (1992). An analytical study of a latent heat storage system in a cylinder. *Energy Conversion and Management, 33*(4), 235-242. doi: 10.1016/0196-8904(92)90113-B

Barreneche, C., Solé, A., Miró, L., Martorell, I., Fernández, A. I., & Cabeza, L. F. (2013). Study on differential scanning calorimetry analysis with two operation modes and organic and inorganic phase change material (PCM). *Thermochimica Acta, 553*(0), 23-26. doi: 10.1016/j.tca.2012.11.027

Bony, J., & Citherlet, S. (2007b). Numerical model and experimental validation of heat storage with phase change materials. *Energy and Buildings, 39*(10), 1065-1072. doi: 10.1016/j.enbuild.2006.10.017

Brent, A. D., Voller, V. R., & Reid, K. J. (1988). Enthalpy-Porosity Technique for Modeling Convection-Diffusion Phase Change: Application to the Melting of a Pure Metal. *Numerical Heat Transfer, 13*(3), 297-318.

Chandrasekharan, R., Lee, E. S., Fisher, D. E., & Deokar, P. S. (2013). An Enhanced Simulation Model for Building Envelopes with Phase Change Materials. *ASHRAE Transactions, 119*(2).

COMSOL. (2015). COMSOL Multiphysics Retrieved Accessed: 10-22-2015, from http://www.comsol.com/

Costa, M., Buddhi, D., & Oliva, A. (1998). Numerical simulation of a latent heat thermal energy storage system with enhanced heat conduction. *Energy Conversion and Management, 39*(3-4), 319-330. doi: 10.1016/S0196-8904(96)00193-8

D'Avignon, K., & Kummert, M. (2013). *Comparison of system-level simulation and detailed models for storage tanks with phase change materials.* Paper presented at the 13th Conference of International Building Performance Simulation Association, Chambéry, France.

D'Avignon, K., & Kummert, M. (2015a). Assessment of T-History Method Variants to Obtain Enthalpy-Temperature Curves for PCMs With Significant Subcooling. *Journal of Thermal Science and Engineering Applications, 7*(4), 041015-041015. doi: 10.1115/1.4031220

D'Avignon, K., & Kummert, M. (2015b). Experimental assessment of a phase change material storage tank. *Applied Thermal Engineering*, Submitted on September 6th, 2015.

de Moura, C. A., & Kubrusly, C. S. (2013). The Courant-Friedrichs-Lewy (CFL) Condition *80 Years After Its Discovery* (pp. 237). Retrieved from http://link.springer.com/10.1007/978-0-8176-8394-8 doi:10.1007/978-0-8176-8394-8

Delcroix, B., Kummert, M., & Daoud, A. (2015). *Thermal behavior mapping of a phase change material between the heating and cooling enthalpy-temperature curves.* Paper presented at the 6th International Building Physics Conference, Torino, Italy.

Dutil, Y., Rousse, D. R., Ben Salah, N., Lassue, S., & Zalewski, L. (2011). A review on phase change materials: Mathematical modeling and simulations. *Renewable and Sustainable Energy Reviews, 15*(1), 112-130. doi: 10.1016/j.rser.2010.06.011

Elsayed, A. O. (2007). Numerical study of ice melting inside rectangular capsule under cyclic temperature of heat transfer fluid. *Energy Conversion and Management, 48*(1), 124-130. doi: 10.1016/j.enconman.2006.05.006

Halawa, E., Saman, W., & Bruno, F. (2010). A phase change processor method for solving a one-dimensional phase change problem with convection boundary. *Renewable Energy, 35*(8), 1688-1695. doi: 10.1016/j.renene.2010.01.016

Hamdan, M. A., & Elwerr, F. A. (1996). Thermal energy storage using a phase change material. *Solar Energy, 56*(2), 183-189. doi: 10.1016/0038-092X(95)00090-E

Incropera, F. P., Dewitt, D. P., Bergman, T. L., & Lavine, A. S. (2007). *Fundamentals of heat and mass transfer* (6th edition ed.). Hoboken: John Wiley & Sons.

International Energy Agency (2008). Energy Technology Perspectives 2008: Scenarios & Strategies to 2050. Retrieved from http://www.iea.org/media/etp/etp2008.pdf

Lacroix, M. (2001). Contact melting of a phase change material inside a heated parallelepedic capsule. *Energy Conversion and Management, 42*(1), 35-47. doi: 10.1016/S0196-8904(00)00047-9

Liu, M., Saman, W., & Bruno, F. (2011). Validation of a mathematical model for encapsulated phase change material flat slabs for cooling applications. *Applied Thermal Engineering, 31*(14-15), 2340-2347. doi: 10.1016/j.applthermaleng.2011.03.034

Marín, J. M., Zalba, B., Cabeza, L. F., & Mehling, H. (2003). Determination of enthalpy-temperature curves of phase change materials with the temperature-history method: improvement to temperature dependent properties. *Journal of Measurement Science and Technology, 14*(2), 184-189. doi: 10.1088/0957-0233/14/2/305

Marín, J. M., Zalba, B., Cabeza, L. F., & Mehling, H. (2005). Improvement of a thermal energy storage using plates with paraffin–graphite composite. *International Journal of Heat and Mass Transfer, 48*(12), 2561-2570. doi: 10.1016/j.ijheatmasstransfer.2004.11.027

Moreno, P., Castell, A., Solé, C., Zsembinszki, G., & Cabeza, L. F. (2014). PCM thermal energy storage tanks in heat pump system for space cooling. *Energy and Buildings, 82*(0), 399-405. doi: 10.1016/j.enbuild.2014.07.044

Patankar, S. V. (1980). *Numerical heat transfer and fluid flow*. Washington: Taylor & Francis.

PCM Products Ltd. (2015). Phase Change Materials Products Ltd. Retrieved 2015-11-02, from http://www.pcmproducts.net

Puschnig, P., Heinz, A., & Steicher, W. (2005). *TRNSYS simulation model for an energy storage for PCM slurries and/or PCM modules.* Paper presented at the Second Conference on Phase Change Material & Slurry: Scientific Conference & Business Forum, Yverdon-les-Bains, Switzerland.

Saman, W., Bruno, F., & Halawa, E. (2005). Thermal performance of PCM thermal storage unit for a roof integrated solar heating system. *Solar Energy, 78*(2), 341-349. doi: 10.1016/j.solener.2004.08.017

Silva, P. D., Gonçalves, L. C., & Pires, L. (2002). Transient behaviour of a latent-heat thermal-energy store: numerical and experimental studies. *Applied Energy, 73*(1), 83-98. doi: 10.1016/S0306-2619(02)00060-0

Tittelein, P., Gibout, S., Franquet, E., Johannes, K., Zalewski, L., Kuznik, F., Dumas, J.-P., Lassue, S., Bédécarrats, J.-P., David, D. (2015). Simulation of the thermal and energy behaviour of a composite material containing encapsulated-PCM: Influence of the thermodynamical modelling. *Applied Energy, 140*(0), 269-274. doi: 10.1016/j.apenergy.2014.11.055

Voller, V. R. (1990). Fast implicit finite-difference method for the analysis of phase change problems. *Numerical Heat Transfer, Part B: Fundamentals, 17*(2), 155-169.

Zalba, B., Marin, J. M., Cabeza, L. F., & Mehling, H. (2004). Free-cooling of buildings with phase change materials. *International Journal of Refrigeration, 27*(8), 839-849. doi: 10.1016/j.ijrefrig.2004.03.015

Zivkovic, B., & Fujii, I. (2001). An analysis of isothermal phase change of phase change material within rectangular and cylindrical containers. *Solar Energy, 70*(1), 51-61. doi: 10.1016/S0038-092X(00)00112-2

CHAPTER 7 GENERAL DISCUSSION

The main objectives of this thesis are to develop a model for the simulation of a horizontal storage tank filled with flat, slab-like phase change material capsules, and to validate the model through experimental testing of a real-scale PCM storage tank in realistic operating conditions.

The literature review (Chapter 2) highlighted the importance of the enthalpy-temperature relation in modelling the phase change process. The scientific community has mainly adopted the DSC and T-History methods to characterize phase change materials and obtain their enthalpy-temperature curves. A recent standard proposed in Germany (RAL Gütezeichen, 2013) specifically refers to these two methods as the only adequate methods to obtain the H-T curves. However, numerous variants of the T-History method have been proposed over the years and there is currently no consensus on the exact methodology that should be applied. Past studies have focussed on comparing the experimental set-ups in each variant and have only made a brief analysis of the different data processing methods. Chapter 4 offers a contribution towards a standardized characterization method of phase change materials through a critical assessment of those data processing methodologies. A detailed analysis of the mathematical formulations and physical principles behind the variants is presented, highlighting their advantages and disadvantages. Original experimental data from the testing of multiple samples is presented in its raw form to highlight the experimental variability that is inherent to the method but has rarely been shown by past authors. The difficulties encountered in applying the methodologies are presented, leading to recommendations on the appropriate data processing variant which should be used to obtain enthalpy-temperature curves for phase change materials exhibiting significant supercooling.

Most recent studies of PCM storage have relied on numerical results for model validation because experimental data is scarce for most geometries. When it exists, data from experimental tests is often limited to a few specific operating conditions, for which only partial measurements are presented. Repeatability is either not analysed or treated by averaging results and presenting punctual deviation measures. As presented in the literature review (Chapter 2), experimental data for this tank configuration is limited to the tests presented by Moreno et al. (2014). Chapter 5 constitutes a significant contribution by presenting original data for a configuration that has not been studied experimentally before, and by providing the full, raw dataset to allow further use by

other researchers. The experimental tests were thorough: 14 distinct operating conditions were tested, varying the inlet flowrate, the temperature interval as well as the load profile to the tank. Tests presented in Chapter 5 were each repeated at least three times and the variability of results is openly presented and discussed. This Chapter also includes an account of the measured behaviour of the phase change material inside its encapsulation, providing valuable insights into the PCM-object behaviour. The experimental dataset has substantial value for all researchers studying thermal energy storage or looking to validate a numerical model.

The literature review (Chapter 2) also highlighted the absence of adequate modelling tools for HVAC system designers to properly predict the behaviour of PCM storage tanks in buildings. None of the existing models have been specifically developed to represent the behaviour of horizontal storage tanks filled with rectangular PCM capsules or experimentally validated to do so. Chapter 6 presents such a model. The pertinence of the modelling assumptions made was verified through the use of detailed, finite-element models. Results indicated the most significant errors appeared after rapid changes in flowrates or inlet temperature due to the simplified flow profile. All other assumptions were proven justified and the proposed model's principles valid for the system-level simulations targeted. The experimental data from the previous chapter was used to perform an exhaustive validation of the model under diverse operating conditions. Comparing numerical and experimental results following the principles of ASHRAE's Guideline 14 confirms the model validity for the simulation of horizontal storage tanks containing rectangular PCM capsules.

Finally, I made a significant contribution to the design, construction and commissioning of the Semi-Virtual Laboratory, which is briefly presented in Chapter 5. It is a testing facility for hydronic (water-side) heating and cooling equipment, especially built to deliver validated, fully dynamic numerical models of HVAC equipment, capable of supporting system-level optimization of complex energy systems. To do this, the Semi-Virtual Laboratory comprises two precision-controlled test loops, capable of imposing dynamic inlet conditions (temperature and flow rate) to the tested equipment. This real testing environment is coupled with a virtual testing environment which can model a full building complete with its HVAC plant. This virtual computer model calculates the inlet conditions that would take place in the modelled building, and the hydronic test bench imposes these conditions to the tested equipment. Outlet conditions from the tested equipment are then fed-back to the computer model in real-time. This "semi-

virtual” principle of operation, similar to the Hardware-In-the-Loop methods used in controls and rapid prototyping, was put in place by Francesca MacDonald and is described in detail in MacDonald et al. (2014). The hardware part of the Laboratory itself was constructed over a period of three years, under my direct responsibility. As such, I designed and calibrated the data acquisition and control system (from sensors to data logging equipment) and proposed modifications to improve the quality of experimental data. The Laboratory allows testing of a variety of hydronic HVAC equipment in diverse building constructions and varied climatic conditions. It will be of great use for future research at Polytechnique towards the development of validated, fully dynamic numerical models of HVAC equipment.

CHAPTER 8 CONCLUSION AND RECOMMENDATIONS

The numerical model presented in this thesis was developed for the simulation of horizontal storage tanks containing flat, rectangular PCM capsules. It is able to represent their behaviour with the accuracy required in traditional building systems, as demonstrated by the experimental validation. Further work should address the model accuracy in the specific conditions that were shown to be more difficult in Chapter 6 and the improvement of computational speed to allow more demanding tasks such as multi-year optimization of complex energy systems.

The experimental characterization of the studied PCM (S27) produced an enthalpy-temperature curve suitable for use in the proposed model and recommendations on PCM characterization methods. Some issues were identified, which would deserve further research. The testing of PCM samples presented in Chapter 4 indicated significant variability amongst samples. The small size of the samples and heterogeneity of the material itself, which appears to be a mixture of two compounds and a nucleation agent, made it difficult to ensure each sample truly represented the "same" material. Tests of a larger volume of PCM or the PCM-object itself would be more likely to resemble the PCM-object's behaviour in the PCM tank. Such tests were performed on the PCM-object though not reported in this thesis. Using inverse methods, an effective enthalpy-temperature curve could be recreated for these objects, likely resulting in an increased accuracy of the model's output.

The effect of supercooling on the outlet fluid temperature from the PCM tank needs to be studied in more detail. The experimental tests presented in Chapter 5 showed that the presence and magnitude of supercooling varied significantly even within a single PCM capsule, under similar test conditions. The concurrent repeatability in the outlet fluid temperature measured exiting the tank led us to conclude that supercooling had little impact on the output from the tank (i.e. that its overall effect cancelled out) and could be neglected in the modelling of the PCM behaviour. This conclusion should be verified by comparison to a model which accounts for supercooling of the material. Work was done to implement the algorithm proposed by Günther et al. (2007) to model supercooling into the TRNSYS model presented in Chapter 6. Before this model version can reasonably be compared against experimental data, additional parameters defining the PCM are required. However, the required information on the material's crystallization speed and nucleation probability as a function of temperature remains unavailable. The determination of

these properties will require additional experimental testing for which no methodology has been found in the literature.

The test bench used to investigate the behaviour of the PCM tank can also be improved. In the tests presented in Chapter 5, only one PCM capsule was instrumented and only one position of the capsule in the tank was tested. Constructing and installing additional instrumented PCM capsules would allow a more detailed portrait of the PCM's behaviour while encapsulated and provide more information, for example, on the prevalence of supercooling. Finally, the full capabilities of the Semi-Virtual Laboratory could be exploited by testing the PCM tank in operating conditions corresponding to potential applications.

BIBLIOGRAPHY

Agyenim, F., Hewitt, N., Eames, P., & Smyth, M. (2010). A review of materials, heat transfer and phase change problem formulation for latent heat thermal energy storage systems (LHTESS). *Renewable and Sustainable Energy Reviews, 14*(2), 615-628. doi: 10.1016/j.rser.2009.10.015

Al-Hinti, I., Al-Ghandoor, A., Maaly, A., Abu Naqeera, I., Al-Khateeb, Z., & Al-Sheikh, O. (2010). Experimental investigation on the use of water-phase change material storage in conventional solar water heating systems. *Energy Conversion and Management, 51*(8), 1735-1740. doi: 10.1016/j.enconman.2009.08.038

Al-Kayiem, H. H., & Alhamdo, M. H. (2012). Thermal behavior of encapsulated phase change material energy storage. *Journal of renewable and Sustainable Energy, 4*(1). doi: 10.1063/1.3683532

Al-Saadi, S. N., & Zhai, Z. (2015). Systematic evaluation of mathematical methods and numerical schemes for modeling PCM-enhanced building enclosure. *Energy and Buildings, 92*(0), 374-388. doi: 10.1016/j.enbuild.2015.01.044

Arkar, C., & Medved, S. (2005). Influence of accuracy of thermal property data of a phase change material on the result of a numerical model of a packed bed latent heat storage with spheres. *Thermochimica Acta, 438*(1-2), 192-201. doi: 10.1016/j.tca.2005.08.032

Arkar, C., & Medved, S. (2007). Free cooling of a building using PCM heat storage integrated into the ventilation system. *Solar Energy, 81*(9), 1078-1087. doi: 10.1016/j.solener.2007.01.010

Arkar, C., Vidrih, B., & Medved, S. (2007). Efficiency of free cooling using latent heat storage integrated into the ventilation system of a low energy building. *International Journal of Refrigeration-Revue Internationale Du Froid, 30*(1), 134-143. doi: 10.1016/j.ijrefrig.2006.03.009

ASHRAE. (2000). ASHRAE Guideline 12-2000 *Minimizing the Risk of Legionellosis Associated with Building Water Systems*. Atlanta, GA, USA: American Society of Heating, Refrigerating and Air-conditioning Engineers

ASHRAE. (2002). ASHRAE Guideline 14-2002 *Measurement of Energy, Demand and Water Savings*. Atlanta, GA, USA: American Society of Heating, Refrigerating and Air-Conditioning Engineers.

Athienitis, A. K., Liu, C., Hawes, D., Banu, D., & Feldman, D. (1997). Investigation of the thermal performance of a passive solar test-room with wall latent heat storage. *Building and Environment, 32*(5), 405-410. doi: 10.1016/S0360-1323(97)00009-7

Awad, M. M. (2010). *Heat transfer for laminar thermally developing flow in parallel-plates using the asymptotic method.* Paper presented at the 3rd International Conference on Thermal Issues in Emerging Technologies Theory and Applications, Cairo, Egypt.

Bansal, N. K., & Buddhi, D. (1992). An analytical study of a latent heat storage system in a cylinder. *Energy Conversion and Management, 33*(4), 235-242. doi: 10.1016/0196-8904(92)90113-B

Barba, A., & Spiga, M. (2003). Discharge mode for encapsulated PCMs in storage tanks. *Solar Energy, 74*(2), 141-148. doi: 10.1016/S0038-092X(03)00117-8

Barreneche, C., Solé, A., Miró, L., Martorell, I., Fernández, A. I., & Cabeza, L. F. (2013). Study on differential scanning calorimetry analysis with two operation modes and organic and inorganic phase change material (PCM). *Thermochimica Acta, 553*(0), 23-26. doi: 10.1016/j.tca.2012.11.027

Bedecarrats, J. P., Castaing-Lasvignottes, J., Strub, F., & Dumas, J. P. (2009). Study of a phase change energy storage using spherical capsules. Part I: Experimental results. *Energy Conversion and Management, 50*(10), 2527-2536. doi: 10.1016/j.enconman.2009.06.004

Behzadi, S., & Farid, M. M. (2011). Experimental and numerical investigations on the effect of using phase change materials for energy conservation in residential buildings. *HVAC&R Research, 17*(3), 366.

Bonacina, C., Comini, G., Fasano, A., & Primicerio, M. (1973). Numerical solution of phase-change problems. *International Journal of Heat and Mass Transfer, 16*(10), 1825-1832. doi: 10.1016/0017-9310(73)90202-0

Bony, J., & Citherlet, S. (2007a, Sept 03-06, 2007). *Comparison between a new TRNSYS model and experimental data of phase change in a solar combisystem.* Paper presented at the

10th Conference of the International Building Performance Simulation Association Beijing, China.

Bony, J., & Citherlet, S. (2007b). Numerical model and experimental validation of heat storage with phase change materials. *Energy and Buildings, 39*(10), 1065-1072. doi: 10.1016/j.enbuild.2006.10.017

Brent, A. D., Voller, V. R., & Reid, K. J. (1988). Enthalpy-Porosity Technique for Modeling Convection-Diffusion Phase Change: Application to the Melting of a Pure Metal. *Numerical Heat Transfer 13*(3), 297-318.

Bruno, F., Tay, N. H. S., & Belusko, M. (2014). Minimising energy usage for domestic cooling with off-peak PCM storage. *Energy and Buildings, 76*(0), 347-353. doi: 10.1016/j.enbuild.2014.02.069

Buick, T. R., O'Callaghan, P. W., & Probert, S. D. (1987). Short-term thermal energy storage as a means of reducing the heat pump capacity required for domestic central heating systems. *International Journal of Energy Research, 11*(4), 583-592. doi: 10.1002/er.4440110414

Cabeza, L. F., Ibanez, M., Sole, C., Roca, J., & Miquel, N. (2006). Experimentation with a water tank including a PCM module. *Solar Energy Material and Solar Cells, 90*(9), 1273-1282. doi: 10.1016/j.solmat.2005.08.002

Canbazoğlu, S., Sahinaslan, A., Ekmekyapar, A., Aksoy, Y. G., & Akarsu, F. (2005). Enhancement of solar thermal energy storage performance using sodium thiosulfate pentahydrate of a conventional solar water-heating system. *Energy and Buildings, 37*, 235-242.

Castellón, C., Günther, E., Mehling, H., Hiebler, S., & Cabeza, L. F. (2008). Determination of the enthalpy of PCM as a function of temperature using a heat-flux DSC - A study of different measurement procedures and their accuracy. *International Journal of Energy Research, 32*(13), 1258-1265. doi: 10.1002/er.1443

Chandrasekharan, R., Lee, E. S., Fisher, D. E., & Deokar, P. S. (2013). An Enhanced Simulation Model for Building Envelopes with Phase Change Materials. *ASHRAE Transactions, 119*(2).

Chen, Z. Q., Gu, M. W., Peng, D. H., Peng, C. H., & Wu, Z. S. (2010). A numerical study on heat transfer of high efficient solar flat-plate collectors with energy storage. *International Journal of Green Energy, 7*(3), 326-336. doi: 10.1080/15435071003796186

Coleman, H. W., & Steele, W. G. (1998). *Experimentation and Uncertainty Analysis for Engineers* (2nd ed.): John Wiley & Sons Inc.

COMSOL. (2015). COMSOL Multiphysics Retrieved 10-22-2015, from http://www.comsol.com/

Costa, M., Buddhi, D., & Oliva, A. (1998). Numerical simulation of a latent heat thermal energy storage system with enhanced heat conduction *Energy Conversion and Management, 39*(3-4), 319-330. doi: 10.1016/S0196-8904(96)00193-8

Crank, J. (1984). *Free and moving boundary problems*. New York: Oxford University Press.

Cristopia Energy Systems. (2011). Cristopia projet reports Retrieved 2012-04-18, from http://www.cristopia.com/

D'Avignon, K., & Kummert, M. (2012). *Proposed TRNSYS model for storage tank with encapsulated phase change materials*. Paper presented at the 5th National Conference of IBPSA-USA, Madison, Wisconsin.

D'Avignon, K., & Kummert, M. (2013). *Comparison of system-level simulation and detailed models for storage tanks with phase change materials*. Paper presented at the 13th Conference of International Building Performance Simulation Association, Chambéry, France.

D'Avignon, K., & Kummert, M. (2015a). Assessment of T-History Method Variants to Obtain Enthalpy-Temperature Curves for PCMs With Significant Subcooling. *Journal of Thermal Science and Engineering Applications, 7*(4), 041015-041015. doi: 10.1115/1.4031220

D'Avignon, K., & Kummert, M. (2015b). Experimental assessment of a phase change material storage tank. *Applied Thermal Engineering*, Submitted on September 6th, 2015.

de Gracia, A., Navarro, L., Castell, A., & Cabeza, L. F. (2015). Energy performance of a ventilated double skin facade with PCM under different climates. *Energy and Buildings, 91*(0), 37-42. doi: 10.1016/j.enbuild.2015.01.011

de Gracia, A., Oró, E., Farid, M. M., & Cabeza, L. F. (2011). Thermal analysis of including phase change material in a domestic hot water cylinder. *Applied Thermal Engineering, 31*(17–18), 3938-3945. doi: 10.1016/j.applthermaleng.2011.07.043

de Moura, C. A., & Kubrusly, C. S. (2013). The Courant-Friedrichs-Lewy (CFL) Condition *80 Years After Its Discovery* (pp. 237). Retrieved from http://link.springer.com/10.1007/978-0-8176-8394-8 doi:10.1007/978-0-8176-8394-8

Delcroix, Kummert, M., & Daoud, A. (2015). *Thermal behavior mapping of a phase change material between the heating and cooling enthalpy-temperature curves.* Paper presented at the 6th International Building Physics Conference, Torino, Italy.

Delcroix, B. (2015). *Modeling of Thermal Mass Energy Storage in Buildings With Phase Change Materials.* Ph. D., École Polytechnique de Montréal, Montréal.

Dolado, P., Lazaro, A., Marin, J. M., & Zalba, B. (2011). Characterization of melting and solidification in a real-scale PCM-air heat exchanger: Experimental results and empirical model *Renewable Energy, 36*(11), 2906-2917. doi: 10.1016/j.renene.2011.04.008

Dolado, P., Lázaro, A., Zalba, B., & Marin, J. M. (2006). *Numerical simulation of the thermal behaviour of an energy storage unit with phase change materials for air conditioning applications between 17°C and 40°C.* Paper presented at the 10th international conference on thermal energy storage, ECOSTOCK 2006, Galloway, NJ.

Dutil, Y., Rousse, D. R., Ben Salah, N., Lassue, S., & Zalewski, L. (2011). A review on phase change materials: Mathematical modeling and simulations *Renewable and Sustainable Energy Reviews, 15*(1), 112-130. doi: 10.1016/j.rser.2010.06.011

Eames, I. W., & Adref, K. T. (2002). Freezing and melting of water in spherical enclosures of the type used in thermal (ice) storage systems. *Applied Thermal Engineering, 22*(7), 733-745. doi: 10.1016/S1359-4311(02)00026-1

Eames, P. C., & Griffiths, P. W. (2006). Thermal behaviour of integrated solar collector/storage unit with 65 degrees C phase change material. *Energy Conversion and Management, 47*(20), 3611-3618. doi: 10.1016/j.enconman.2006.02.029

Elsayed, A. O. (2007). Numerical study of ice melting inside rectangular capsule under cyclic temperature of heat transfer fluid. *Energy Conversion and Management, 48*(1), 124-130. doi: 10.1016/j.enconman.2006.05.006

Esen, M. (2000). Thermal performance of a solar-aided latent heat store used for space heating by heat pump. *Solar Energy, 69*(1), 15-25. doi: 10.1016/S0038-092X(00)00015-3

Farid, M. M., Khudhair, A. M., Razack, S. A. K., & Al-Hallaj, S. (2004). A review on phase change energy storage: Materials and applications. *Energy Conversion and Management, 45*(9-10), 1597-1615. doi: 10.1016/j.enconman.2003.09.015

Figliola, R. S., & Beasley, D. E. (2011a). Theory and Design for Mechanical Measurements (5th ed., pp. 309-374): Wiley.

Figliola, R. S., & Beasley, D. E. (2011b). Theory and Design for Mechanical Measurements (5th ed., pp. 161-208): Wiley.

Fiorito, F. (2012). Trombe Walls for Lightweight Buildings in Temperate and Hot Climates. Exploring the Use of Phase-change Materials for Performances Improvement. *Energy Procedia, 30*, 1110-1119. doi: 10.1016/j.egypro.2012.11.124

Gong, Z.-X., & Mujumdar, A. S. (1997). Non-convergence versus non-conservation in effective heat capacity methods for phase-change problems. *International Journal of Numerical Methods for Heat & Fluid Flow, 7*(6), 565-579. doi: 10.1108/09615539710170754

Günther, E., Hiebler, S., Mehling, H., & Redlich, R. (2009). Enthalpy of Phase Change Materials as a Function of Temperature: Required Accuracy and Suitable Measurement Methods. *International Journal of Thermophysics, 30*(4), 1257-1269. doi: 10.1007/s10765-009-0641-z

Günther, E., Mehling, H., & Hiebler, S. (2007). Modeling of subcooling and solidification of phase change materials *Modeling and Simulation in Materials Science and Engineering, 15*(8). doi: 10.1088/0965-0393/15/8/005

Halawa, E., Saman, W., & Bruno, F. (2010). A phase change processor method for solving a one-dimensional phase change problem with convection boundary. *Renewable Energy, 35*(8), 1688-1695. doi: 10.1016/j.renene.2010.01.016

Hamdan, M. A., & Elwerr, F. A. (1996). Thermal energy storage using a phase change material. *Solar Energy, 56*(2), 183-189. doi: 10.1016/0038-092X(95)00090-E

Hong, H., Kim, S. K., & Kim, Y.-S. (2004). Accuracy improvement of T-history method for measuring heat of fusion of various materials. *International Journal of Refrigeration, 27*(4), 360-366. doi: 10.1016/j.ijrefrig.2003.12.006

Hydro-Quebec. (2014). Annual Report 2014: Hydro-Quebec.

Ibáñez, M., Cabeza, L. F., Sole, C., Roca, J., & Nogues, M. (2006). Modelization of a water tank including a PCM module. *Applied Thermal Engineering, 26*(11-12), 1328-1333. doi: 10.1016/j.applthermaleng.2005.10.022

Incropera, F. P., Dewitt, D. P., Bergman, T. L., & Lavine, A. S. (2007). *Fundamentals of heat and mass transfer* (6th edition ed.). Hoboken: John Wiley & Sons.

International Energy Agency. (2008). Energy Technology Perspectives 2008: Scenarios & Strategies to 2050 Retrieved from http://www.iea.org/media/etp/etp2008.pdf

Kalnæs, S. E., & Jelle, B. P. (2015). Phase change materials and products for building applications: A state-of-the-art review and future research opportunities. *Energy and Buildings, 94*(0), 150-176. doi: 10.1016/j.enbuild.2015.02.023

Kenisarin, M., & Mahkamov, K. (2007). Solar energy storage using phase change materials. *Renewable and Sustainable Energy Reviews, 11*(9), 1913-1965. doi: 10.1016/j.rser.2006.05.005

Khudhair, A. M., & Farid, M. M. (2004). A review on energy conservation in building applications with thermal storage by latent heat using phase change materials. *Energy Conversion and Management, 45*(2), 263-275. doi: 10.1016/S0196-8904(03)00131-6

Klein, J. S., Beckman, W. A., Mitchell, J. W., Duffie, J. A., Duffie, N. A., Freeman, T. L., Mitchell, J. C., Braun, J. E., Evans, B. L., Kummer, J. P., Urban, R. E., Fiksel, A., Thornton, J. W., Blair, N. J., Williams, P. M., Bradley, D. E., McDowell, T. P., Kummert,

M., & Duffy, M. J. (2011). *TRNSYS 17 - A TRaNsient System Simulation program, User manual* Madison: University of Wisconsin-Madison.

Kousksou, T., Bruel, P., Cherreau, G., Leoussoff, V., & El Rhafiki, T. (2011). PCM storage for solar DHW: From an unfulfilled promise to a real benefit. *Solar Energy, 85*(9), 2033-2040. doi: 10.1016/j.solener.2011.05.012

Kozlowski, T. (2009). Some factors affecting supercooling and the equilibrium freezing point in soil–water systems. *Cold Regions Science and Technology, 59*(1), 25-33. doi: 10.1016/j.coldregions.2009.05.009

Kravvaritis, E. D., Antonopoulos, K. A., & Tzivanidis, C. (2010). Improvements to the measurement of the thermal properties of phase change materials. *Journal of Measurement Science and Technology, 21*(4), 1-9. doi: 10.1088/0957-0233/21/4/045103

Kravvaritis, E. D., Antonopoulos, K. A., & Tzivanidis, C. (2011). Experimental determination of the effective thermal capacity function and other thermal properties for various phase change materials using the thermal delay method. *Journal of Applied Energy, 88*(12), 4459-4469. doi: 10.1016/j.apenergy.2011.05.032

Lacroix, M. (1989). Computation of heat transfer during melting of a pure substance from an isothermal wall. *Numerical Heat Transfer, Part B: Fundamentals, 15*(2), 191-210. doi: 10.1080/10407798908944900

Lacroix, M. (1999). Electric water heater designs for load shifting and control of bacterial contamination. *Energy Conversion and Management, 40*(12), 1313-1340. doi: 10.1016/S0196-8904(99)00013-8

Lacroix, M. (2001). Contact melting of a phase change material inside a heated parallelepedic capsule. *Energy Conversion and Management, 42*(1), 35-47. doi: 10.1016/S0196-8904(00)00047-9

Langlois, A. (2011). *Pompes a chaleur geothermiques utilisant des banques thermiques a materiau a changement de phase.* M.Sc.A., Ecole Polytechnique de Montreal, Canada.

Larocque, S. (2014, 04-17-2014). L'entreprise du président de l'OIQ condamnée, *La Presse*. Retrieved from http://affaires.lapresse.ca/dossiers/litiges-economiques/201404/17/01-4758454-lentreprise-du-president-de-loiq-condamnee.php

Lázaro, A., Dolado, P., Marín, J. M., & Zalba, B. (2009). PCM–air heat exchangers for free-cooling applications in buildings: Experimental results of two real-scale prototypes. *Energy Conversion and Management, 50*(3), 439-443. doi: 10.1016/j.enconman.2008.11.002

Lázaro, A., Günther, E., Mehling, H., Hiebler, S., Marín, J. M., & Zalba, B. (2006). Verification of a T-history installation to measure enthalpy versus temperature curves of phase change materials. *Journal of Measurement Science and Technology, 17*(8), 2168-2174. doi: 10.1088/0957-0233/17/8/01

Lázaro, A., Peñalosa, C., Solé, A., Diarce, G., Haussmann, T., Fois, M., Zalba, B., Gshwander, S., & Cabeza, L. F. (2013). Intercomparative tests on phase change materials characterisation with differential scanning calorimeter. *Applied Energy, 109*(0), 415-420. doi: 10.1016/j.apenergy.2012.11.045

Liu, K., Güven, H., Beyene, A., & Lowrey, P. (1994). A comparison of the field performance of thermal energy storage (TES) and conventional chiller systems. *Energy, 19*(8), 899-900. doi: 10.1016/0360-5442(94)90041-8

Liu, M., Bruno, F., & Saman, W. (2011). Thermal performance analysis of a flat slab phase change thermal storage unit with liquid-based heat transfer fluid for cooling applications. *Solar Energy, 85*(11), 3017-3027. doi: 10.1016/j.solener.2011.08.041

Liu, M., Saman, W., & Bruno, F. (2011). Validation of a mathematical model for encapsulated phase change material flat slabs for cooling applications. *Applied Thermal Engineering, 31*(14-15), 2340-2347. doi: 10.1016/j.applthermaleng.2011.03.034

Liu, S., & Li, Y. (2015). An experimental study on the thermal performance of a solar chimney without and with PCM. *Renewable Energy, 81*(0), 338-346. doi: 10.1016/j.renene.2015.03.054

MacDonald, F., D'Avignon, K., Kummert, M., & Daoud, A. (2014). *A TRNSYS-LabVIEW bi-directional connection for HVAC equipment testing using hardware-in-the-loop simulation.* Paper presented at the 9th International Conference on System Simulation in Buildings 2014, Liege, Belgium.

Malvi, C. S., Dixon-Hardy, D. W., & Crook, R. (2011). Energy balance model of combined photovoltaic solar-thermal system incorporating phase change material. *Solar Energy, 85*(7), 1440.

Marín, J. M., Zalba, B., Cabeza, L. F., & Mehling, H. (2003). Determination of enthalpy-temperature curves of phase change materials with the temperature-history method: improvement to temperature dependent properties. *Journal of Measurement Science and Technology, 14*(2), 184-189. doi: 10.1088/0957-0233/14/2/305

Marín, J. M., Zalba, B., Cabeza, L. F., & Mehling, H. (2005). Improvement of a thermal energy storage using plates with paraffin–graphite composite. *International Journal of Heat and Mass Transfer, 48*(12), 2561-2570. doi: 10.1016/j.ijheatmasstransfer.2004.11.027

Mehling, H., & Cabeza, L. F. (2008). *Heat and cold storage with PCM - An up to date introduction into basics and applications*. Berlin: Springer.

Mehling, H., Cabeza, L. F., Hippeli, S., & Hiebler, S. (2003). PCM-module to improve hot water heat stores with stratification. *Renewable Energy, 28*(5), 699-711. doi: 10.1016/S0960-1481(02)00108-8

Moffat, R. J. (1982). Contributions to the Theory of Single-Sample Uncertainty Analysis. *Transactions of the ASME, 104*(2), 250-260.

Moreno, P., Castell, A., Solé, C., Zsembinszki, G., & Cabeza, L. F. (2014). PCM thermal energy storage tanks in heat pump system for space cooling. *Energy and Buildings, 82*(0), 399-405. doi: 10.1016/j.enbuild.2014.07.044

Nallusamy, N., Sampath, S., & Velraj, R. (2007). Experimental investigation on a combined sensible and latent heat storage system integrated with constant/varying (solar) heat sources *Renewable Energy, 32*(7), 1206-1227. doi: 10.1016/j.renene.2006.04.015

National Instruments Corporation. Retrieved 2014-10-29, from www.ni.com

Natural Resources Canada. (2013). Energy Efficiency Trends in Canada - 1990 to 2010: Natural Resources Canada.

Nikoofard, S., Ugursal, V. I., & Beausoleil-Morrison, I. (2015). Techno-economic assessment of the impact of phase change material thermal storage on the energy consumption and GHG

emissions of the Canadian Housing Stock. *Building Simulation, 8*(2), 225-238. doi: 10.1007/s12273-014-0204-5

Nkwetta, D. N., & Haghighat, F. (2014). Thermal energy storage with phase change material—A state-of-the art review. *Sustainable Cities and Society, 10*, 87-100. doi: 10.1016/j.scs.2013.05.007

Nkwetta, D. N., Vouillamoz, P.-E., Haghighat, F., El Mankibi, M., Moreau, A., & Desai, K. (2014). Phase change materials in hot water tank for shifting peak power demand. *Solar Energy, 107*(0), 628-635. doi: 10.1016/j.solener.2014.05.034

Paré, D., & Bilodeau, S. (2007). TES without ice. *ASHRAE Journal, 49*(7), 46-49.

Patankar, S. V. (1980). *Numerical heat transfer and fluid flow*. Washington: Taylor & Francis.

PCM Products Ltd. (2009). Setting a new world standard in green building design Retrieved 2013-10-08, from http://www.pcmproducts.net/files/melbourne_city_council_ch2_plusice_application.pdf

PCM Products Ltd. (2015). Phase Change Materials Products Ltd. Retrieved 2015-11-02, from http://www.pcmproducts.net

Peck, J. H., Kim, J.-J., Kang, C., & Hong, H. (2006). A study of accurate latent heat measurement for a PCM with a low melting temperature using T-history method. *International Journal of Refrigeration, 29*(7), 1225-1232. doi: 10.1016/j.ijrefrig.2005.12.014

Pomianowski, M., Heiselberg, P., & Zhang, Y. (2013). Review of thermal energy storage technologies based on PCM application in buildings. *Energy and Buildings, 67*(0), 56-69. doi: 10.1016/j.enbuild.2013.08.006

Popiel, C. O., Wojtkowiak, J., & Bober, K. (2007). Laminar free convective heat transfer from isothermal vertical slender cylinder. *Experimental Thermal and Fluid Science, 32*(2), 607-613. doi: 10.1016/j.expthermflusci.2007.07.003

Puschnig, P., Heinz, A., & Steicher, W. (2005). *TRNSYS simulation model for an energy storage for PCM slurries and/or PCM modules*. Paper presented at the Second Conference on

Phase Change Material & Slurry: Scientific Conference & Business Forum, Yverdon-les-Bains, Switzerland.

Rabin, Y., Bar-Niv, I., Korin, E., & Mikic, B. (1995). Integrated solar collector storage system based on a salt-hydrate phase-change material. *Solar Energy, 55*(6), 435-444.

Raj, V. A. A., & Velraj, R. (2010). Review on free cooling of buildings using phase change materials. *Renewable and Sustainable Energy Reviews, 14*(9), 2819-2829. doi: 10.1016/j.rser.2010.07.004

RAL Gütezeichen. (2013). Phase Change Material Quality Assurance *RAL-GZ 896*. Sankt Augustin, Germany: German Institute for Quality Assurance and Certification e.V.

Rathgeber, C., Miró, L., Cabeza, L. F., & Hiebler, S. (2014). Measurement of enthalpy curves of phase change materials via DSC and T-History: When are both methods needed to estimate the behaviour of the bulk material in applications? *Thermochimica Acta, 596*(0), 79-88. doi: 10.1016/j.tca.2014.09.022

Regin, A. F., Solanki, S. C., & Saini, J. S. (2008). Heat transfer characteristics of thermal energy storage system using PCM capsules: A review *Renewable and Sustainable Energy Reviews, 12*(9), 2438-2458. doi: 10.1016/j.rser.2007.06.009

Richardson, M. J. (1997). Quantitative aspects of differential scanning calorimetry. *Thermochimica Acta, 300*(1-2), 15-28. doi: 10.1016/S0040-6031(97)00188-3

Riffat, S. B., Omer, S. A., & Ma, X. (2001). A novel thermoelectric refrigeration system employing heat pipes and a phase change material: an experimental investigation. *Renewable Energy, 23*(2), 313-323. doi: 10.1016/S0960-1481(00)00170-1

Rodriguez-Ubinas, E., Ruiz-Valero, L., Vega, S., & Neila, J. (2012). Applications of Phase Change Material in highly energy-efficient houses. *Energy and Buildings, 50*, 49-62. doi: 10.1016/j.enbuild.2012.03.018

Rudtsch, S. (2002). Uncertainty of heat capacity measurements with differential scanning calorimeters. *Thermochimica Acta, 382*(1-2), 17-25. doi: 10.1016/S0040-6031(01)00730-4

Saman, W., Bruno, F., & Halawa, E. (2005). Thermal performance of PCM thermal storage unit for a roof integrated solar heating system. *Solar Energy, 78*(2), 341-349. doi: 10.1016/j.solener.2004.08.017

Sandnes, B., & Rekstad, J. (2006). Supercooling salt hydrates: Stored enthalpy as a function of temperature. *Journal of Solar Energy, 80*(5), 616-625. doi: 10.1016/j.solener.2004.11.014

Sharma, A., Tyagi, V. V., Chen, C. R., & Buddhi, D. (2009). Review on thermal energy storage with phase change materials and applications. *Renewable and Sustainable Energy Reviews, 13*(2), 318-345. doi: 10.1016/j.rser.2007.10.005

Shirazi, A. S. (2012). *Transient Heat Transfer in Vertical Ground Heat Exchangers.* Ph. D., École Polytechnique de Montréal, Montréal.

Shyy, W., Udaykumar, H. S., Rao, M. M., & Smith, R. W. (1996). *Computational fluid dynamics with moving boundaries*. Washington: Taylor & Francis.

Siemens Canada ltée c. Groupe Enerstat inc., No. 450-17-002827-088, 2014 QCCS 1601, CanLII (Superior Court of Québec 2014).

Silva, P. D., Gonçalves, L. C., & Pires, L. (2002). Transient behaviour of a latent-heat thermal-energy store: numerical and experimental studies *Applied Energy, 73*(1), 83-98. doi: 10.1016/S0306-2619(02)00060-0

Sohn, C. W., & Nixon, J. L. (2001). Long-term experience with external-melt ice-on-coil storage cooling system. *ASHRAE Transactions, 107*, 532-537.

Solé, A., Miró, L., Barreneche, C., Martorell, I., & Cabeza, L. F. (2013). Review of the T-history method to determine thermophysical properties of phase change materials (PCM). *Renewable and Sustainable Energy Reviews, 26*(0), 425-436. doi: 10.1016/j.rser.2013.05.066

Solomon, G. R., Karthikeyan, S., & Velraj, R. (2013). Sub cooling of PCM due to various effects during solidification in a vertical concentric tube thermal storage unit. *Applied Thermal Engineering, 52*(2), 505-511. doi: 10.1016/j.applthermaleng.2012.12.030

Systemex Energies inc. c. Groupe Enerstat inc., No. 500-17-061210-103, 500-17-059433-105, 500-17-059375-108, 2015 QCCS 1038, CanLII (Superior Court of Québec 2015).

Tabares-Velasco, P. C., Christensen, C., & Bianchi, M. (2012). Verification and validation of EnergyPlus phase change material model for opaque wall assemblies. *Building and Environment, 54*(0), 186-196. doi: 10.1016/j.buildenv.2012.02.019

Talmatsky, E., & Kribus, A. (2008). PCM storage for solar DHW: An unfulfilled promise? *Solar Energy, 82*(10), 861-869. doi: 10.1016/j.solener.2008.04.003

Tartaglino, U., Zykova-Timan, T., Ercolessi, F., & Tosatti, E. (2005). Melting and nonmelting of solid surfaces and nanosystems. *Physics Reports, 411*(5), 291-321. doi: 10.1016/j.physrep.2005.01.004

Tittelein, P., Gibout, S., Franquet, E., Johannes, K., Zalewski, L., Kuznik, F., Dumas, J.-P., Lassue, S., Bédécarrats, J.-P., & David, D. (2015). Simulation of the thermal and energy behaviour of a composite material containing encapsulated-PCM: Influence of the thermodynamical modelling. *Applied Energy, 140*(0), 269-274. doi: 10.1016/j.apenergy.2014.11.055

Turnpenny, J. R., Etheridge, D. W., & Reay, D. A. (2000). Novel ventilation cooling system for reducing air conditioning in buildings. Part I: testing and theoretical modelling. *Applied Thermal Engineering, 20*(11), 1019-1037. doi: 10.1016/S1359-4311(99)00068-X

Turnpenny, J. R., Etheridge, D. W., & Reay, D. A. (2001). Novel ventilation cooling system for reducing air conditioning in buildings. Part II: testing of prototype. *Applied Thermal Engineering, 21*(12), 1203-1217. doi: 10.1016/S1359-4311(01)00003-5

Tyagi, V. V., & Buddhi, D. (2007). PCM thermal storage in buildings: A state of art. *Renewable and Sustainable Energy Reviews, 11*(6), 1146-1166. doi: 10.1016/j.rser.2005.10.002

Vakilaltojjar, S. M. (2000). *Phase Change Thermal Storage System For Space Heating And Cooling.* Ph. D., University of South Australia. Retrieved from http://arrow.unisa.edu.au:8081/1959.8/82317

Vakilaltojjar, S. M., & Saman, W. (2001). Analysis and modelling of a phase change storage system for air conditioning applications. *Applied Thermal Engineering, 21*(3), 249-263. doi: 10.1016/S1359-4311(00)00037-5

Voller, V. R. (1990). Fast implicit finite-difference method for the analysis of phase change problems. *Numerical Heat Transfer, Part B: Fundamentals, 17*(2), 155-169.

Voller, V. R., Cross, M., & Markatos, N. C. (1987). Enthalpy method for convection/diffusion phase change. *International Journal for Numerical Methods in Engineering, 24*(1), 271-284.

Voller, V. R., & Prakash, C. (1987). A fixed grid numerical modelling methodology for convection-diffusion mushy region phase-change problems. *International Journal of Heat and Mass Transfer, 30*(8), 1709-1719.

Wang, M. J., & Kusumoto, N. (2001). Ice slurry based thermal storage in multifunctional buildings. *Heat and Mass Transfer, 27*(6), 597-604.

Wang, X., Zhang, Y. P., Xiao, W., Zeng, R. L., Zhang, Q. L., & Di, H. F. (2009). Review on thermal performance of phase change energy storage building envelope. *Chinese Science Bulletin, 54*(6), 920-928. doi: 10.1007/s11434-009-0120-8

Wei, D., Liang, C., Xing, X., & Yun, Z. (2009). *Phase change materials in building envelopes - state of the art review.* Paper presented at the 5th International Workshop on Energy and Environment of Residential Buildings and 3rd International Conference on Built Environment and Public Health, Guilin, China.

Wei, J., Kawaguchi, Y., Hirano, S., & Takeuchi, H. (2005). Study on a PCM heat storage system for rapid heat supply. *Applied Thermal Engineering, 25*(17-18), 2903-2920. doi: 10.1016/j.applthermaleng.2005.02.014

Xie, J., Li, Y., Wang, W., Pan, S., Cui, N., & Liu, J. (2013). Comments on Thermal Physical Properties Testing Methods of Phase Change Materials. *Advances in Mechanical Engineering, 2013*, 1-9. doi: 10.1155/2013/695762

Yamaha, M., & Misaki, S. (2006). The evaluation of peak shavings by a thermal storage system using phase-change materials in air distribution systems. *HVAC&R Research, 12*(Supplement 3), 861-869. doi: 10.1080/10789669.2006.10391213

Yang, H., & He, Y. (2010). Solving heat transfer problems with phase change via smoothed effective heat capacity and element-free Galerkin methods. *International communications in heat and mass transfer, 37*(4), 385-392. doi: 10.1016/j.icheatmasstransfer.2009.12.002

Zalba, B. (2002). *Thermal energy storage with phase change. Experimental procedure.* Ph.D., University of Zaragoza, Zaragoza, Spain.

Zalba, B., Marin, J. M., Cabeza, L. F., & Mehling, H. (2003). Review on thermal energy storage with phase change: Materials, heat transfer analysis and applications. *Applied Thermal Engineering, 23*(3), 251-283. doi: 10.1016/S1359-4311(02)00192-8

Zalba, B., Marin, J. M., Cabeza, L. F., & Mehling, H. (2004). Free-cooling of buildings with phase change materials. *International Journal of Refrigeration, 27*(8), 839-849. doi: 10.1016/j.ijrefrig.2004.03.015

Zhang, Y., Jiang, Y., & Jiang, Y. (1999). A simple method, the T-history method, of determining the heat of fusion, specific heat and thermal conductivity of phase-change materials. *Journal of Measurement Science and Technology, 10*(3), 201-205.

Zhou, G. B., Zhang, Y. P., Wang, X., Lin, K. P., & Xiao, W. (2007). An assessment of mixed type PCM-gypsum and shape-stabilized PCM plates in a building for passive solar heating. *Solar Energy, 81*(11), 1351-1360. doi: 10.1016/j.solener.2007.01.014

Zhu, N., Ma, Z. J., & Wang, S. W. (2009). Dynamic characteristics and energy performance of buildings using phase change materials: A review. *Energy Conversion and Management, 50*(12), 3169-3181. doi: 10.1016/j.enconman.2009.08.019

Zivkovic, B., & Fujii, I. (2001). An analysis of isothermal phase change of phase change material within rectangular and cylindrical containers *Solar Energy, 70*(1), 51-61. doi: 10.1016/S0038-092X(00)00112-2

Zukowski, M. (2007). Experimental study of short term thermal energy storage unit based on enclosed phase change material in polyethylene film bag. *Energy Conversion and Management, 48*(1), 166-173. doi: 10.1016/j.enconman.2006.04.020

APPENDIX A – ADDITIONAL S27 PROPERTIES

This appendix presents the properties of phase change material S27 required for adequate numerical simulation of the PCM object's behaviour. Phase change material S27 is a salt hydrate, i.e. a mixing of salt and water in a fixed ratio. Because salt hydrates consist of several components they can separate into different phases which leads to stability problems after numerous heating/cooling cycles (Mehling & Cabeza, 2008). As can be seen on Figure A-1, material S27 is heterogeneous and appears to be composed of a clear liquid component, a viscous translucent liquid component and numerous beads the size of grains of sand. The latter are special additives (i.e. nucleators) meant to cause heterogeneous nucleation and reduce the likeliness of supercooling.

Figure A-1: Image of S27 sample equipped with a thermocouple sensor

As shown in Table A.1, only some properties were supplied by the manufacturer. The properties specified by the manufacturer are somewhat ambiguous. It is unclear whether the density and thermal conductivity values specified are associated with the liquid state or solid state of the phase change material. Only the container weight is listed when it is the phase change material weight that is required for adequate simulation. The single phase change temperature indicated

implies the latent heat of fusion is released at a specific temperature rather than over a temperature range which is rare for heterogeneous PCMs. Also, most salt hydrates will exhibit supercooling (Mehling & Cabeza, 2008) but no information is specified by the manufacturer in that regard.

Table A.1: S27 properties supplied by the manufacturer[7]

Phase change temperature	27 °C
Density	1530 kg/m^3
Latent heat of fusion	183 kJ/kg
Volumetric heat capacity	280 MJ/m^3
Specific heat capacity	2.20 kJ/kg-K
Thermal conductivity	0.540 W/m-K
Container weight	5.81 kg

Some properties had to be determined from experimentation and others specified by the manufacturer had to be validated. The experimental procedure used for measuring each property is described in the next sections, followed by a presentation of the uncertainty on that measurement.

Measurement procedure

Four glass cylinders graduated from 50 ml to 1000 ml were identified with letters A through D, cleaned and weighed on a QUINTIX2102-1S balance from Sartorius Weighing Technology GmbH. Five weightings were made, labelled E1 through E5, in order to reduce random errors caused by variations in air movements, user error etc. A single PCM object was heated in a controlled chamber to a temperature of 65 °C, when its content was completely liquefied. The capsule was vigorously shaken to maximise homogeneity of its contents and emptied into the four graduated cylinders. Each graduated cylinders was then put through five separate weightings, labelled R1 through R5, and the volume of its content measured by two different observers, labelled V1 and V2. The temperature of each cylinder was taken both before and after the series of weight and volume measurements using a Type-T thermocouple connected with a hand-held HH501BT Omega data acquisition system.

[7] The properties listed have been copied exactly as found in manufacturer data.

Table A.1: PCM temperature before and after measurements

	Cylinder identifier	A	B	C	D
Temperature readings [g]	T1 [°C]	64.0	64.1	61.5	63.7
	T2 [°C]	63.3	61.5	61.4	61.2

Temperature readings T1 were taken before any measurements were made of the graduated cylinder in question and readings T2 were taken after all measurements. The temperature readings listed in Table A.2 indicate the PCM was clearly in its liquid phase during the whole measurement process and so all properties can be safely attributed to the PCM's liquid state.

PCM mass

The results from each weight reading are presented in Table A.3 below.

Table A.2: Weight measurements of the graduated cylinders

	Cylinder identifier	A	B	C	D
Empty cylinder weight [g]	E1	394.13	396.93	395.05	397.48
	E2	394.12	396.95	395.02	397.50
	E3	394.14	396.96	395.04	397.49
	E4	394.13	396.94	395.04	397.50
	E5	394.13	396.94	395.04	397.48
	Sample mean, $\overline{E}_i$	394.13	396.94	395.04	397.49
	Sample standard deviation, S_{E_i}	0.00707	0.01140	0.01095	0.01000
	Sample standard deviation of the mean, $S_{\overline{E}_i}$	0.003162	0.005099	0.004899	0.004472
Full cylinder weight [g]	R1	1827.33	1638.79	1532.90	1596.48
	R2	1827.32	1638.76	1532.85	1596.43
	R3	1827.30	1638.73	1532.82	1596.38
	R4	1827.27	1638.69	1532.81	1596.06
	R5	1827.25	1638.69	1532.79	1596.02
	Sample mean, $\overline{R}_i$	1827.29	1638.73	1532.83	1596.27
	Sample standard deviation, S_{R_i}	0.0336	0.0438	0.0428	0.2170
	Sample standard deviation of the mean, $S_{\overline{R}_i}$	0.0150	0.0196	0.0191	0.0970

In this case, the average mass of each filled graduated cylinder ($\overline{R}_A$ through $\overline{R}_D$) are variables independent from one another. The average mass of each empty graduated cylinder ($\overline{E}_A$ through $\overline{E}_D$) are likewise independent and accordingly the mass of the PCM inside a capsule, m_{pcm}., is determined through Equation A.1. The result is a PCM mass of 5011.53 g inside the capsule tested.

$$m_{pcm} = \sum_{i=A}^{D} \overline{R}_i - \sum_{i=A}^{D} \overline{E}_i = (\overline{R}_A + \overline{R}_B + \overline{R}_C + \overline{R}_D) - (\overline{E}_A + \overline{E}_B + \overline{E}_C + \overline{E}_D) \qquad (A.1)$$

The uncertainty on the measurement of the PCM mass inside the capsule, m_{pcm}, is obtained through the technique of propagation of uncertainties described by Figliola & Beasley (2011b). As detailed in Equation A.2, the combined standard uncertainty, u_c, is determined from the standard deviation estimate for the random uncertainty, S_i, and the standard deviation estimated for the systematic uncertainty, S_{Bi}, of each measured variable i. In this case, the variables, i, that must be considered are the average mass of each graduated cylinder both when empty and when filled; for a total of 10 variables.

$$u_c{}^2 = \sum_i \{S_{Bi}{}^2 + S_i{}^2\} = \sum_i \left\{ \left(\frac{B_i}{2}\right)^2 + \left(\frac{S_X}{\sqrt{N}}\right)^2 \right\} \qquad (A.2)$$

The balance's repeatability is ± 0.01 g according to the manufacturer's specifications. This is assumed to approximate with a 95% confidence level the limits of the systematic error, B_i, for all weight readings. Assuming a Gaussian distribution of the possible systematic errors, the standard deviation of the systematic uncertainty, S_{Bi}, of the average weight measurements is half of B_i, or 0.005 g for every variable. The standard deviation of the random uncertainty, S_i, is approximated as the sample standard deviation of the mean for each variable, $S_{\overline{R}_i}$ and $S_{\overline{E}_i}$, presented in Table A.3 above.

This results in a combined standard uncertainty, u_c, of 0.10 g, to which a coverage factor must be applied, t_{95}, to state the expanded uncertainty, U_{95}, with a 95% confidence level. The coverage factor is determined from Student's t-distribution for an effective number of degrees of freedom, ν_i, approximated through the Welch-Satterthwaite formula (Equation A.3).

$$v_i = \frac{\left\{\sum_{i=A}^{D}(S_{\bar{R}})_i^{\,2} + \sum_{i=A}^{D}(B_{\bar{R}})_i^{\,2} + \sum_{i=A}^{D}(S_{\bar{E}})_i^{\,2} + \sum_{i=A}^{D}(B_{\bar{E}})_i^{\,2}\right\}^2}{\sum_{i=A}^{D}\left(\frac{(S_{\bar{R}})_i^{\,2}}{v_{Si}}\right) + \sum_{i=A}^{D}\left(\frac{(B_{\bar{R}})_i^{\,2}}{v_{Bi}}\right) + \sum_{i=A}^{D}\left(\frac{(S_{\bar{E}})_i^{\,2}}{/v_{Si}}\right) + \sum_{i=A}^{D}\left(\frac{(B_{\bar{E}})_i^{\,2}}{v_{Bi}}\right)} \qquad \text{(A.3)}$$

In this case, the number of degree of freedom associated with the systematic uncertainty, v_{Bi}, can be considered very large so the second term of the denominator is neglected. The result is that the PCM mass inside a capsule, m_{pcm}, is evaluated at 5011.53 ± 0.27 g with a 95% confidence level. It must be noted that this uncertainty does not quantify the expected variability in the PCM mass between capsules. To do that, numerous capsules would have to have been opened and weighted which would have rendered them unusable for testing in the PCM tank afterwards. Due to the limited number of capsules available, only one was measured.

PCM volume

The two volume readings, V1 and V2, described previously are indicated in Table A.4 for each graduated cylinder.

Table A.3: Volume measurements

Cylinder identifier	A	B	C	D
V1	925	800	725	775
V2	920	800	740	775
Sample mean, $\overline{V}_i$	922.5	800	732.5	775
Standard deviation, S_V	3.536	0.000	10.607	0.000
Sample standard deviation of the mean, $S_{\overline{V}}$	2.5	0.0	7.5	0.0
Expected range of systematic error, B_i	46.125	40.000	36.625	38.750
Systematic uncertainty, S_{Bi}	23.0625	20.0000	18.3125	19.3750

Again, the measurements of the volume of PCM inside each graduated cylinder, A through D, are independent from one another, so the PCM volume inside the capsule, V_{pcm}, is calculated through Equation A.4. The result is a PCM volume of 3230 ml inside the capsule tested.

$$V_{pcm} = \sum_{i=A}^{D} \overline{V}_i = \overline{V}_A + \overline{V}_B + \overline{V}_C + \overline{V}_D \quad (A.4)$$

The cylinders are graduated every 50 ml, from 100 ml to 1000 ml and the manufacturer indicates an accuracy of ± 5 %. The resolution error due to the 50 ml graduations will be present in the data scatter of the readings and so it will figure in the evaluation of the random uncertainty. Taking the mean value of the volume readings made by two different observers is considered to render negligible any systematic reading error they might introduce. The systematic error, B_i, on volume readings is considered to involve only the ± 5 % accuracy expected by the manufacturer, so the associated uncertainty is illustrated in Table A.4 for each cylinder under the heading "B_i". Assuming a Gaussian distribution of the possible systematic errors, the standard deviation of the systematic uncertainty, S_{Bi}, of the volume measurements is half of B_i.

The standard deviation of the random uncertainty, S_i, is approximated as the sample standard deviation of the mean, $S_{\overline{V}}$, presented in Table A-3. This results in a combined standard uncertainty, u_c, of 41 ml and expanded uncertainty of 81 ml with a 95% confidence level. Therefore, the PCM volume inside the tested capsule, V_{pcm}, is evaluated at 3230 ± 81 ml. Again, this uncertainty does not assess the variability of the PCM volume amongst different capsules for the same reasons as those stipulated concerning the PCM mass.

PCM density

Though the capsule was shaken before being emptied into the graduated cylinders, we do not believe the PCM contained inside each cylinder is an identical sample of S27. Therefore, the average PCM mass and volume of each graduated cylinder are independent variables and are presented in Table A below.

Table A.4: Resulting PCM density

Cylinder identifier	A	B	C	D
$\overline{m}_{pcm}$ [kg]	1433.16	1241.79	1137.80	1198.78
$\overline{V}$ [ml]	922.5	800	732.5	775

The PCM density is calculated using the mass of PCM inside a capsule, m_{pcm}, and the volume of PCM inside that capsule, V_{pcm}, as indicated in Equation A.5. The resulting PCM density, ρ_{pcm}, is 1551.56 kg/m^3, which compares favourably with the manufacturer's reported value of 1530 kg/m^3.

$$\rho_{pcm} = \frac{m_{pcm}}{V_{pcm}} = \frac{\sum_{i=A}^{D} \overline{m}_{pcm_i}}{\sum_{i=A}^{D} \overline{V}_i} \tag{A.5}$$

The uncertainty on the liquid phase PCM density value, u_c, is determined from Equation A.6 using the uncertainty, u_i, and sensitivity index, θ_i, of each variable, *i*.

$$u_R{}^2 = \sum_i \{\theta_i u_i{}^2\} \tag{A.6}$$

In this case, the variables that must be considered are the total PCM mass in the capsule and the total PCM volume in that capsule; a total of two variables. The sensitivity index for the PCM mass and the PCM volume are respectively 3.1*10^{-4} and -4.8*10^{-4}, given by Equations A.7 and A.8 below.

$$\theta_{m_{pcm}} = \frac{\partial \rho}{\partial m_{pcm}} = \frac{\partial \left\{\frac{m_{pcm}}{V_{pcm}}\right\}}{\partial m_{pcm}} = \frac{1}{V_{pcm}} = 3.1 \cdot 10^{-4} \tag{A.7}$$

$$\theta_{V_{pcm}} = \frac{\partial \rho}{\partial V_{pcm}} = \frac{\partial \left\{\frac{m_{pcm}}{V_{pcm}}\right\}}{\partial V_{pcm}} = \frac{-m_{pcm}}{V_{pcm}{}^2} = -4.8 \cdot 10^{-4} \tag{A.8}$$

This results in a combined standard uncertainty in the result, u_R, of 2.19, therefore, the liquid phase PCM density, ρ_{pcm}, is evaluated at 1551.56 ± 2.19 kg/m^3.

Though no measurements were taken in the solid state, it can be stated that the solid phase density is higher than the liquid phase density as the PCM's volume reduces upon solidification. The above liquid phase value for density contradicts the value of 1530 kg/m^3 given by the manufacturer. A possible explanation would be that a significant variation exists in the composition of the material inserted in the PCM capsules produced, making the value reported by

the manufacturer closer to the average PCM density while still allowing certain capsules so see a density as low as that measured here.

References

Figliola, R. S., & Beasley, D. E. (2011a). Theory and Design for Mechanical Measurements (5th ed., pp. 309-374): Wiley.

Mehling, H., & Cabeza, L. F. (2008). *Heat and cold storage with PCM - An up to date introduction into basics and applications*. Berlin: Springer.

APPENDIX B – TEMPERATURE SENSOR CALIBRATION AND UNCERTAINTY

Temperature sensors of different types were used in the various experimental works of this thesis: 2 Type-K and 8 Type-T thermocouples, 16 platinum resistance temperature detectors (RTDs) and a prefabricated thermopile. A complete list of the various temperature sensors is given in Table B.1.

In this appendix, the experimental procedure used to calibrate the temperature sensors is defined followed by a presentation of the resulting sensor uncertainty. The sensors were calibrated in order to reduce their bias (systematic error) and to obtain a measure of the uncertainty associated with their measurements. Their calibration is based upon the method of R. J. Moffat (1982) used by Ali Salim Shirazi in his thesis (Shirazi, 2012) described in a Section below.

The prefabricated thermopile TP 2671 was not calibrated. It is a differential temperature transducer composed of 20 junctions of Type-T thermocouples. Each junction is electrically isolated, shielded against electromagnetic radiation and enclosed in an individual thermowell. This specific thermopile has dual housing so the two fluid passages can be installed at a certain distance from one another. The accuracy specified by the manufacturer is ± 0.04 °C on the temperature difference measurement.

The two Type-K thermocouples are also uncalibrated at the moment. Their accuracy as specified by ASTM E230-ANSI MC 96.1 is ± 2.20 °C over the temperature range used in this thesis. The uncertainty from the data-acquisition module, terminal block and the reference junction compensation is ± 0.36 °C. Combining both uncertainties through Equation B.6 (defined further) leads to a global uncertainty of ± 2.23 °C for these sensors.

Table B.2: List of temperature sensors

Sensor ID	Sensor type	Measured value ID	Usage
TK - 1	Type-K thermocouple, 304 SS sheath	$T3_{PCM}$	Capsule temperature measurements
TK - 2	Type-K thermocouple, 304 SS sheath	$T4_{PCM}$	
TC - 12	Type-T thermocouple, PFA insulated	$T2_{PCM}$	Characterization of PCM Object
TC - 16	Type-T thermocouple, PFA insulated	$T1_{PCM}$	
TC - 18	Type-T thermocouple, PFA insulated	$T2_{water}$	
TC - 21	Type-T thermocouple, PFA insulated	$T1_{water}$	
TC - 13	Type-T thermocouple, PFA insulated	T_{in}	
TC - 14	Type-T thermocouple, PFA insulated	T_{over}	
TC - 15	Type-T thermocouple, PFA insulated	T_{under}	
TC - 17	Type-T thermocouple, PFA insulated	T_{out}	
1/10 - 1	Platinum RTD, Class 1/10 DIN	Reference	Sensor calibration
1/10 - 5	Platinum RTD, Class 1/10 DIN	Reference	
1/10 - 14	Platinum RTD, Class 1/10 DIN	T201	Semi-virtual test bench test zone
1/10 - 16	Platinum RTD, Class 1/10 DIN	T202	
1/10 - 17	Platinum RTD, Class 1/10 DIN	T301	
1/10 - 18	Platinum RTD, Class 1/10 DIN	T302	
TP - 2671	Differential temperature transducer, 20 junctions of Type-T thermocouples	TP	
1/3 - 16	Platinum RTD, Class 1/3 DIN	T101	Semi-virtual test bench production zone
1/3 - 1	Platinum RTD, Class 1/3 DIN	T102	
1/3 - 2	Platinum RTD, Class 1/3 DIN	T103	
1/3 - 3	Platinum RTD, Class 1/3 DIN	T104	
1/3 - 4	Platinum RTD, Class 1/3 DIN	T105	
1/3 - 5	Platinum RTD, Class 1/3 DIN	T001	
1/3 - 6	Platinum RTD, Class 1/3 DIN	T002	
1/3 - 7	Platinum RTD, Class 1/3 DIN	T003	
1/3 - 8	Platinum RTD, Class 1/3 DIN	T004	
1/3 - 9	Platinum RTD, Class 1/3 DIN	T005	

Calibration

Experimental procedure

The experimental setup consisted on inserting the sensors to be calibrated in individual holes in a machined cylindrical copper block of 7.6 cm in diameter and 10 cm in height. The copper block is inserted into a constant temperature bath (Neslab RTE 220) filled with a 30% water-glycol mixture. Data acquisition is done via a CompactRio System. The Type-T thermocouples are connected to a 24-bit ADC isothermal thermocouple input module NI 9214 with built-in cold-junction compensation and the 4-wire platinum resistance sensors are connected to a 24-bit analog input module NI 9217 with built-in excitation and noise rejection.

The calibration is performed for target temperatures steps of 5 °C over the interval -10 °C to 70 °C. The temperature is measured and recorded by the data acquisition system every 1 second, for a time period of five minutes (300 data points recorded for each sensor) for each target temperature.

Calibration procedure

For the target temperature of 0 °C, the temperature measurements obtained from sensor *i* are averaged. The average temperature difference, $\Delta\overline{T}$, between that sensor's average temperature, $\overline{T}_i$, and the average reference temperature, $\overline{T}_{ref}$, is calculated as per Equation B.1 below.

$$\Delta\overline{T} = \overline{T}_{ref} - \overline{T}_i \qquad (B.1)$$

The procedure is repeated for each target temperature from -10 °C to 70 °C. The average temperature difference, $\Delta\overline{T}$, is then plotted against the corresponding average reference temperature, $\overline{T}_{ref}$, for each target temperature, leading to a plot such as illustrated in Figure B-1 for each sensor.

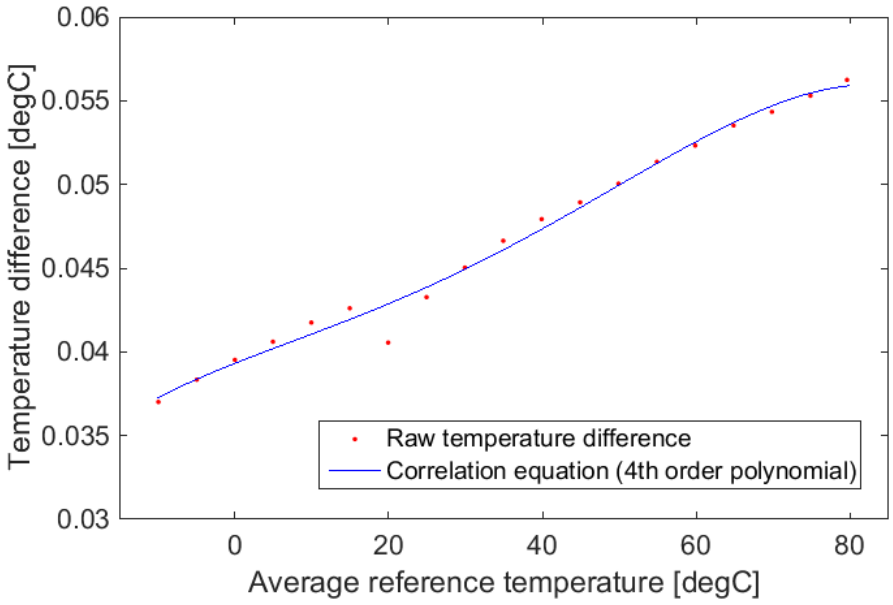

Figure B-1: Raw experimental and correlation predicted temperature difference plotted against the average reference temperature for sensor « 1/10 - 4 »

A polynomial is fitted to the data using a least square procedure. A fourth order polynomial of the form of Equation B.2 was found to predict the temperature difference with good accuracy.

$$\Delta\overline{T} = p_{5,i} + p_{4,i} \cdot \overline{T}_i + p_{3,i} \cdot \overline{T}_i^{\,2} + p_{2,i} \cdot \overline{T}_i^{\,3} + p_{1,i} \cdot \overline{T}_i^{\,4} \qquad \text{(B.2)}$$

In this equation, $\overline{T}_i$ is the average of the un-calibrated measured temperature for sensor *i* and $\Delta\overline{T}$ is the average temperature difference and coefficients $p_{j,i}$ represent the *j*th order coefficient of the polynomial for sensor *i*. The calibration correlation for each sensor can then be used to correct the measured temperature readings in the following way:

$$T_{i,cal} = T_i + \left\{p_5 + p_4 \cdot T_i + p_3 \cdot T_i^{\,2} + p_2 \cdot T_i^{\,3} + p_1 \cdot T_i^{\,4}\right\} \qquad \text{(B.3)}$$

where T_i is the un-calibrated temperature measured by sensor *i* and $T_{i,cal}$ is the resulting calibrated measurement.

Uncertainty

The uncertainty on the temperature sensor readings is obtained through the technique described by Figliola & Beasley (2011b). The uncertainty for the whole measurement system is determined from the uncertainty of each system component; the data-acquisition module and terminal block,

the reference junction compensation (in the case thermocouples are used as sensors), the calibration equation and the sensor itself.

A list of all uncertainties associated with the measurement system used with thermocouple sensors is detailed in Table B.5. The list also includes safeguards put in place in the measurement or calibration process to reduce each uncertainty source and the resulting conclusion on the significance of considering this source in the overall uncertainty calculation.

The list of uncertainties detailed in Table B.5 for thermocouples also applies to the platinum probe sensors, with the exception of the linearization error which does not exist as the data acquisition of RTDs does not require reference junction compensation. The same methodology is applied to both types of sensors.

Uncertainty of the data acquisition system

For the thermocouples, data acquisition is done via a CompactRio System using 24-bit ADC isothermal thermocouple input module NI 9214. The manufacturer specifies a measurement accuracy which includes all measurement errors from the data-acquisition system (terminal bock and module) including RMS noise. The built-in cold-junction compensation of the NI 9214 module introduces a linearization error which is also included in the specified measurement accuracy. The systematic uncertainty associated with the thermocouple data acquisition system will be removed through calibration. However the measurement accuracy of the reference sensor data acquisition system will have to be included in the overall uncertainty.

The reference sensors are 4-wire platinum RTDs which are connected to 24-bit analog input module NI 9217 with built-in excitation and noise rejection. The temperature accuracy specified by the manufacturer for the measurement system (including noise) is indicated in Table B.2 for different measured temperature ranges, ambient temperatures and RTD types.

Table B.3: Measurement accuracy for NI 9217 specified by the manufacturer

Sensor type, measurement mode	**Measured value**	**Typical ambient (25 °C)**	**Maximum ambient (-40 °C to 70 °C)**
4-wire, High-resolution mode	-200 °C to 150 °C	0.15 °C	0.35 °C
	150 °C to 850 °C	0.20 °C	1.00 °C

Table B.2 (continued): Measurement accuracy for NI 9217 specified by the manufacturer

3-wire,	-200 °C to 150 °C	0.20 °C	0.50 °C
High-resolution mode	150 °C to 850 °C	0.30 °C	1.00 °C

The temperature interval of the experiments considered here spanned up to 15 °C above and below the predicted phase change temperature of 27 °C of the phase change material, so the accuracy was taken as 0.15 °C. This leads to a data acquisition system uncertainty, denoted here as U1, of 0.15 °C.

Uncertainty of the reference sensor

As the averaged value of the 300 readings is used in determining the calibration equation coefficients, any random error of the reference sensors is negligible and only the systematic error is evaluated. The reference sensors are ultra-precise platinum RTDs with a 1/10 DIN accuracy in accordance with DIN/IEC 60751. The accuracy specification of class 1/10DIN sensors is specified by Equation B.4, where T is a measure temperature from 0.0 °C to 100.0 °C.

$$u_2 = \pm {}^{1}/_{10} \{0.3 + 0.005 \cdot |T|\} \text{ [°C]} \quad \text{(B.4)}$$

This results in the systematic uncertainty values for the reference sensor listed as U2 in Table B.3 for every average target temperature, $\overline{T}_{ref}$.

Uncertainty of the calibrated sensor

During the calibration experiment, each sensor performs 300 readings of the temperature at each of the target temperatures. The averaged value of these readings is used in determining the calibration equation coefficients so any random error of the sensors during calibration is negligible.

However, each reading performed by these sensors after having been calibrated will still include random errors. A component of the overall uncertainty must account for the fact that, at a specific reference temperature, the mean sample value is not the value which will be measured in the future by the calibrated sensor. Instead, measurements will be randomly distributed around this mean. The uncertainty associated with this random error is evaluated from the fluctuations in readings during the calibration experiment, for each target temperature. As an example, the

standard deviation of the 300 measurements, S_{T_i}, is calculated for thermocouple TC - 12 for each target temperature and presented in Table B.3.

Table B.4: Detailed calculation of random uncertainty for thermocouple TC - 12

$\overline{T}_{ref}$ **[°C]**	U2 **[°C]**	$\overline{T}_i$ **[°C]**	S_{T_i} **[°C]**	$2 * S_{T_i} = U3$ **[°C]**	$T_{i,cal}$ **[°C]**	U4 **[°C]**	u_c **[°C]**
-9.8745	0.0349	-10.0047	0.0070	0.0141	-9.8560	0.0185	0.1558
-4.8737	0.0324	-5.0350	0.0070	0.0140	-4.8995	0.0258	0.1562
0.0700	0.0300	-0.0588	0.0068	0.0136	-0.0619	0.0081	0.1538
5.0112	0.0325	4.9149	0.0068	0.0135	5.0193	0.0081	0.1543
10.0024	0.0350	9.9216	0.0071	0.0141	10.0086	0.0062	0.1548
15.0026	0.0375	14.9359	0.0067	0.0134	15.0046	0.0020	0.1552
19.9922	0.0400	19.9387	0.0065	0.0131	19.9885	0.0037	0.1558
24.9837	0.0425	24.9564	0.0068	0.0136	24.9870	0.0033	0.1565
29.9683	0.0450	29.9632	0.0070	0.0140	29.9749	0.0066	0.1574
34.9565	0.0475	34.9666	0.0068	0.0136	34.9597	0.0033	0.1580
39.9461	0.0500	39.9711	0.0067	0.0135	39.9468	0.0006	0.1587
44.9440	0.0525	44.9825	0.0067	0.0135	44.9418	0.0022	0.1595
49.9340	0.0550	49.9809	0.0070	0.0141	49.9258	0.0082	0.1606
54.9253	0.0575	54.9824	0.0065	0.0129	54.9152	0.0101	0.1615
59.9098	0.0600	59.9799	0.0067	0.0135	59.9033	0.0065	0.1623
64.8967	0.0624	64.9815	0.0068	0.0136	64.8988	0.0021	0.1631
69.8851	0.0649	69.9817	0.0070	0.0140	69.8967	0.0116	0.1644

As suggested by Figliola & Beasley (2011a), the random standard uncertainty, denoted as U3, is estimated to be twice the sample standard deviation of the 300 measurements for each sensor, S_{T_i}. A value for U3 is presented in Table B.3 for thermocouple TC - 12 for each target temperature.

Uncertainty of the calibration equation

Applying the calibration equation to the average of the temperature measurements for each sensor does not allow to reproduce the average reference sensor temperature perfectly; a difference remains. As an example, the temperature resulting from the calibration equation, $T_{i,cal}$, is

indicated in Table B.3 above for thermocouple TC – 12 for every target temperature. The uncertainty of the calibration equation is estimated by the absolute difference between the reference temperature and the temperature resulting from the correlation equation; it is illustrated in detail for thermocouple TC – 12 in Table B.3 under the heading U4.

Global uncertainty of thermocouple measurements

The square value of the different uncertainties presented above are added as indicated in Equation B.6 to produce a combined standard uncertainty, u_c, indicated in Table B.3.

$$u_c = \sqrt{U1^2 + U2^2 + U3^2 + U4^2} \quad \text{(B.6)}$$

From the combined standard uncertainty obtained for each target temperature, only the greatest value is retained for each temperature sensor and presented in Table B.4.

Table B.5: Maximum combined uncertainty for every sensor

Sensor ID	**Sensor type**	**Measured value ID**	**Max u_c [°C]**
TK - 1	Type-K thermocouple, 304 SS sheath	$T3_{PCM}$	2.23
TK - 2	Type-K thermocouple, 304 SS sheath	$T4_{PCM}$	2.23
TC - 12	Type-T thermocouple, PFA insulated	$T2_{PCM}$	0.1644
TC - 16	Type-T thermocouple, PFA insulated	$T1_{PCM}$	0.1642
TC - 18	Type-T thermocouple, PFA insulated	$T2_{water}$	0.1642
TC - 21	Type-T thermocouple, PFA insulated	$T1_{water}$	0.1650
TC - 13	Type-T thermocouple, PFA insulated	T_{in}	0.1641
TC - 14	Type-T thermocouple, PFA insulated	T_{over}	0.1643
TC - 15	Type-T thermocouple, PFA insulated	T_{under}	0.1642
TC - 17	Type-T thermocouple, PFA insulated	T_{out}	0.1662
1/3 - 16	Platinum RTD, Class 1/3 DIN	T101	0.1635
1/3 - 1	Platinum RTD, Class 1/3 DIN	T102	0.1635
1/3 - 2	Platinum RTD, Class 1/3 DIN	T103	0.1635
1/3 - 3	Platinum RTD, Class 1/3 DIN	T104	0.1635
1/3 - 4	Platinum RTD, Class 1/3 DIN	T105	0.1635
1/3 - 5	Platinum RTD, Class 1/3 DIN	T001	0.1635
1/3 - 6	Platinum RTD, Class 1/3 DIN	T002	0.1635
1/3 - 7	Platinum RTD, Class 1/3 DIN	T003	0.1635
1/3 - 8	Platinum RTD, Class 1/3 DIN	T004	0.1635
1/3 - 9	Platinum RTD, Class 1/3 DIN	T005	0.1635
1/10 - 14	Platinum RTD, Class 1/10 DIN	T201	0.1638
1/10 - 16	Platinum RTD, Class 1/10 DIN	T202	0.1655
1/10 - 17	Platinum RTD, Class 1/10 DIN	T301	0.1635
1/10 - 18	Platinum RTD, Class 1/10 DIN	T302	0.1635

Results indicate it is the data acquisition system uncertainty of 0.15 °C which dominates the combined uncertainty value. All calibrated sensors (i.e. excluding the two Type-K thermocouples) have a combined uncertainty which is lower or equal to 0.165 °C so a conservative estimate was made that a combined uncertainty of 0.165 °C could be assigned to all. The global uncertainty on all calibrated temperature measurements is therefore ± 0.165 °C with a 95% confidence level.

References

Figliola, R. S., & Beasley, D. E. (2011a). Theory and Design for Mechanical Measurements (5th ed., pp. 309-374): Wiley.

Figliola, R. S., & Beasley, D. E. (2011b). Theory and Design for Mechanical Measurements (5th ed., pp. 161-208): Wiley.

Moffat, R. J. (1982). Contributions to the Theory of Single-Sample Uncertainty Analysis. *Transactions of the ASME, 104*(2), 250-260.

Shirazi, A. S. (2012). *Transient Heat Transfer in Vertical Ground Heat Exchangers.* Ph. D., École Polytechnique de Montréal, Montréal.

Table B.6: List of uncertainty sources, associated uncertainty reduction methods and conclusion

Uncertainty sources		**Uncertainty reduction method**	**Conclusion**
Calibration uncertainty	For a defined target temperature, the real temperature of the water bath might oscillate depending on the precision of the bath's controls.	All measurements being taken inside a copper block, the effect of any oscillation of the bath's water temperature will be reduced. To further reduce thermal gradients in the copper block, before recording any measurements at a target temperature, the reference temperature will have to have varied by less than ± 0.05 °C over a period of five (5) minutes.	Negligible
	The reference sensor measurements will have random errors.	Using the average of 300 measurements to determine the target temperature used in the sensor calibration will reduce the effect of random errors in the reference sensor reading versus the real bath temperature (Coleman & Steele, 1998).	Negligible
	The reference sensor measurements will have systematic errors.		To be evaluated
	Error from calibration equation		To be evaluated
	The calibrated sensor will have random errors.	Each reading performed by the sensors after having been calibrated will not always be the mean used in the calibration equation. The uncertainty associated with this random error will be evaluated from the fluctuations in readings for each target temperature.	To be evaluated
	The sensor to be calibrated will have systematic errors.	The systematic errors of the sensors to be calibrated will be defined by the calibration equation.	Negligible
Data acquisition system uncertainty	Data-acquisition system resolution error and calibration uncertainty	The manufacturer specifies a measurement accuracy which includes all measurement errors from the data-acquisition system (terminal bock and module) including RMS noise.	To be evaluated
	The linearization error due to built-in reference junction compensation	The error induced by the built-in reference junction compensation of the thermocouple data acquisition module is a systematic error and as such it will be replaced by the calibration error.	Negligible